AFIT/GE/ENG/04-05

SIMULATING A CHROMOTOMOGRAPHIC SENSOR FOR HYPERSPECTRAL IMAGING

IN THE INFRARED

THESIS

Anthony J. Dearinger
Flight Lieutenant, Royal Australian Air Force

AFIT/GE/ENG/04-05

DEPARTMENT OF THE AIR FORCE

AIR UNIVERSITY

AIR FORCE INSTITUTE OF TECHNOLOGY

Wright-Patterson Air Force Base, Ohio

SIMULATING A CHROMOTOMOGRAPHIC SENSOR FOR
HYPERSPECTRAL IMAGING IN THE INFRARED

THESIS

Presented to the Faculty

Department of Electrical and Computer Engineering

Graduate School of Engineering and Management

Air Force Institute of Technology

Air University

Air Education and Training Command

In Partial Fulfillment of the Requirements for the

Degree of Master of Science in Electrical Engineering

Anthony J. Dearinger, B.E.(Electrical) (Hons) *UNSW*

Flight Lieutenant, Royal Australian Air Force

March, 2004
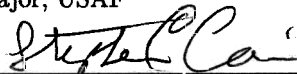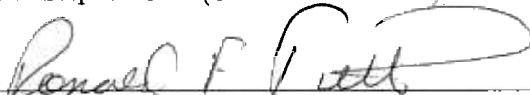
AFIT/GE/ENG/04-05

SIMULATING A CHROMOTOMOGRAPHIC SENSOR FOR HYPERSPECTRAL IMAGING IN THE INFRARED

THESIS

Anthony J. Dearinger, B.E.(Electrical) (Hons) *UNSW*

Flight Lieutenant, Royal Australian Air Force

Approved:

_____   _____
Dr. Matthew Goda (Thesis Advisor)   Date

Major, USAF

_____   _____
Dr. Stephen Cain (Committee Member)   Date

_____   _____
Dr. Ronald Tuttle (Committee Member)   Date

_____   _____
Dr. Glenn Perram (Committee Member)   Date

Dedicated to my wife and our darling children
Your love and devotion sustains my will and motivation in all that I do
Thank you

Table of Contents

viii

List of Tables

AFIT/GE/ENG/04-05

Abstract

Hyperspectral imaging systems passively sense radiant electromagnetic energy from a remote scene to form a three dimension profile of the remote scene. The data contained in this profile describes real images of the remote scene (two spatial dimensions) for a certain number of spectral wavelength bands across a finite spectral range of electromagnetic radiation (one spectral dimension). Typical grating type hyperspectral imaging systems collect spectral electromagnetic radiation in the visible and near infrared spectral range, by incrementally scanning across the spatial extent of the remote scene. Due to the very low optical throughput used in these systems, a legacy of the optical techniques employed to scan for spectral and spatial information, adapting these systems for spectral ranges extending into the mid wave and long wave infrared is difficult. Utilising an optical arrangement that delivers significantly greater optical throughput for collecting radiant electromagnetic energy from remote scenes, the chromotomographic imaging system has been reported to demonstrate reasonable quality hyperspectral images for finite spectral ranges in the visible, mid wave, and long wave infrared.

This thesis investigates the design for a software model that emulates the attributes of the optics system loosely detailed in reports of the chromotomographic imaging system. The optical system angularly multiplexes the spatial electromagnetic radiation collected from a remote scene onto a focal plane array detector using a rotating prism to disperse the electromagnetic radiation. Using optics principles and wave optics propagation theory, the software model has been designed to simulate the point spread function characteristics of the optics system in the chromotomographic real image plane. The software model can be used as an aid to develop and test the characteristics of an optics system through simulation, or simulate acquiring actual chromotomographic real image based on spectral information about a remote scene, or explore certain hyperspectral image reconstruction techniques suited to the chromotomograhic imaging system.

SIMULATING A CHROMOTOMOGRAPHIC SENSOR FOR HYPERSPECTRAL IMAGING IN THE INFRARED

I. Introduction

Interest in recording visual events as images continues to evolve as advances in various technologies and the application of these technologies continue to progress according to the pace of changing demands and desires of human societies around the world. Photography is recognised as the first advance in technology by mankind for directly recording real world scenery. The application of photography over the years has influenced innovation and inventions with commercial investment to explore different methods for essentially recording real world scenery. In the engineering discipline of remote sensing, photography has served as the foundation for advancements that have been made in remote sensing to record images of real world scenery.

As an engineering discipline, remote sensing can be viewed as applying scientific techniques for an observer to gather useful information about a remotely located subject. In this context, photography is certainly a form of remote sensing, where the useful information acquired from photography is typically a two-dimension image of the subject remotely located within a line of sight from the observer. One particular remote sensing application that continues to realise potential for further advancement is the field of hyperspectral imagery systems.

1.1   Hyperspectral Imaging

Aerial photography is probably the best known application of remote sensing where hyperspectral imagery systems have been developed for the purpose of capturing and recording two dimension images. Individually each image covers different finite spectral bands, and collectively form a data set of real images across a finite range of the electromagnetic spectrum. This data

<div align="center">(a)   (b)</div>
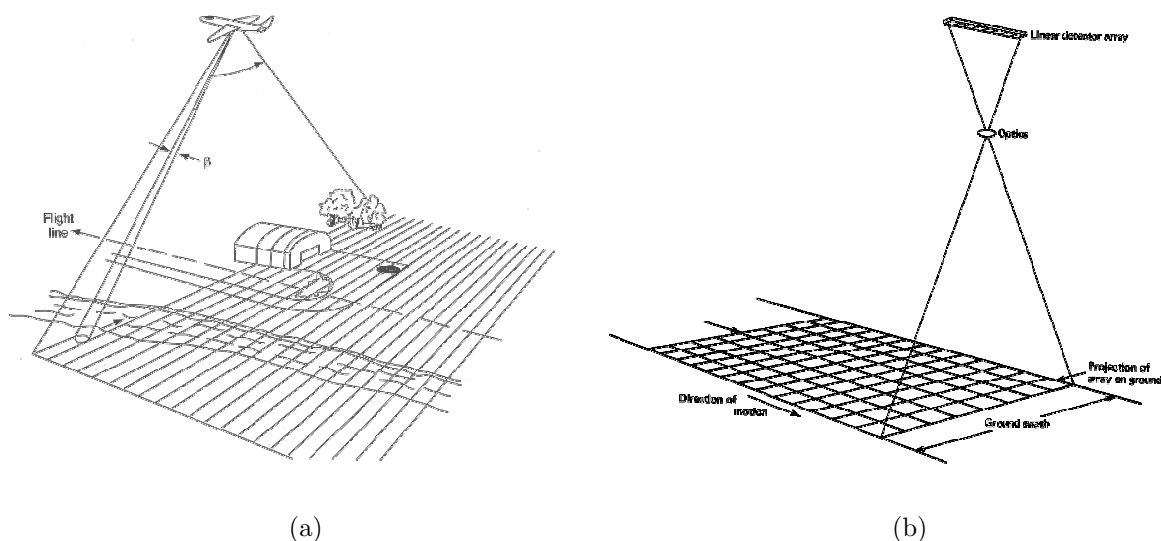
Figure 1.1:   Hyperspectral remote sensing techniques. Aerial scanning techniques that employ dispersive optical systems to record the spectral details of each spatial sample of the remote scene are the (a) whiskbroom (across track) [3: 311] and (b) pushbroom (along track) [3: 315]. These techniques incrementally scan across the entire spatial extent of the remote scene over time, capturing the hyperspectral details for the remote scene.

set captures the spectral and spatial fidelity of information about the remotely located subject or scene.

During the process of sensing and recording data from the remote scene, the collected spatial and spectral details must be in a format at the time of recording that enables spectral images of the remote scene to be constructed from the recorded data. The images of the same remote scene collected over a spectral range of the electromagnetic spectrum collectively form a hyperspectral data set for the remote scene.

During the past development of hyperspectral imaging systems, certain techniques have endured success with sensing multispectral remote scenes and representing this information as hyperspectral data sets. The whiskbroom (across track) and the pushbroom (along track) techniques for collecting multispectral remote scene data are two better known approaches employed for hyperspectral image remote sensing. Diagrams representing each technique appear in Figure 1.1.

These techniques scan piecewise subareas from a large area, progressively collecting the complete spatial extent of the large area to steadily build a spectral information set for the large area. The collection of hyperspectral image data with these techniques endures a time penalty, the duration of time required to scan the large area and appropriately record the spectral information. This time requirement has confined the use of hyperspectral imaging systems to applications where prominent features in the remote scenery do not change over extended periods of time. Platforms that are available to undertake the role of carrying hyperspectral imaging systems to collect this form of data are aircraft and satellites. Consequently, aerial surveillance of geographic regions on Earth has pioneered the application of hyperspectral imaging systems, where community or rural centres regions may be surveyed typically with aircraft platforms, and large regions of continents or oceans surveyed with satellite platforms.

1.2   Airborne Visible / Infrared Imaging Spectrometer

One well known application of employing a hyperspectral imaging system is the Airborne Visible / Infrared Imaging Spectrometer (AVIRIS) project. The AVIRIS project continues to be undertaken by NASA's Jet Propulsion Laboratory (JPL) to identify, measure and monitor major constituents of the Earth's surface and atmosphere based on molecular absorption and particle scattering signatures.

AVIRIS uses an imaging spectrometer to obtain spectral information of the remote scene, by scanning subregions as piecewise components of the entire region contained in the remote scene. Spectral information for each subregion is recorded during the scan period allocated for each subregion, so progressively the hyperspectral image data set of the entire remote scene is recorded. Figure 1.2 is a representative sketch of the spectral information this project collects from remote scenes. Figure 1.3 is a sketch of a representative spectroscopic profile for a subregion or pixel from the remote scene. Figure 1.4 is a hyperspectral image data set, represented here as an image cube,
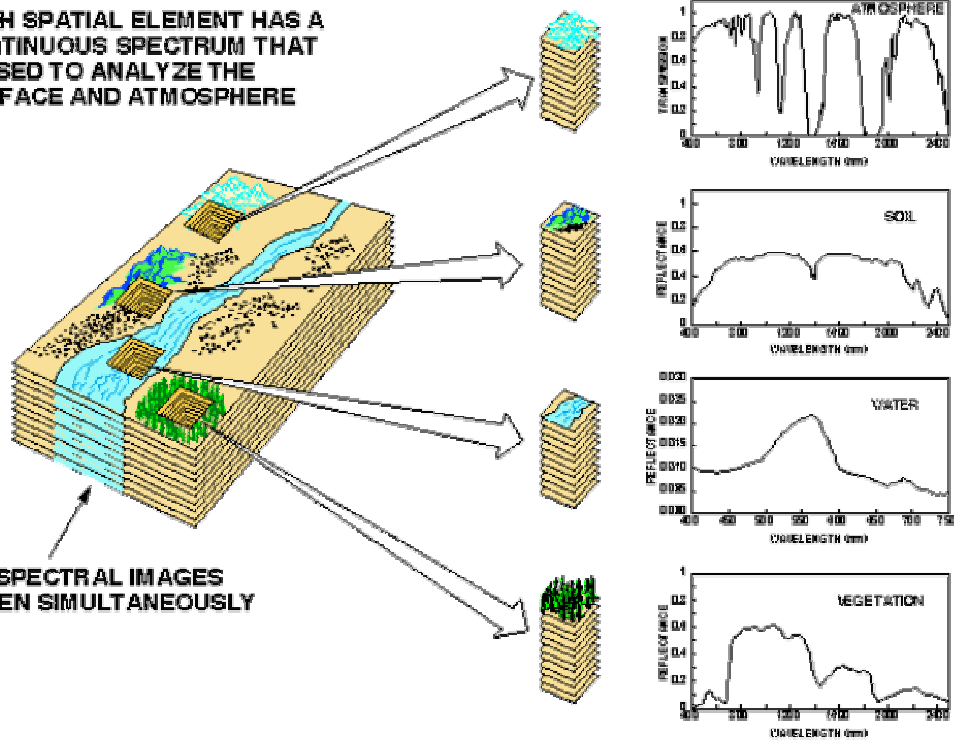
Figure 1.2:   AVIRIS concept of Hyperspectral Imaging [1]

of Moffett Field at the southern end of San Francisco Bay, California. The false colour image on top of the image cube has been established to highlight the structure of the water and evaporation ponds in the lower right region of the remote scene. The sides of the cube represent spectral slices of the respective edges of the remote scene represented on top, across the spectrum of electromagnetic radiation from 400 nm (near ultraviolet) to 2,500 nm (near infrared).

1.3   Conventional Hyperspectral Imaging Limitation

The AVIRIS approach with collecting multispectral remote scene image data highlights the characteristic limitation of information throughput with conventional hyperspectral imaging techniques that scan across one dimension, whether spatially or spectrally, to obtain the complete set

4
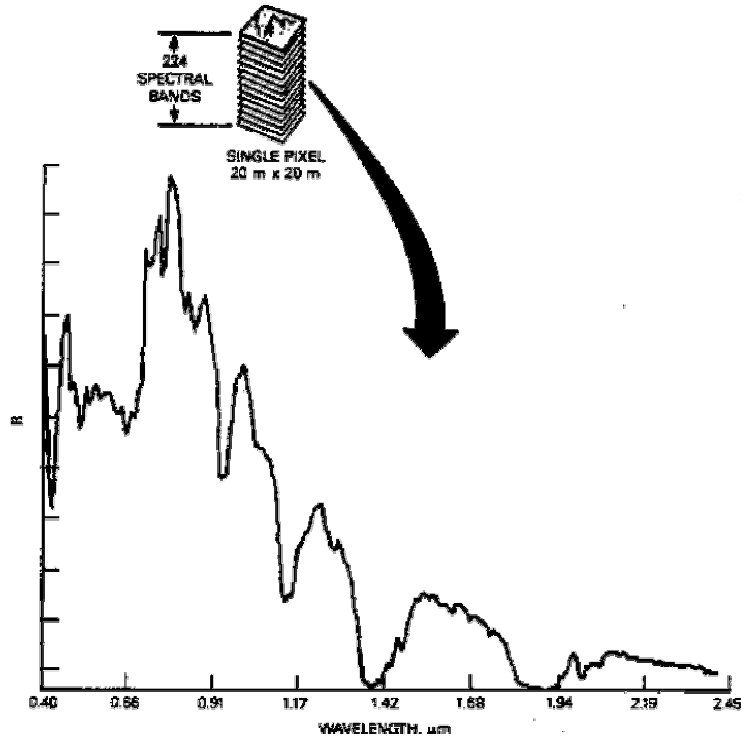
Figure 1.3:   AVIRIS sample profile of Intensity for a single pixel on the detector [1]

of spatial and spectral information from the remote scene. The limitation of this throughput is
further compounded by the time interval needed to completely scan the remote scene.

Adapting conventional state-of-the-art hyperspectral imaging systems for spectral ranges in
the mid wave and long wave infrared regions of the electromagnetic spectrum is compounded by
the very low optical throughput techniques used these systems. At infrared spectral wavelengths
features in the remote scene characteristically have low contrast between energy levels of electro-
magnetic radiation. For remote sensing in the infrared and overcome the low contrast between
radiant energy levels, a hyperspectral imaging system would require an optical system arrangement
that offered significantly higher optical throughput.

The chromotomographic imaging system was developed by Jonathon M. Mooney and col-
leagues of AFRL/SNHI at Hanscom Air Force Base [4–6], utilising an optical system with high op-
tical throughput that angularly multiplexes the spatial electromagnetic radiation collected from a

5
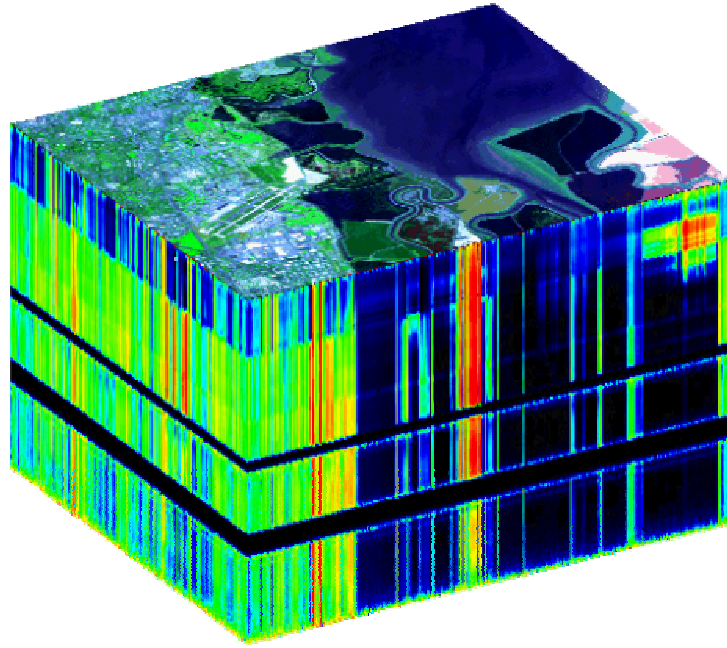
Figure 1.4:   AVIRIS Hyperspectral Image Cube (Hyperspectral Data Set) [1]

remote scene onto a focal plane array detector, to provide significantly greater optical throughput for collecting radiant electromagnetic energy from remote scenes. Comparisons of optical throughput between conventional hyperspectral imaging systems and the chromotomographic imaging system are worth noting with respect to the hyperspectral data cube, which describes the three dimension image data remotely sensed by these systems. Figure 1.5 shows this comparison for the hyperspectral image remote sensing techniques of spatial scanning, spectral filtering, and chromotomography.

1.4   Spectrotomography

Adapting the application of hyperspectral imaging systems for other uses is a current challenge in the remote sensing community, particularly over the past decade. Using hyperspectral imaging systems for surveying features in remote scenes that are characteristically transient over time is the challenge being tackled as the next advancement in the application of hyperspectral imaging systems.
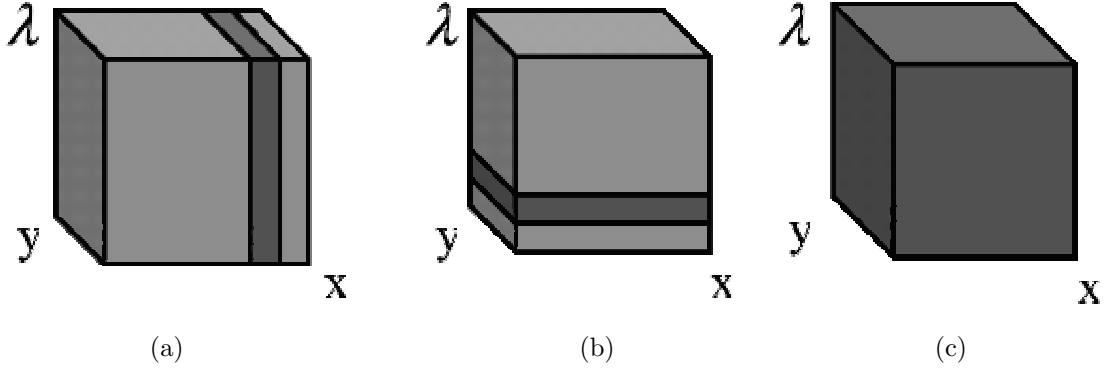
Figure 1.5: Optical throughput characteristics with conventional hyperspectral imaging systems can be compared from the hyperspectral data cube where (a) spatial scanning (b) spectral filtering methods deliver low optical throughput. The spatial and spectral slices respectively demonstrate this throughput. A higher optical throughput (c) chromotomography is achieved with the optical sensor used in the chromotomographic imaging system [7].

Studies by Bulygin *et al* [8] and Okamoto *et al* [9] pioneered the development of techniques that demonstrate how multispectral spatial data from a remote scene can be collected and recorded using an optical system in a manner suited to hyperspectral imaging. A computed tomography approach is adopted to construct the spectral real images of the remote scene across the spectral range of electromagnetic radiation obtained with the optics system. Computed tomography was pioneered in the medical science discipline to obtain the three dimension spatial impression of a subject from the collection of two dimension spatial image slices of the subject. Applying the concept of computed tomography to hyperspectral imaging, the impression of the subject (remote scene) is obtained as a collection of two dimension spatial images slicing piecewise through a spectral range of the electromagnetic spectrum in spectral wavelength bands. This computed tomography collection of spatial images is more accurately known as the spectrotomography collection of the remote scene, analogous to a hyperspectral data set of images.

Further research over the past decade in spectral imagery that employs the concept of spatially separating spatial images of a subject according to spectral content has been reported in various forums by Mooney et al [4–6], Brodzik and Mooney [10], Descour and Dereniak *et al* [11, 12], Volin

et al [13], Scholl *et al* [14], and Ford *et al* [15]. These reported works contain explanations of the top-level detail for the actual systems of optics respectively used, but do not contain sufficient detail that would allow these efforts in spectrotomography to be replicated easily. This list of works is by no means an exhaustive representation of the research activity experienced in the field of spectrotomography.

1.5   Research Motivation

The Center for Measurement and Signature Intelligence (MASINT) Studies and Research (CMSR) at the United States Air Force Institute of Technology (AFIT) is interested in acquiring a sensor capable of hyperspectral imaging in the infrared region of the electromagnetic spectrum to capture and record dynamic real world remote scenes in real time. A sensor that employs the techniques of spectrotomography can realistically meet this capability. The sensor could also be regarded at this time a technologically leading-edge concept, and worthy of researching with a goal of designing a sensor suitable for use over predetermined spectral ranges of the electromagnetic spectrum.

Improving upon the MASINT understanding of the radiant energy phenomenology in the fireball resulting from an explosion or explosions in the remote scene is the foundation of interest behind this research of the chromotomographic sensor. To capture the spectral and spatial details from transient events in the remote scene, such as explosions, in the context of hyperspectral imagery, a sensor with the optical throughput characteristics of the chromotomographic sensor is needed.

The chromotomographic sensor's high optical throughput feature offers the ability to collect the spectral electromagnetic radiation content from the remote scene to form a hyperspectral real image data set representing the remote scene in a significantly lower duration of time (seconds) compared with other grating type conventional scanning hyperspectral imaging systems (hours).

This lower time duration with the staring chromotomographic sensor allows for speedier sequential collection over time of radiant energy from the remote scene to obtain a time resolved series of hyperspectral real image data sets representing the remote scene. Achieving time-resolved hyperspectral imagery of transient events elevates the dimensionality of for this type of imagery with the inclusion of time as a dimension to a four dimension real image data set.

The work reported by Mooney *et al* [4–6] explored recording remote scenes in the infrared range of the electromagnetic spectrum as hyperspectral image data sets. Recent descriptions of this work refers to the complete system of collecting the spatial and spectral information from a multispectral remote scene for constructing the remote scene as a hyperspectral image data set as a Chromotomographic Imaging System (CTIS). Instead of referring to spectrotomography, this thesis refers to chromotomography and the Chromotomographic Imaging System in recognition of the preceding work by Mooney *et al.*

To augment AFIT's research effort, this thesis reports the research undertaken with developing a software model that simulates the entire optics element of the chromotomographic imaging system. This software model employs a wave optics approach for representing the propagation of electromagnetic field wavefronts through the entire optics element of the system. Mooney *et al* presented a simplistic description of the optics element of the CTIS. This description has been used loosely as an aid to developing the software model reported in this thesis.

1.6 Research Goals

The goal of the research effort reported in this thesis is to develop a software model of the entire optics element of the chromotomographic imaging system. The software model is intended to be a software tool to enable understanding of the optics element of the CTIS through exercising the software model for different optics configurations. Gaining a deeper understanding and appreciation of constraints and freedoms that can be utilised for certain design parameters in developing an

optics element using the software model is intended to provide the user a realistic expectation of performance from a physical optics element with equivalent design parameters.

The nature of constructing hyperspectral image data sets with the post-processing element of the chromotomographic imaging system relies on obtaining the point spread functions related to the collected hyperspectral data set of the optics element of the system. With an established optic element baseline of design, the software model may be used to provide this information for the purpose of aiding with constructing hyperspectral image data sets.

Furthermore with an established optic element baseline of design, the software model could be utilised to obtain simulated a priori information regarding the remote scene as an aid for reconstruction. The accuracy of this information would depend on the accuracy to which the software model could simulate the behaviour of the real-world sensor.

1.7   Organisation

Chapter 2 introduces the chromotomographic imaging system chosen for the basis of developing the software model of the system and discusses some of the fundamentals with optics considered in the synthesis of developing the software model.

Chapter 3 introduces the specifics of the simulation model, separating the entire sensor optics system situated in an environment as a defined system, into manageable components of the simulation model, explaining the choices and decisions made with developing each component of the model.

Chapter 4 discusses the software model, examines the various parameters used in the software model, explains the approach undertaken to evaluate these parameters sufficiently for a sensible configuration of parameters, so these parameters can be used to simulate the chromotomographic sensor that comprises the sensor optics system of the chromotomographic imaging system. The software model simulates the spectral point spread functions for the chromotomographic sensor

for a scenario configuration that comprises the sensor optics system and the separation distance between the sensor and the remote scene. Evaluation of a scenario configuration is presented to give an insight about the type of information the software model provides toward understanding the simulated chromotomographic sensor system.

Chapter 5 reviews the attributes reported in this thesis that contributed during the research effort for designing a software model to simulate the chromotomographic sensor system.

II. Background

This chapter introduces the chromotomographic imaging system (CTIS) as presented by Mooney *et al* [4–6]. The research presented in this thesis used the description of the CTIS system to loosely guide the development of the software model. Geometric optics and Fourier optics are introduced as alternate approaches to modelling the optics component of the CTIS. Understanding where each approach has relevance in the design of the software model is important. Introducing the concept of propagating light as a spatial and spectral waveform, the genesis of wave optics, as the backbone of the software model.

2.1 Chromotomographic Imaging System

The concept of the CTIS used as the guide for developing the software model was described originally by Mooney *et al* [4] as an Angularly Multiplexed Spectral Imager (AMSI). An impression of the optical system arrangement used in the CTIS is shown at Figure 2.1.
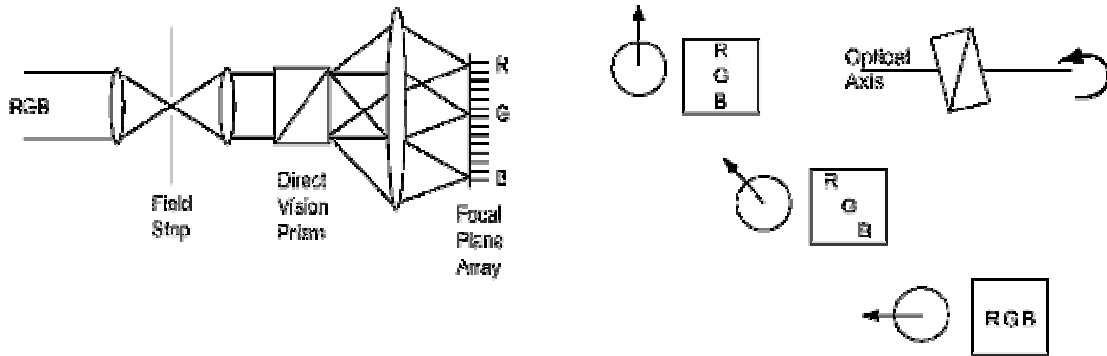
Figure 2.1:   Optical system arrangement for the chromotomographic imaging system [6]

The CTIS as a complete system can be viewed to contain two sub-system components, the chromotomographic sensor system and the digital post-processing and image construction system, which stand alone separately as significant systems. Previously these systems were discussed as the optics component and the digital post-processing component of the CTIS respectively. The
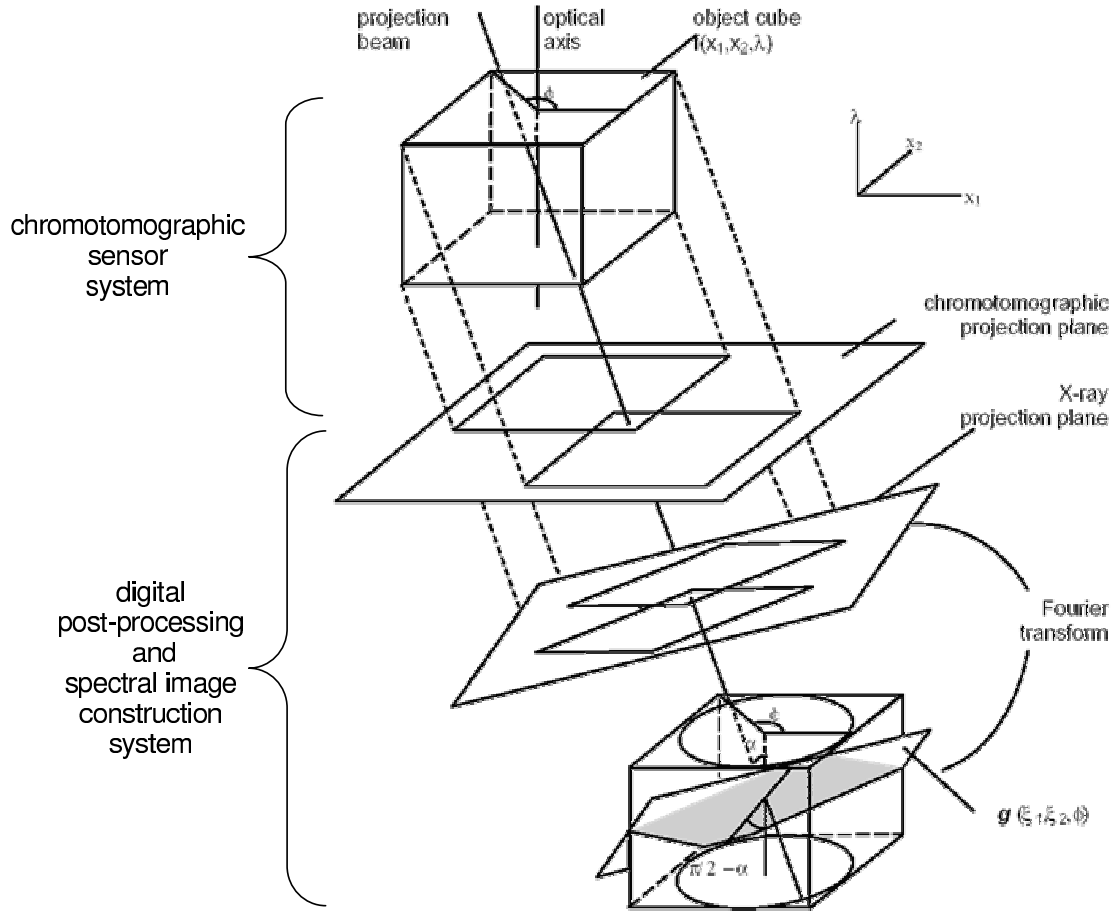
Figure 2.2:   Arrangement of projection planes for the chromotomographic imaging system [7, 10]

separation between these systems is described in Figure 2.2 from the viewpoint of projection planes that characterise key stages of the information process for the chromotomographic imaging system.

Although the process of achieving hyperspectral imaging from the CTIS has been described [4–7, 10], the science used for designing a chromotomographic sensor system to achieve image spectroscopy by spatially separating spectral images in the chromotomographic real image plane is not clearly outlined. Research reported in this thesis was focussed on understanding the science of wave optics propagation and establishing a software model that accurately represents the performance

of a physically equivalent chromotomographic sensor system. In the software model design, the sensor optics system represents the chromotomographic sensor system.

2.1.1 Description. The chromotomographic sensor system is comprised of a double lens arrangement separated with a field stop aperture, followed with a prism, a detector focussing lens and focal plane array. Figure 2.1 details this arrangement where the double lens and field stop arrangement collect the multispectral electromagnetic radiation and spatial features from a remotely located subject. The electromagnetic radiation that propagates beyond the second lens is expected to be collimated.

These collimated wavefronts enter the prism, called the direct vision prism, which is designed for the purpose of dispersing the spectral wavefront fields contained in the multispectral electromagnetic radiation in angular directions with respect to the optic axis. The design of the prism affords for a certain wavelength contained in the finite spectral range to propagate through the prism to the detector focussing lens undeviated. The reference to undeviated means the spectral field for the specific undeviated wavelength should propagate from the prism to the focussing lens parallel to the optic axis, thus exhibiting no net deviation in angular direction of propagation with respect to the optic axis after propagating through the prism. All other spectral wavefront fields propagate from the prism adjacent to the optic axis with some net angular change in direct of propagation with respect to the optic axis.

The dispersed spectral wavefront fields propagate from the prism as incident radiation on the focussing lens of the detector. Propagating through the focussing lens, the spectral wavefront fields are focussed at the detector focal plane array as real images of the remote scene, separated spatially according to the spectral wavelength of intensity contained in each real image. The spatial separation between real images is governed by the angular dispersion encountered from propagation through the direct vision prism.

For the task of constructing the spectral real images from the spatial intensity data available at the focal plane array, the CTIS uses the point spread function (PSF) characteristics of the chromotomographic sensor system. The PSF for each spectral wavelength band represented with a real image differ in location on the focal plane array for each angular position of orientation for the prism. At the chromotomographic projection plane, the point spread functions for each spectral wavelength band that uniquely characterise the chromotomographic sensor system are dependent on: (1) the spectral wavelength of electromagnetic radiation for spatial extent and intensity level; and (2) the net angular direction of propagation and prism angular position of rotation for spatial location in the chromotomographic projection plane.

To form the hyperspectral image data cube, the CTIS separately convolves each spatial point spread function with the spatial characteristics of the remote scene at each spectral wavelength. For each angular position of prism rotation, summing the outcomes from each two dimension convolution operation according to the spatial locations of the point spread functions in the chromotomographic projection plane results in real images of the remote scene that are spatially offset according to the spectral wavelength band for each point spread function. These real images arranged spatially represent the chromotomographic real image (spectral real image data) for a single angular position of prism rotation (frame of data collection) recorded on the detector focal plane array. Illustrating this explanation, the mathematical expressions used to describe the CTIS [4] have been adapted here to represent four spectral wavelength bands and four angular positions of rotation for the direct vision prism, which correspond to four frames of chromotomographic real images. Equations 2.1 to 2.4 describe this relationship.

$$r_1(x,y) = p_{1,1}(x,y) \otimes c_1(x,y) + p_{1,2}(x,y) \otimes c_2(x,y) + p_{1,3}(x,y) \otimes c_3(x,y) + p_{1,4}(x,y) \otimes c_4(x,y)$$

$$(2.1)$$

$$r_2(x,y) = p_{2,1}(x,y) \otimes c_1(x,y) + p_{2,2}(x,y) \otimes c_2(x,y) + p_{2,3}(x,y) \otimes c_3(x,y) + p_{2,4}(x,y) \otimes c_4(x,y)$$

$$(2.2)$$

$$r_3(x, y) = p_{3,1}(x, y) \otimes c_1(x, y) + p_{3,2}(x, y) \otimes c_2(x, y) + p_{3,3}(x, y) \otimes c_3(x, y) + p_{3,4}(x, y) \otimes c_4(x, y)$$

$$(2.3)$$

$$r_4(x, y) = p_{4,1}(x, y) \otimes c_1(x, y) + p_{4,2}(x, y) \otimes c_2(x, y) + p_{4,3}(x, y) \otimes c_3(x, y) + p_{4,4}(x, y) \otimes c_4(x, y)$$

$$(2.4)$$

Introducing the parameter, $p_{a,b}$ describes the point spread function (denoted, p) for the spectral wavelength band (denoted, b) resulting from the specific angular position of prism rotation (denoted, a). The parameter, $r_a(x, y)$ describes the chromotomographic real image frame recorded (denoted, r), and this real image frame is linked to the specific angular position of prism rotation. The parameter $c_b(x, y)$ describes the spatial details of the remote scene (denoted, c) with electromagnetic radiation in the spectral wavelength band (denoted, b). The symbol $\otimes$ represents the two-dimension spatial convolution operation.

The hyperspectral image reconstruction approach described for the CTIS [4] relies on obtaining the system transfer function matrix from the complete set of point spread functions. The inverse of the system transfer function matrix together with the two-dimension spatial Fourier Transform of each recorded frame of chromotomographic real images formed on the detector focal plane array, enables the spectral real images of the remote scene to be computed. The outcome is a hyperspectral image data set that spectrally reconstructs the remote scene.

A further observation to note: each angular position of prism rotation corresponds to a chromotomographic real image frame of recorded data. There must be at least as many frames (one for each specific angular position of prism rotation) as spectral wavelength bands to be reconstructed for the digital post-processing approach to have enough parameters for successful hyperspectral image reconstruction.

2.1.2   Linear Shift and Time Invariant System.   The CTIS chromotomographic sensor system has the attributes of a typical optics system, with lenses and a prism being the only optical components in the system. These components do not introduce electromagnetic uncertainties with
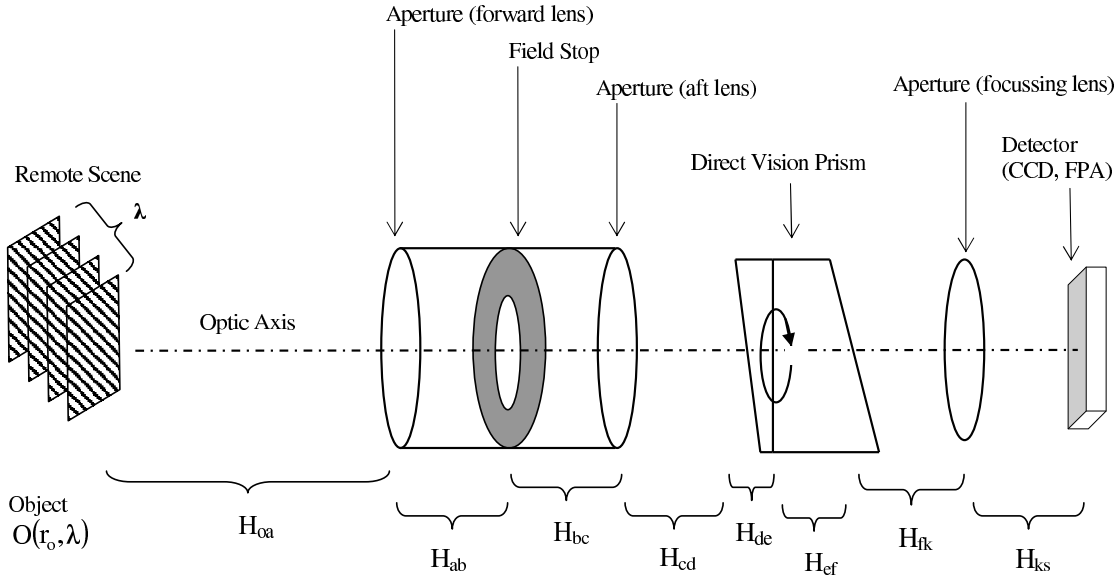
Figure 2.3:   Linear System Interpretation of Sensor Optics System

field propagation that would prohibit treating the system as a linear shift and time invariant (LSTI) system [2: 519-556]. Figure 2.3 shows the linear systems viewpoint of the chromotomographic sensor system with the remote scene included to completely characterise the remote sensing scenario.

From a linear system perspective, each point spread function represents a separate impulse response characteristic of the chromotomographic sensor system. For each specific angular position of prism rotation, the corresponding spectral point spread functions across the finite spectral range of electromagnetic radiation summed together according to spatial location, forms a chromotomographic real image frame. This frame may also be interpreted as the chromotomographic point spread function for the angular position of prism rotation, or prism prism orientation.

2.1.3 Geometric optics interpretation.   Geometric optics is very useful for interpreting the stages of propagation the software model of the sensor optics system is expected to simulate. Electromagnetic radiation is treated as rays in the direction of propagation with geometric optics, and is also referred to as ray optics. The paths of propagation for the electromagnetic radiation

17
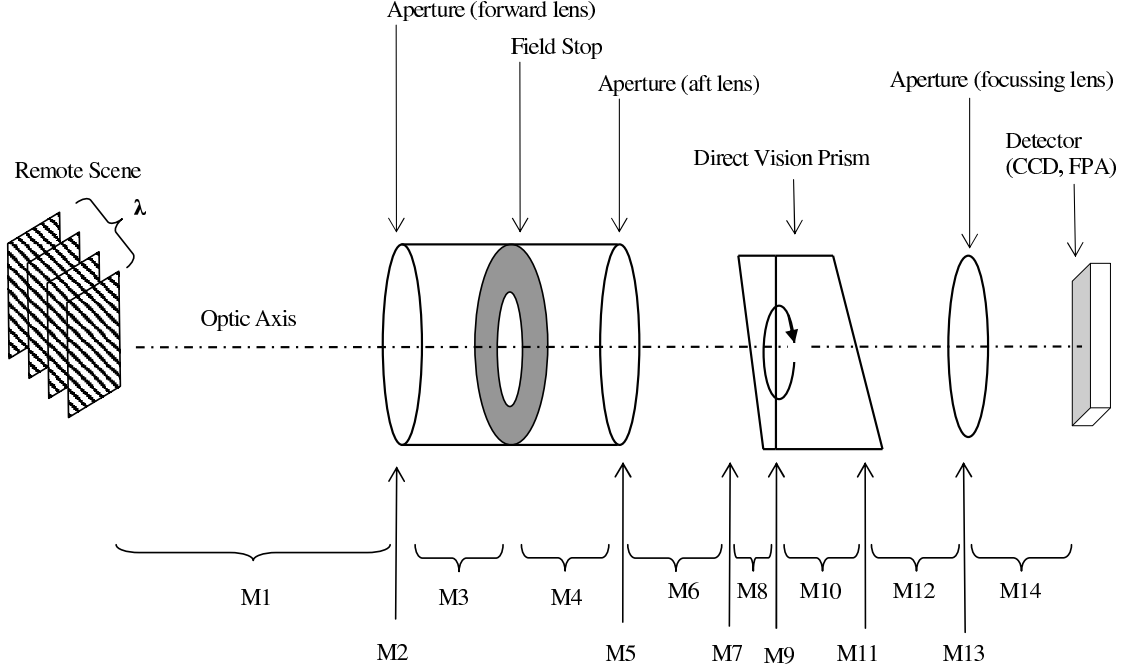
Figure 2.4:   Geometric Optics Interpretation of Sensor Optics System

wavefront are captured with sufficient accuracy that allow for the direction of propagation behaviour of radiation through a system to be readily identified.

Rays of electromagnetic radiation propagating through each stage of the sensor optics system can be expressed with a matrices that characterise the propagation in terms of the vertical displacement and angle subtended to the horizontal plane with the optic axis. More precise details about the propagation of electromagnetic radiation, like phase information across the wavefront of the electromagnetic field, are not treated with a geometric optics approach.

Figure 2.4 shows the sensor optics system from the software modelling viewpoint and the transformation matrices for each stage of propagation. These matrices for the different subsystems of the sensor optics system are described in Table A.1 for the forward optics system, Table A.2 for the prism optics system, and Table A.3 for the detector optics system.
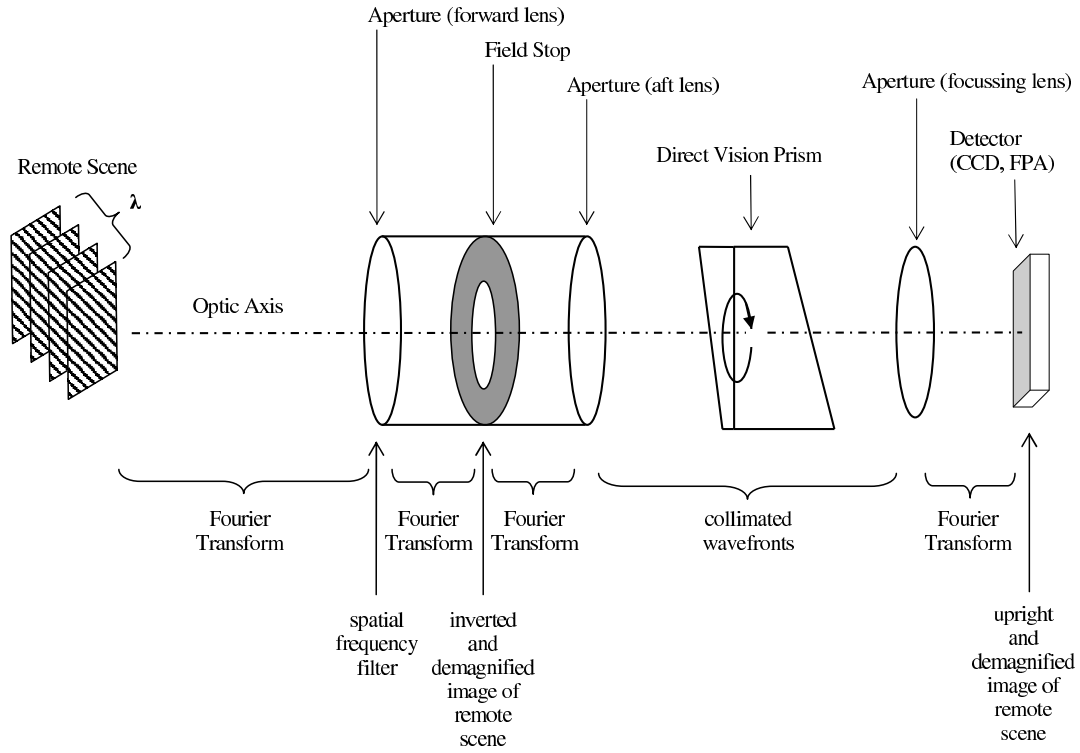
Figure 2.5:   Fourier Optics Interpretation of Sensor Optics System

Phenomena with the propagation of light as an electromagnetic wavefront, like interference patterns in the wavefront along the path of propagation due to the diffraction of light through an aperture and the incoherence of light propagating as photon radiation, are not represented with geometric optics.

As a technique to aid with modelling the sensor optics system, geometric optics is a simple technique for implementing the appropriate distances between lenses and imaging planes in the system. Establishing the transverse plane locations along the optic axis where real images of the remote scene should be observed is readily possible with use of the Lensmaker's formula for lenses, and Snell's Law of Refraction for the prism. Expressions for the Lensmaker's formula and Snell's Law of Refraction are presented in section 2.2.

2.1.4 Fourier optics interpretation.   Fourier optics is another alternate approach for describing the transitions of the electromagnetic field for the electromagnetic radiation wavefront. Propagating through lenses and the direct vision prism, the wavefront experiences changing optical path lengths that influence whether the wavefront beam converges, diverges, or is collimated for different stages of propagation. Figure 2.5 represents the sensor optics system this time described from the Fourier optics viewpoint.

Fourier optics employs approximations for the optical path lengths for points along the wavefront to propagate between transverse planes. These approximations enable the stages of propagation characterised by Fourier optics to be evaluated with the two-dimension Fourier Transform for each spectral wavelength.

From a software modelling viewpoint, using the Fourier optics approach to model these stages of propagation offers the computational advantage of speed at the legacy of amount of data. Simulation packages like MatLab® have dedicated fast Fourier Transform algorithms that are significantly quicker than separate instructions, however using these algorithms for cascading stages of propagation can attract a significant increase in generated electronic data.

Using Fourier Transforms to simulate the electric field propagation of electromagnetic radiation generally requires the source of radiation to be located on and symmetric with respect to the optic axis. Using Fourier Transforms as the basis of simulating the electric field propagation in a software model may limit the versatility of the software model with computing an off-axis point spread function for the simulated sensor optics system.

2.2 Propagation with wave optics

The complex electric field for electromagnetic radiation is used in wave optics models to simulate the propagation of electromagnetic radiation through a medium. During propagation through different optical components the complex electric field across the wavefront of radiation

experiences effects optical path lengths due to the type of medium and length of propagation through the medium. For the sensor optics system, the lenses and direct vision prism have mediums of propagation that differ from air and will impart different optical path lengths of propagation for each region of the electric field wavefront.

2.2.1 Propagation through media. The optical path lengths are influenced by the speed of propagation and the duration of propagation through the medium. The speed of propagation, more commonly described as the speed of light, through a medium depends on the index of refraction for the medium. Index of refraction for a certain medium describes the ratio of the speed of light in a vacuum $c = \frac{1}{\sqrt{\epsilon_0 \mu_0}}$, with respect to the speed of light in a certain medium $v = \frac{1}{\sqrt{\epsilon \mu}}$, and is generally expressed as $n = \frac{c}{v} = \sqrt{\frac{\epsilon \mu}{\epsilon_0 \mu_0}}$. The terms in these expressions are index of refraction, n, dielectric constants of permeability for a vacuum ϵ_0, permeability for a certain medium ϵ, permittivity for a vacuum μ_0, and permittivity for a certain medium μ. The duration of propagation depends on the distance of propagation through the medium.

These considerations with wave optics thus captures the change in direction of the propagation due to a change in propagation medium. The mathematical relationship that describes the change in wavefront orientation and so the direction of propagation, is Snell's Law of Refraction stated in equation 2.5,

$$n_1 \sin \theta_1 = n_2 \sin \theta_2 \tag{2.5}$$

where the angle of incidence θ_1 in the first media at the surface interface between two different media, and the index of refraction of the first medium n_1 where the angle of incidence occurs, is related to the angle of refraction θ_2 from the surface interface between the two media, and the index of refraction of the second medium n_2 where the angle of refraction occurs.

The Lensmaker's formula uses Snell's Law of Refraction for the interface between propagation media at each surface of the lens to paraxially approximate the optical path length for propagation

21

through the lens. This approximation also treats the lens as a thin lens, and so the Lensmaker's formula expressed at equation 2.6 is also referred to as the Gauss Thin Lens formula for lenses,

$$\frac{1}{\text{s}_{\text{observe}}} + \frac{1}{\text{s}_{\text{image}}} = \frac{1}{\text{f}} \tag{2.6}$$

where f denotes the focal length of the lens, $\text{s}_{\text{observe}}$ denotes the distance the subject is located from the lens, and s_{image} the distance the real image is located from the lens.

2.2.2 Propagation of point sources. Interference patterns in the wavefront along the path of propagation due to the diffraction of light passing through an aperture, is a phenomena with the propagation of light that can be emulated with simulation, provided an appropriate approach is used to represent the propagation of light as a complex electromagnetic field. An approach that captures the essence of the diffraction experienced in the electromagnetic field wavefront propagation of light is desirable for this purpose.

The Rayleigh-Sommerfield diffraction theory [16: 52] describes the diffraction effects resulting from the propagation of a spherical electromagnetic field wavefront through an aperture. Correct use of the Rayleigh-Sommerfield diffraction formula representing this theory and described at equation 2.7 in the software model should achieve simulating the diffraction effects inherent with this wavefront propagation.

$$\text{U}_1(\text{x}_1, \text{y}_1) = \frac{1}{\text{j}\lambda} \iint \frac{\text{U}_0(\text{x}_0, \text{y}_0)}{\text{r}} \; \text{e}^{\text{j k r}} \; \cos\theta \; \text{dx}_0 \; \text{dy}_0 \tag{2.7}$$

This equation describes the complex electromagnetic field wavefront $\text{U}_0(\text{x}_0, \text{y}_0)$ propagating from the transverse plane with ordinates x_0 and y_0, to another transverse plane with ordinates x_1 and y_1, resulting in the complex electromagnetic field wavefront $\text{U}_1(\text{x}_1, \text{y}_1)$. The distance of propagation for a point source on the wavefront of the electromagnetic radiation is,
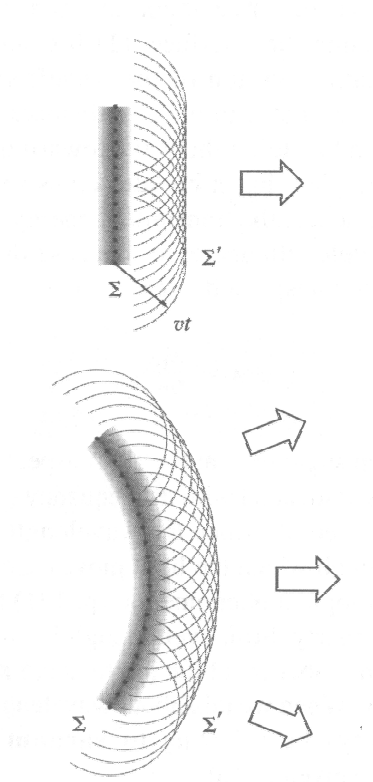
Figure 2.6:   Huygens's Principle [2: 104]

$r(x_0, y_0, x_1, y_1) = \sqrt{(x_1 - x_0)^2 + (y_1 - y_0)^2 + z^2}$ in metres, and the wave number for each wavelength in the spectrum of electromagnetic radiation is, $k = \frac{2\pi}{\lambda}$ in metres^{-1}.

To appreciate how wave optics treats a propagating electromagnetic field of light, a sketch representing Huygens's Principle is included at Figure 2.6. This figure shows the wavefront of the electromagnetic field of light propagating as many (uncountable) point sources distributed along the wavefront, each emitting spherical wave fields of electromagnetic radiation.

Although the propagation of a field of electromagnetic radiation as light has vectorial properties, the Rayleigh-Sommerfield diffraction theory applies scalar properties to describe the propagation of this field in an optics system based on certain key simplifications and assumptions. Electromagnetic interactions, described by Maxwell's equations, between the propagating field and other electromagnetic fields at surface boundaries and apertures of optical components in the optics system are disregarded in the Rayleigh-Sommerfield diffraction theory. Coupling between electric

and magnetic fields in the propagating electromagnetic radiation are also disregarded since the propagation media at all stages of propagation through the system does not support this coupling, earlier referred to as electromagnetic uncertainties in section 2.1.2.

Treating the propagation of electromagnetic radiation as a scalar phenomenon is acceptable provided two conditions in the circumstances of propagation are satisfied. These conditions are (1) the diffracting aperture must be significantly large compared to the wavelength of electromagnetic radiation, and (2) the electromagnetic field resulting after the diffracting aperture must be observed from a sufficiently distant location from the diffracting aperture [16: 35].

The criteria for the terminology *significantly large* and *a sufficiently distant location* is not specifically defined. For a typical aperture or lens diameter from 2 cm to 20 cm, and typical observation distances from 10 cm to 100 cm respectively, in the infrared spectrum in terms of wavelength from 2 μm to 5 μm, the relationship between these distances and wavelength can be described in terms of ratios with magnitudes of at least $\frac{2\text{cm}}{5.0\mu\text{m}} = 4,000$. This represents at least three orders of magnitude in size between the spectral wavelength and the distances mentioned in the typical conditions.

Another requirement of the Rayleigh-Sommerfield diffraction theory is for each diffracting aperture to be planar [16: 51]. This criteria is represented in the expression for the propagation distance (denoted, r) and the term $\cos\theta$ which describes the orientation of the direction of propagation with respect to the surface normal of the aperture plane. This condition can be satisfied at each stage of propagation for the software model, since the field and intensity of the electromagnetic radiation are sampled across a planar cross-section of the sensor optics system.

2.3 Proposed system requirements and specifications

With developing a model to simulate an actual system of interest for physical design and operation, the requirements of any system should be translated to the design of the model. For the

purpose of constructing this hyperspectral imaging system, certain attributes of the system may be more restrictive on choices for the sensor design than others, so it is important to capture all the attributes that may influence how the design is undertaken.

The principle aim of this software model is to retain sufficient flexibility with defining system parameters, so that design choices can be evaluated effectively using the model.

2.3.1 Hardware.   Some hardware attributes of the system that must be accommodated with developing the model of the sensor optics system include the following notes.

2.3.1.1 Detector - focal plane array.   The infrared detector is an Indium Antimonide (InSb) focal plane array, comprising 512 pixels by 640 pixels with a 0.24 μm pitch per pixel for height and width equally across the array.

2.3.1.2 Detector - focussing lens.   The choice focussing lens that focuses radiation incident on the infrared detector to the InSb focal plane array can be selected to have an effective focal length of either 50 mm, 100 mm, 150 mm, 200 mm, 250 mm, and 500 mm.

2.3.1.3 Stepper Motor.   The direct vision prism will be mounted in a high precision axially tubular stepper motor, that can hold and axially rotate optical components that do not exceed 2 inches in diameter. The direct vision prism diameter must not exceed 2 inches (approximately 50.8 mm).

2.3.1.4 Direct Vision Prism.   The direct vision prism diameter is one inch. The minimum axial distance along the outer axial surface for each bulk media stage of the prism is 3 mm.

2.3.2 Performance.   Some hardware attributes of the system that must be accommodated with developing the model of the sensor optics system include the following notes.

2.3.2.1   Spectral coverage.   The spectral range of infrared electromagnetic radiation to be collected and imaged by the sensor optics system is 1.8 to 5.2 μm.

2.3.2.2   Undeviated spectral wavelength.   The undeviated spectral wavelength of infrared electromagnetic radiation is to be $3.6 \pm 0.1\mu$m.

2.3.2.3   Usable aperture.   The diameter of the collimated beam of infrared electromagnetic radiation entering the direct vision prism and propagating through the prism is to be at minimum 25 percent of the prism height without reflecting off the outer axial surface of the prism .

2.3.2.4   Spatial extent of images.   The spatial extent of the imaging area for each spectral wavelength band is not to exceed 128 pixels by 128 pixels on the focal plane array of the infrared detector.

III. Methodology

T his chapter covers the design of the software model for simulating the sensor optics system. The functional attributes of the system are covered in general at section 3.1. A generic treatment of the spatial sampling requirements in order to accurately sample the simulated electromagnetic radiation wavefront is outlined at section 3.2. The system coordinates and sign conventions defined for the software model are presented at section 3.3. The impetus for pursuing the software model is restated at section 3.4 before the functional sub-systems of the software model are discussed at section 3.5 (forward optics system), section 3.6 (prism optics system) and section 3.7 (detector optics system).

3.1 General Description

Designing the software model of the sensor optics system involved dividing the whole system into subsystems that were logically separable. Fortunately most optics systems can be viewed in simple terms as cascading stages of electromagnetic field wavefront propagation, and the sensor optics system is an excellent example of this.

The principal influences on the remote scene radiation performed by the system are collection, dispersion, and recording, so a logical approach was to divide the LSTI system described at section 2.1.2 into three sub-systems. Figure 3.1 shows the sensor optics system divided into three separable subsystems designated, forward optics system, prism optics system, and detector optics system, according to the influences of collecting, dispersing and detecting the remote scene radiation .

3.1.1 Forward Optics System.   From collecting all the incident fields of electromagnetic radiation from the remote scene and surrounding environment propagating through the forward lens is the incoming wavefront of electromagnetic radiation to the forward optics system. This electromagnetic field wavefront is focussed in the field stop transverse plane. The aperture size set
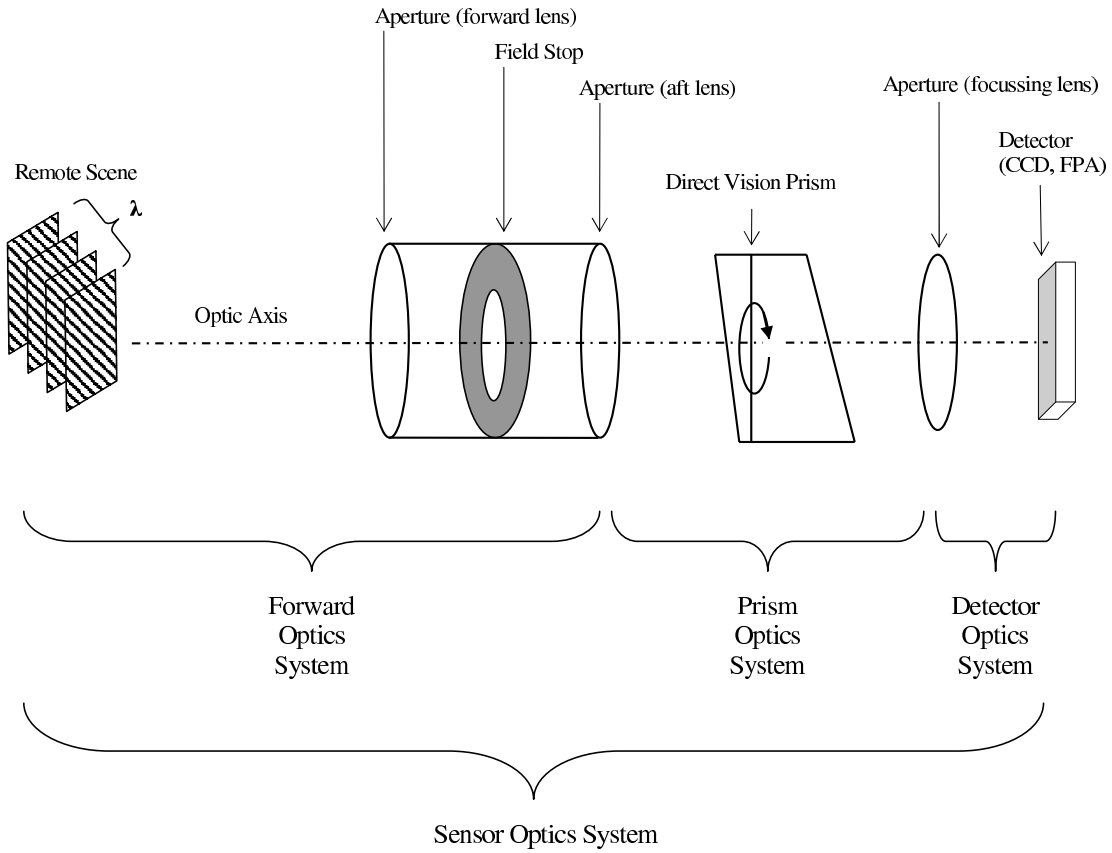
Figure 3.1:   Description of the CTIS Sensor Optics System as separate subsystems

at the field stop determines the angular extent of the collected electromagnetic radiation propagates from the field stop through to the aft lens. With the distances between each lens and the field stop set appropriately so a minified real image of the remote scene is formed in the field stop, the field of electromagnetic radiation propagating from the aft lens should be a collimated wavefront. As described here, the task of collecting electromagnetic radiation from the remote scene is achieved with the forward optics system.

3.1.2   Prism Optics System.   The field of electromagnetic radiation leaving the aft lens is the incoming wavefront of electromagnetic radiation to the prism optics system. The description of the wavefront as a field here implies there are many spectral wavelengths contained in the wavefront, effectively many (uncountable) fields of discrete electromagnetic radiation. The incoming wavefront

28

propagates through the different stages of media as material for the direct vision prism. The separation of air between the prism and the aft lens and detector focussing lens are also considered stages of propagation in the prism optics system. The materials that comprise the prism are selected as a media of propagation to offer more favourable transmission properties and some dispersion for the range of spectral wavelengths of interest for detection. The collimated wavefront entering the prism media experiences dispersion according to the spectral wavelengths in one direction along the transverse plane of the prism optics system in the course of propagating through the direct vision prism. The wavefront incident at the detector focussing lens is the result of dispersion on the wavefront of collected electromagnetic radiation from the remote scene, due to propagation through the prism optics system. This system achieves the task of dispersing the collected remote scene electromagnetic radiation.

The prism used in this system is permitted to rotate around the optic axis and disperses the collected radiation across the transverse plane along an axis of the prism cross section aligned with the transverse plane to the optic axis. The orientation of the direction of dispersion depends on the orientation of the prism with respect to the sensor optics system coordinates. As the prism is rotated angularly around the optic axis, the real image of the remote scene formed on the detector focal plane array as a dispersed image, also rotates around the optic axis. The spectral content of the collected radiation is dispersed in the transverse plane in both directions from the optic axis according to wavelength, with the exception of one wavelength band. This exclusive wavelength band of the remote scene forms a real image of the remote scene centred on the optic axis, and is referred to as the undeviated wavelength. For this wavelength band, the real image of the remote scene does not change location on the focal plane array as the angular orientation of the prism changes.

3.1.3 Detector Optics System.   The field of electromagnetic radiation entering the detector focussing lens is the incoming wavefront of electromagnetic radiation to the detector optics system.

The dispersion contained in this wavefront establishes different angular directions of propagation with respect to the optic axis for the spectral wavefront fields of electromagnetic radiation contained in the incident wavefront of electromagnetic radiation at the detector focussing lens. The lens focusses the incident spectral wavefront fields on the detector focal plane array.

The detector focussing lens interrogates each spectral wavefront field of electromagnetic radiation in a transverse plane to the horizontal plane of the sensor optics system that contains the optic axis. The view of the wavefront obtained by the detector focussing lens differs according to the angular direction of propagation for each spectral wavelength of electromagnetic fields in the wavefront. In essence this view conveys a certain gradient or tilt in phase (phase tilt) across the wavefront in the direction of dispersion from the direct vision prism. The amount of phase tilt for the electromagnetic field of each spectral wavelength can be gauged by comparing these wavefronts incident on the detector focussing lens with equivalent wavefronts propagating with no angular direction of propagation with respect to the optic axis (ie. along the optic axis). The location in the transverse plane of the detector focal plane array where the real image of the remote scene for a spectral wavelength of electromagnetic radiation is influenced by the phase tilt on the spectral wavefront field.

The detector optics system achieves the task of recording the collected remote scene electromagnetic radiation in a format that separates the spectral wavelength content of the remote scene to enable retrieval of real images of the remote scene for each spectral wavelength of electromagnetic radiation recorded. For an upright oriented direct vision prism, the angular directions of propagation for every spectral wavefront field of electromagnetic radiation in the wavefront change along the vertical axis of the system, applying vertical phase tilts to the spectral wavefront fields.

The purpose of the software model is to represent a discrete version of the collected fields of electromagnetic radiation from the remote scene that propagate through the sensor optics system. To ensure these fields are accurately represented as discretely sampled spectral fields, the requirements of spatial sampling across the apertures contained in the sensor optics system must be assessed.

3.2.1   General Description.   Imaging systems typically consist of lenses and apertures, and the optical performance of these systems is limited by the propagation of electromagnetic fields through the imaging system. These fields carrying the remote scene spatial feature information, and the size of apertures and lenses influences the optical performance of imaging systems with reproducing the real image of the remote scene.

Using Fourier optics analysis between two transverse planes, the spatial frequency response of an imaging system can be evaluated with some important fundamentals for diffraction-limited imaging [16: 134-144]. An Amplitude Transfer Function (ATF) describes the spatial frequency response for a coherent imaging system, whereas an Optical Transfer Function (OTF) describes the spatial frequency response for an incoherent imaging systems. So for one physical configuration of optics, the optical performance related to the diffraction-limited spatial frequency cut-off, can be assessed from the ATF, whether the optics system is used in a coherent or incoherent imaging system.

The diffraction-limited spatial frequency cut-off for a field of electromagnetic radiation with spectral wavelength, λ, propagating through an aperture with diameter, dia, in a direction adjacent to the optic axis to some location in a transverse plane to the optic axis, with the distance, z, separating the aperture and the transverse plane measured along the optic axis, is described at

equation 3.1 for coherent imaging, and at equation 3.2 for incoherent imaging,

$$f_{co(f)} = \frac{dia}{2\lambda z} \qquad (3.1)$$

$$f_{co(i)} = \frac{dia}{\lambda z} \qquad (3.2)$$

where $f_{co(f)}$ describes the cut-off spatial frequency for the field amplitude related to the ATF of the optics system, and $f_{co(i)}$ describes the cut-off spatial frequency for the field intensity related to the OTF of the optics system. Comparing these cut-off spatial frequencies, $f_{co(i)} = 2\ f_{co(f)}$.

3.2.2 Software Model. The sensor optics system of the CTIS is used for incoherent imaging, so the sampling requirements for the software model to represent the incident fields of electromagnetic radiation as discretely sampled fields were treated for incoherent imaging. The principles of geometric optics will be used to define the relationships for obtaining the discretely sampled fields.

Viewing the arrangement of the software model for the sensor optics system between the remote scene and the field stop with the forward lens situated between these transverse planes as shown in Figure 3.2, the geometric optics principle that rays propagating through the centre of the lens pass through undeviated, establishes the following relationship at equation 3.3 between the sampling intervals at the field stop transverse plane ds_3, and the remote scene transverse plane ds_1.

$$\frac{ds_1}{z_1} = \frac{ds_3}{z_2} \qquad (3.3)$$

For the aperture of the forward lens with a diameter dia_2, the cut-off spatial frequency at the field stop is expressed at equation 3.4 for a diffraction-limited system based on coherent imaging.

$$f_{3co(f)} = \frac{dia_2}{2}\frac{1}{\lambda z_2} \qquad (3.4)$$
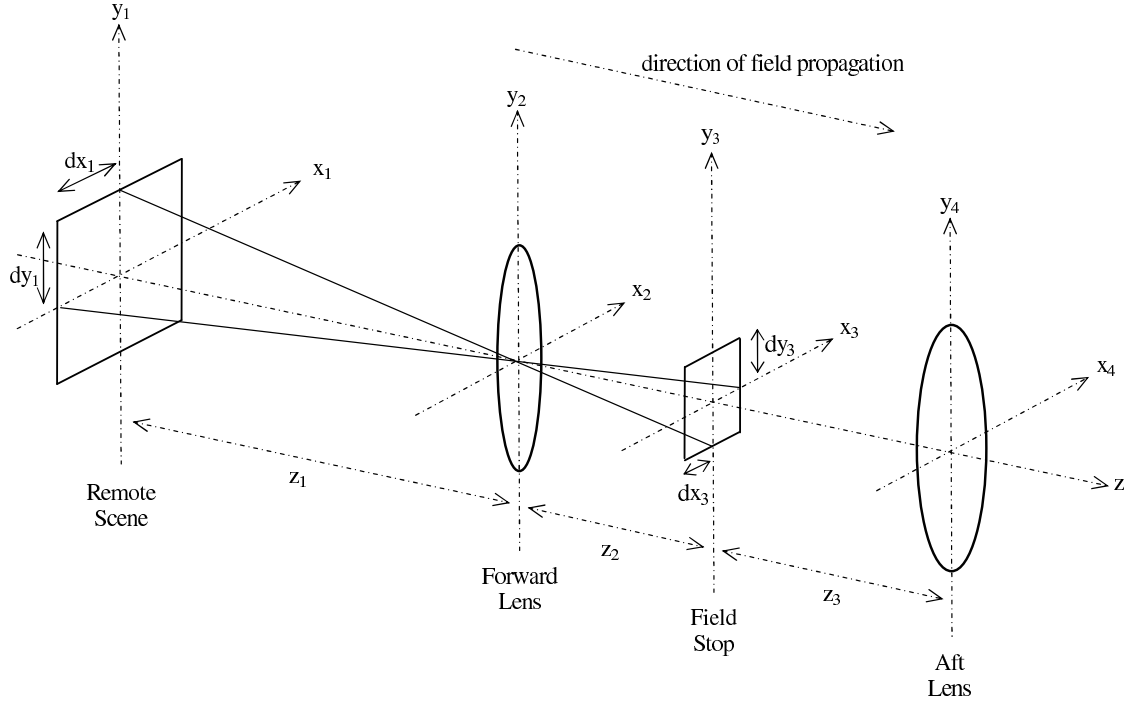
Figure 3.2:   Interpretation of spatial sampling intervals for the forward lens with geometric optics

Modifying this cut-off spatial frequency for an optics system used for incoherent imaging, the cut-off spatial frequency for forming a real image at the field stop described at equation 3.5.

$$f_{3co(i)} = 2f_{3co(f)} = \frac{dia_2}{\lambda z_2} \qquad (3.5)$$

The spatial rate of sampling, termed the spatial sampling frequency, must record this cut-off spatial frequency, so obeying the Nyquist criteria for spatial sampling so the complete extent of phase variations in the fields of electromagnetic radiation are accurately recorded, the spatial sampling frequency as a minimum must be twice the cut-off spatial frequency as described in equation 3.6.

$$f_{3s} = 2f_{2co(i)} = \frac{2dia_2}{\lambda z_2} \qquad (3.6)$$

The spatial sampling interval in the transverse plane of the field stop is the inverse of this spatial sampling frequency and is described in equation 3.7.

$$ds_3 = \frac{1}{f_{3s}} = \frac{\lambda z_2}{2 dia_2} \tag{3.7}$$

Revisiting the relationship between the spatial sampling intervals ds_1 and ds_3 at equation 3.3, the spatial sampling interval in the transverse plane of the remote scene can be described in equation 3.8.

$$ds_1 = ds_3 \left(\frac{z_1}{z_2} \right) \;\; \Rightarrow \;\; ds_1 = \left(\frac{\lambda z_2}{2 dia_2} \right) \left(\frac{z_1}{z_2} \right) \;\; \Rightarrow \;\; ds_1 = \frac{\lambda z_1}{2 dia_2} \tag{3.8}$$

An aperture located in the remote scene can be notionally formed around the extent of the remote scene observed through the sensor optics system, for the purpose of evaluating the number of samples required to discretely represent the remote scene, and described to have a diameter, $dia_1 = Nds_1$. The cut-off spatial frequency at the forward lens $f_{2co(f)}$ for the notional aperture in the remote scene is described in equation 3.9, for a diffraction-limited system based on coherent imaging. The number of samples N, represents the total number of samples across the extent of the remote scene.

$$f_{2co(f)} = \left(\frac{dia_1}{2} \right) \left(\frac{1}{\lambda z_1} \right) \;\; \Rightarrow \;\; f_{2co(f)} = \left(\frac{Nds_1}{2} \right) \left(\frac{1}{\lambda z_1} \right) \tag{3.9}$$

This expression represents the field amplitude cut-off spatial frequency at the forward lens. For sampling the fields of electromagnetic radiation at the forward lens, this cut-off spatial frequency can be retained because there is no real image formed at the forward lens. Obeying the Nyquist sampling criteria, the spatial sampling frequency as a minimum is set to twice this cut-off spatial

frequency, as described in equation 3.10.

$$f_{2s} = 2f_{2co(f)} = \frac{Nds_1}{\lambda z_1} \tag{3.10}$$

The sampling spatial interval at the forward lens is the inverse of this spatial sampling frequency, as described in equation 3.11.

$$ds_2 = \frac{1}{f_{2s}} = \frac{\lambda z_1}{Nds_1} \tag{3.11}$$

Noting the spatial sampling interval at the remote scene ds_1 from equation 3.3 and the number of spatial samples across the spatial extent of the remote scene N, the size of the remote scene can be described as Nds_1, and used to evaluate the spatial sampling interval at the forward lens ds_2. The expression used to evaluate ds_2 appears at equation 3.12.

$$ds_2 = \frac{\lambda z_1}{Nds_1} \;\Rightarrow\; ds_2 = \left(\frac{\lambda z_1}{N}\right)\left(\frac{2dia_2}{\lambda z_1}\right) \;\Rightarrow\; ds_2 = \frac{2dia_2}{N} \tag{3.12}$$

The diameter of the forward lens reveals the total number of spatial samples M across the diameter of the forward lens required to sample the incident fields of electromagnetic radiation described at equation 3.13 represents half the number of spatial samples required to discretely sample the remote scene.

$$M = \frac{dia_2}{ds_2} = \frac{N}{2} \tag{3.13}$$

With the real image of the remote scene formed in the field stop, the ray propagation principles of geometric optics were used to establish the spatial sampling intervals for the aft lens transverse plane. Propagating rays of electromagnetic radiation incident on the field stop converge at the field stop, then diverge past the field stop to propagate toward the aft lens as shown in Figure 3.3. The geometry of this propagation for the respective spatial sampling intervals at the forward lens

aperture ds_2 and aft lens aperture ds_4 is expressed in equation 3.14.

$$\frac{ds_2}{z_2} = \frac{ds_4}{z_3} \qquad (3.14)$$
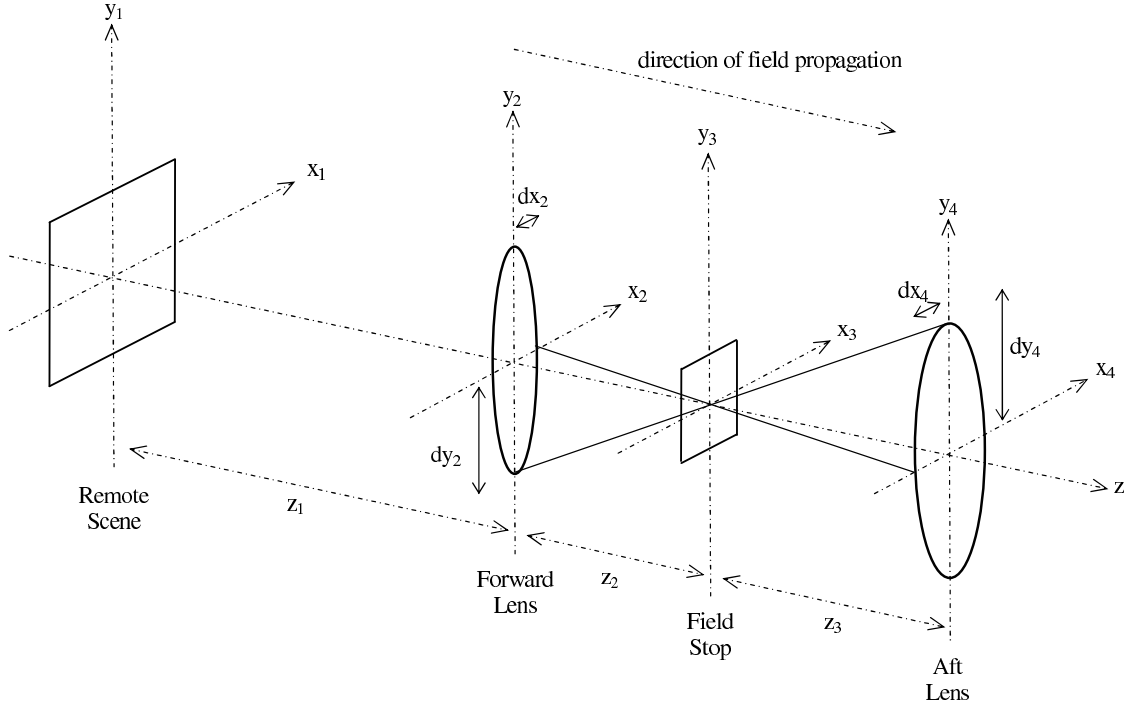
Figure 3.3:   Interpretation of spatial sampling intervals for the field stop with geometric optics

Using the forward lens expression from equation 3.12 and sampling the spectral wavefront fields of electromagnetic radiation at the aft lens for the same reasons described previously for the forward lens, the spatial sampling interval in the transverse plane of the aft lens ds_4 was evaluated using equation 3.15.

$$ds_4 = ds_2 \left(\frac{z_3}{z_2}\right) \quad \Rightarrow \quad ds_4 = \left(\frac{2\mathrm{dia}_2}{N}\right)\left(\frac{z_3}{z_2}\right) \qquad (3.15)$$

The spatial sampling intervals have a dependence on the spectral wavelength of every spectral field of electromagnetic radiation being discretely sampled. To sample these fields sufficiently for all spectral wavelengths the spatial sampling interval required for the minimum spectral wavelength

of electromagnetic radiation is used in the software model for all spectral wavelengths, ensuring all spectral wavefront fields are sufficiently sampled.

3.3 System coordinates and sign conventions

A system defining the orientations of position in an arbitrary transverse vertical plane, and angles of trajectory with respect to the optic axis lying in an axial horizontal plane, was required for developing the software model. The reference system used throughout the software model and shown at Figure 3.4 defines the positions and angles of propagation for the simulate electromagnetic field, by orientation and sign convention.
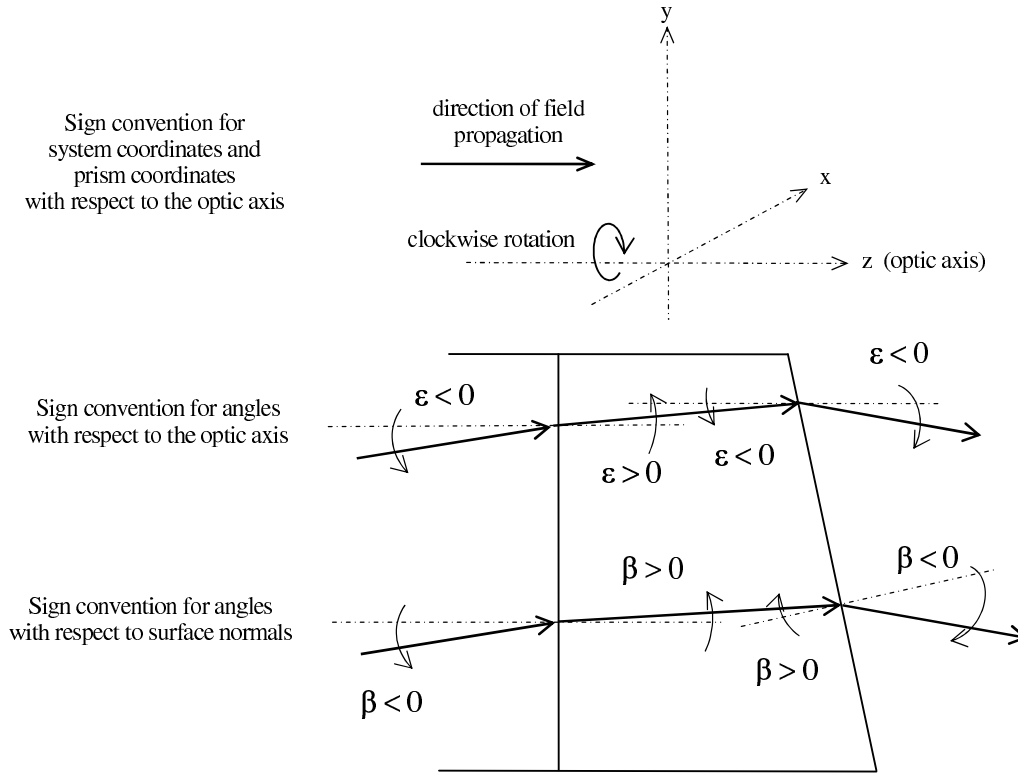
Figure 3.4: Sensor optics system sign conventions and coordinate system defined for the designing the software model

The system coordinates chosen for the software model align the x-axis horizontal, the y-axis vertical, so both axes lie in a transverse plane to the horizontal optic axis oriented as the z-axis.

37

The sign convention for locations of position follows the right-hand rule used in electromagnetic theory, where the direction of propagation is defined as the positive direction along the z-axis.

The sign convention for angles of propagation follows typical geometric optics sign convention. A plane of propagation oriented vertically (in yz-plane), where the angular direction of dispersion varies vertically according to the relationships between angles of incidence and angles of refraction, was used to establish the sign convention use in the software model. Positive angles represent angles subtended to the propagation ray of electromagnetic radiation from the optic axis in the upward direction, and negative angles represent angles subtended to the propagation ray from the optic axis in the downward direction.

3.4   Software Model Development

Development of the sensor optics system software model closely followed the subsystems identified previously in section 3.1. The mathematics and graphics laboratory tool MatLab® was chosen as the facilitating software to perform the instructions scripted for simulating the system. Figure 3.5 describes the simplified block diagram of the software model and includes the forward optics system, prism optics system, and detector optics system as subsystems of the entire system.

The significance of defining the point spread functions for the sensor optics system to aid with characterising the system and aid with reconstruction of the remote scene as a hyperspectral real image set were discussed at section 2.1. The software model simulates the point spread functions for the system. The source of electromagnetic radiation used for the software model simulates fields of electromagnetic radiation across the range of spectral wavelengths from 2 μm to 5 μm emitted from the remote scene as spherical wavefronts of electromagnetic radiation from a non-discernible point source.
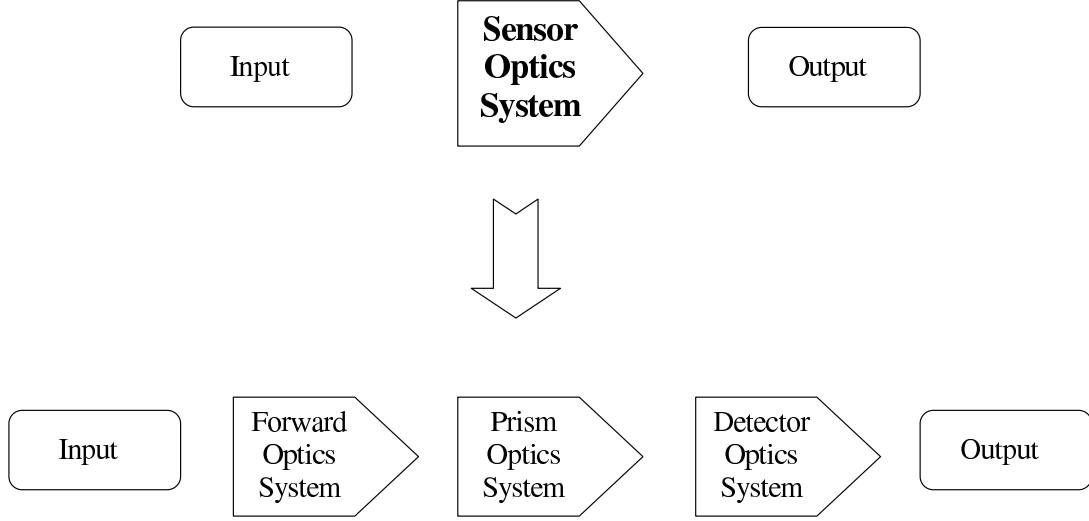
Figure 3.5:   CTIS Sensor Optics System description for software model

3.5 Forward Optics System

The design of the forward optics system as a software model is represented as a simple block diagram at Figure 3.6.

The point source was simulated as a non-discernible source emitting spherical wavefronts of electromagnetic radiation in the discrete spectral wavelength region between 2 μm and 5 μm. Propagation of this radiation as spherical electromagnetic wavefronts is simulated using the Rayleigh-Sommerfield diffraction formula through the various stages of propagation in the forward optics system. The discrete version of the Rayleigh-Sommerfield diffraction formula used to compute discrete samples of the electromagnetic field for each spectral wavelength at the destination aperture of propagation, is represented at equation 3.16 where N_x and N_y represent the number of discrete samples dx_0 and dy_0 across the forward lens aperture of the electromagnetic field wavefront in directions along the x-axis and y-axis respectively. N_x and N_y were chosen to be odd integers for
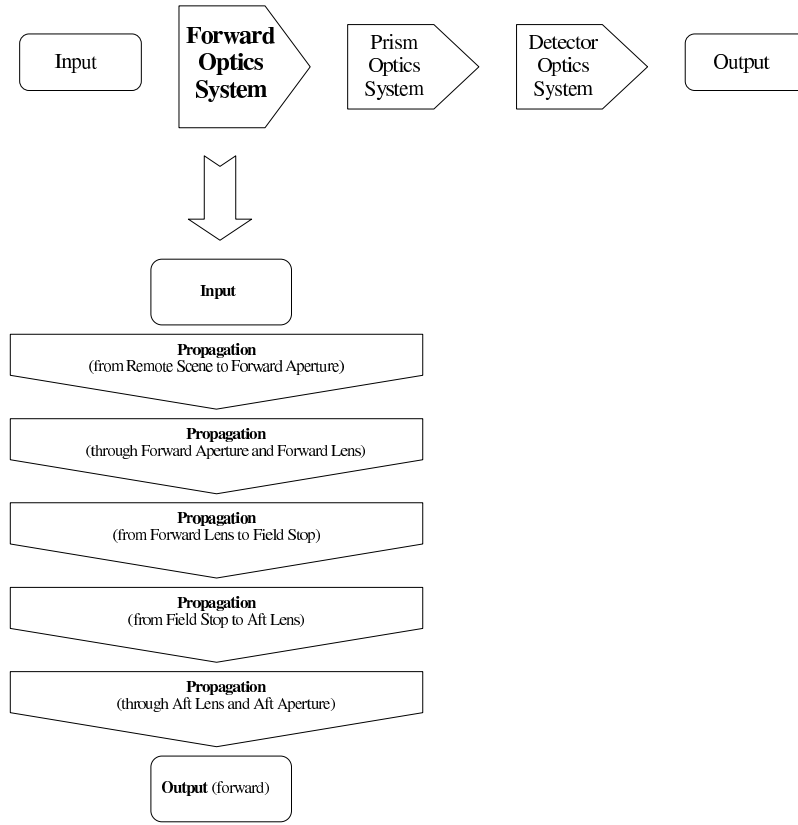
Figure 3.6:   Forward Optics System description for software model

symmetry around the optic axis.

$$U_1(x_1, y_1, \lambda) = \frac{1}{j\lambda} \sum_{n_x=-\frac{1}{2}(N_x-1)}^{\frac{1}{2}(N_x-1)} \sum_{n_y=-\frac{1}{2}(N_y-1)}^{\frac{1}{2}(N_y-1)} \frac{U_0(n_x dx_0, n_y dy_0, \lambda)}{r} \; e^{j \; \frac{2\pi}{\lambda} \; r} \; \cos\theta \; n_x dx_0 \; n_y dy_0 \quad (3.16)$$

The distance of propagation r, to the destination transverse plane from the emitting transverse plane is described at equation 3.17.

$$r \; = \; r(x_0, y_0, x_1, y_1) \; = \; r(n_x x_0, n_y y_0, x_1, y_1) \; = \; \sqrt{(x_1 - x_0)^2 + (y_1 - y_0)^2 + z^2} \qquad (3.17)$$

Simulating the electromagnetic fields discretely with the Rayleigh-Sommerfield diffraction formula in this way provides a wave optics treatment of the propagation of electromagnetic radiation

40

through the forward optics system. Once the sampling requirements are established for each transverse plane, and the image distance for the spectral wavelengths evaluated for locating the field stop along the optic axis, the wave optics propagation of the electromagnetic radiation was simulated for the stages of propagation: (1) between the point source and the forward lens transverse planes; (2) between the forward lens and the field stop transverse planes; and (3) between the field stop and the aft lens transverse planes, using the Rayleigh-Sommerfield diffraction formula.

Simulating the wave optics propagation through the forward and aft lenses respectively involved computing additional phase to each sample of the electromagnetic field. Using the lens thickness formula for each lens, the optical path length for each sample of the electromagnetic field was evaluate and used to compute the additional phase. The lens thickness formula, including the paraxial approximation used for representing a spherical lens surface as a parabolic surface, is described at equation 3.18.

$$\triangle_1(x_0, y_0) \;=\; \triangle_0 - \left(x_0{}^2 + y_0{}^2\right)\left(\frac{1}{2R_1} - \frac{1}{2R_2}\right) \tag{3.18}$$

Using this lens thickness expression, the additional phase for all spatial samples across every spectral wavefront field of electromagnetic radiation incident on the lens $U_0(x_0, y_0, \lambda)$ after propagation through the lens $U_1(x_0, y_0, \lambda)$ was evaluated using equation 3.19.

$$U_1(x_0, y_0, \lambda) \;=\; U_0(x_0, y_0, \lambda)e^{\,j\,\frac{2\pi}{\lambda}\,\triangle_1(x_0, y_0)\,(n_{lens}-1)} \tag{3.19}$$

3.6   Prism Optics System

The general overview for designing the prism optics system as a software model is represented by the simple block diagram at Figure 3.7.

The fields of electromagnetic radiation entering the prism optics system are simulated as a combined collimated wavefront of electromagnetic radiation. The wavefront passes through each

41
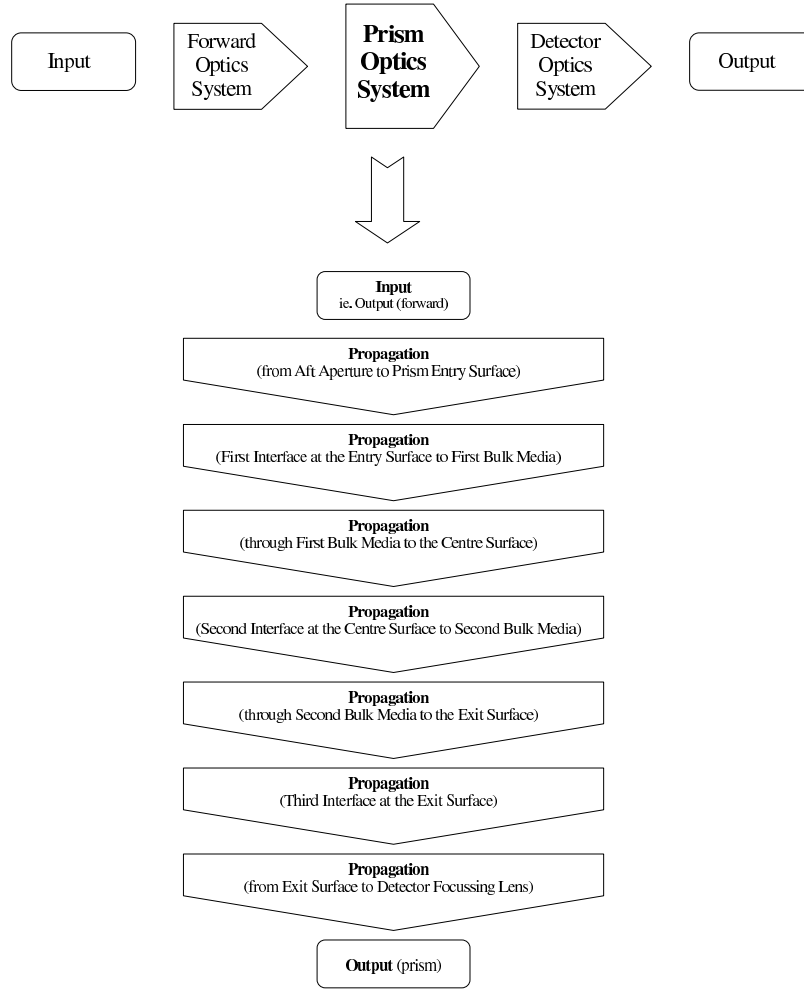
Figure 3.7:   Prism Optics System description for software model

stage of prism bulk media, experiencing the effects of refraction in the course of propagating through the prism optics system. The direction of propagation for each spectral field of electromagnetic radiation is altered at each interface between different prism bulk media according to Snell's Law of Refraction described at equation 2.5. Altering the direction of propagation for the collimated wavefront is simulated by varying the angle of propagation with respect to the optic axis along the direction of dispersion. Each spectral field of electromagnetic radiation in the collimated wavefront experiences a different change in direction of propagation at each interface between prism bulk media.

The prism optics system in the software model consists of five separate bulk media propagation elements, meaning there are four separate interfaces in the software model. The air separation between the aft lens and direct vision prism, also the detector focussing lens and direct vision prism, are also treated as propagation bulk media in the simulated prism optics system. The optical path lengths for each sample across each spectral field of electromagnetic radiation are computed so the properties of wave optics are represented in the simulated spectral fields computed in the software model for the prism optics system.

Dispersion of the wavelengths (spreading in location of separate wavelengths) contained in the broadband electric field is achieved from two effects resulting from the propagation through the prism. The refraction that occurs at the surface interface between two different propagation media, resulting from the contrast in index of refraction between the two propagation media, is one effect. The variation of index of refraction for the propagation media with respect to wavelength, for the broadband electric field is the other effect.

The angles measured with respect to the surface normal for each surface interface between separate propagation bulk media in the prism are designated β. Figure 3.8 and Figure 3.9 show the arrangement of these angles, with the electromagnetic field propagation represented by the ray. The set of equations at equation 3.20 describe these angles.
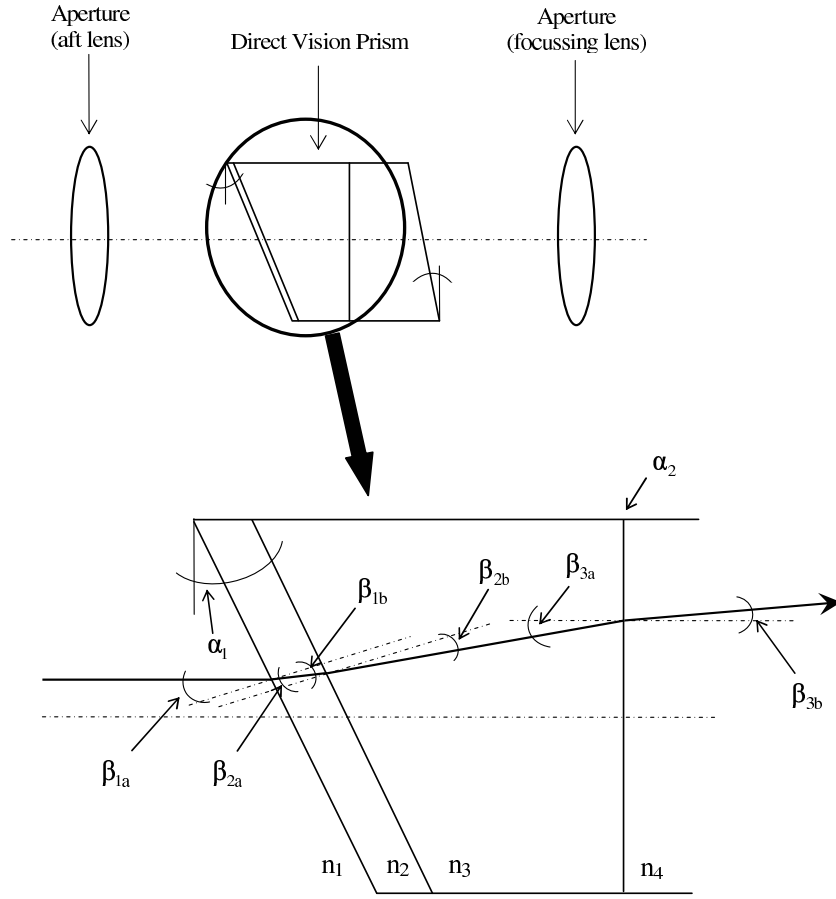
Figure 3.8:   Angles of refraction through the forward section of the direct vision prism

$$\beta_{1a} = \alpha_1$$

$$\beta_{1b} = -\arcsin\left(\frac{n_1}{n_2}\right)\sin\beta_{1a}$$

$$\beta_{2a} = -\beta_{1b}$$

$$\beta_{2b} = -\arcsin\left(\frac{n_2}{n_3}\right)\sin\beta_{2a}$$

$$\beta_{3a} = -(\alpha_1 + \beta_{2b})$$

$$\beta_{3b} = -\arcsin\left(\frac{n_3}{n_4}\right)\sin\beta_{3a}$$

$$\beta_{4a} = \alpha_3 - \beta_{3b}$$

$$\beta_{4b} = -\arcsin\left(\frac{n_4}{n_5}\right)\sin\beta_{4a}$$

(3.20)
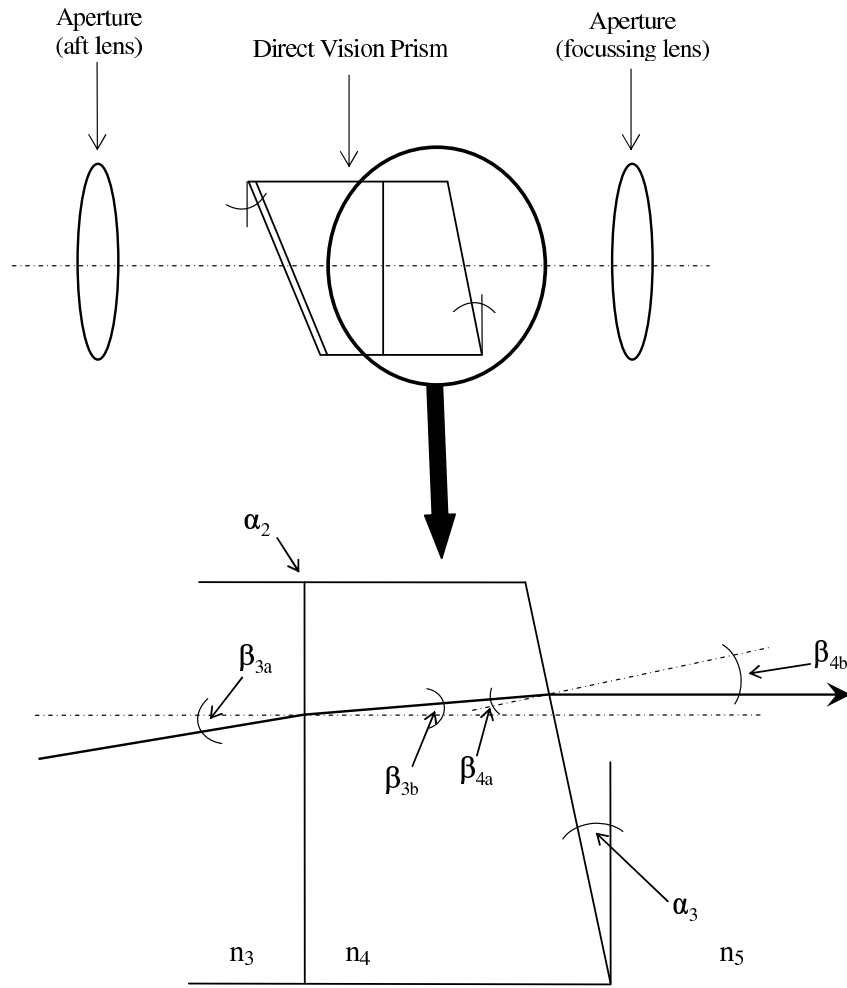
Figure 3.9:   Angles of refraction through the aft section of the direct vision prism

The angles measured with respect to the optics axis are designated as ϵ. The set of equations at equation 3.21 describe these angles.

$$\epsilon_{1a} = 0$$

$$\epsilon_{1b} = \alpha_1 + \beta_{1b}$$

$$\epsilon_{2a} = -\epsilon_{1b}$$

$$\epsilon_{2b} = \alpha_1 + \beta_{2b}$$

$$\epsilon_{3a} = -\epsilon_{2b}$$

$$\epsilon_{3b} = \beta_{3b}$$

$$\epsilon_{4a} = -\epsilon_{3b}$$

$$\epsilon_{4b} = \alpha_3 + \beta_{4b}$$

$$(3.21)$$

The speed of propagation through bulk media, v, for an electromagnetic field is related to the index of refraction for the media, n, and the speed of propagation in free space, c, expressed in equation 3.22. Knowing the distance of propagation, d, and the speed of propagation, the duration of propagation, t, or time of flight for the electromagnetic radiation can be determined.

$$v = \frac{c}{n} = \frac{d}{t} \Rightarrow t = \frac{nd}{c} \tag{3.22}$$

The time of flight for each sample of electromagnetic field across the collimated wavefront is used to evaluate the optical path lengths for each sample propagating through the prism optics system. The time of flight for the entire prism optics system can be represented by taking the sum of all times of flight through the separate bulk media propagation elements for each sample of the collimated wavefront, as described in equation 3.23.

$$t_0 = t_1 + t_2 + t_3 + t_4 + t_5 \tag{3.23}$$

Substituting the time of flight expression from equation 3.22, the time of flight for samples across each spectral field of electromagnetic radiation can be alternately expressed by equation 3.24.

$$t_0 = \frac{n_1 d_1}{c} + \frac{n_2 d_2}{c} + \frac{n_3 d_3}{c} + \frac{n_4 d_4}{c} + \frac{n_5 d_5}{c} \tag{3.24}$$

The optical path length (OPL) for each sample across the spectral field propagating through the separate bulk media propagation elements is related by the product between speed of light in free space and the time of flight to propagate the length of media in free space, as described in equation 3.25,

$$ct_0 = n_1 d_1 + n_2 d_2 + n_3 d_3 + n_4 d_4 + n_5 d_5 \tag{3.25}$$

where the expression, $n_1 d_1$, used separately for each spectral field, represents the OPLs of each sample of the field for the first bulk media propagation element in the prism optics system.

The distances of propagation for each spectral wavelength field of electromagnetic radiation simulated through the prism optics system were evaluated according to the system coordinates and sign conventions stated in section 3.3. The distances of propagation for each stage of propagation through the prism optics system is described from section 3.6.1 to section 3.6.5. Figure 3.10 shows the propagation for the first, second and third bulk media stages of propagation, and Figure 3.11 shows the propagation for the fourth and fifth stages of propagation through the prism optics system.

3.6.1 First bulk media propagation. Propagation from the aft aperture of the forward optics system to the first surface interface of the prism. Treat the propagation of the wavefront for each wavelength as a collimated beam propagating along the optic axis of the system.
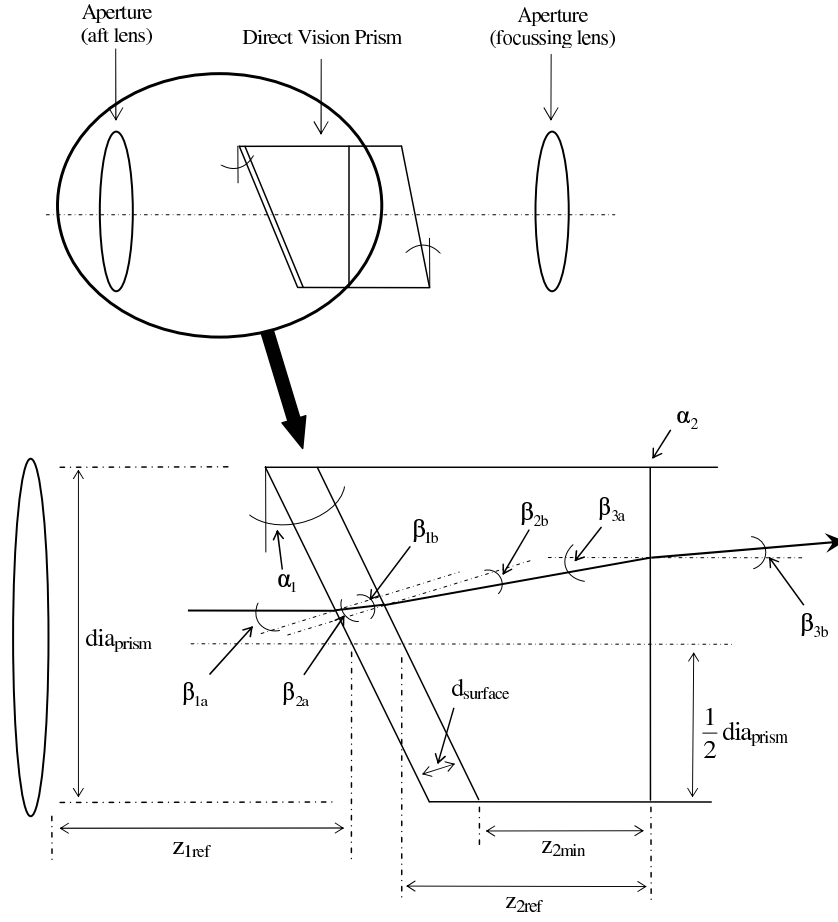
Figure 3.10:   Paths of propagation through the forward section of the prism optics system

$$z_{1(\text{offset})} = y_{1(\text{total})} \ \tan \alpha_1$$

$$z_{1(\text{total})} = z_{1(\text{ref})} - z_{1(\text{offset})}$$

$$r_1 = z_{1(\text{total})}$$

$$(3.26)$$

The OPLs for this propagation element of the prism optics system are described by the expression, $n_1 r_1$.

48

3.6.2 Second bulk media propagation. Propagation through the first media of the prism, which is a thin uniform coating of sapphire of thickness $d_{surface}$ on the surface of the bevelled forward face of the prism. Treat the propagation of the wavefront for each wavelength as a collimated beam propagating at an angle to the optic axis of the system.

$$r_2 = \frac{d_{surface}}{\cos \beta_{1b}}$$

$$y_{2(total)} = r_2 \ \sin(\alpha_1 + \beta_{1b}) + y_{1(total)}$$

(3.27)

The OPLs for this propagation element of the prism optics system are described by the expression, $n_2 r_2$.

3.6.3 Third bulk media propagation. Propagation through the second media of the prism, which is the first actual bulk media stage of the prism. The forward surface for this stage of propagation is set at an angle α_1 with respect to the optic axis of the system, therefore giving the appearance of a bevelled prism face. Treat the propagation of the wavefront for each wavelength as a collimated beam propagating at an angle to the optic axis of the system.

The equation list described at equation 3.28 reveals the detail of computation used to obtain the length of propagation r_3 and the cumulative vertical displacement of the simulated electromagnetic radiation wavefront $y_{3(total)}$ after completing this stage of propagation.

$$z_{2(\text{ref})} = \tfrac{1}{2} \, \text{dia}_{\text{prism}} \, \tan \alpha_1 \; + \; z_{2(\text{min})}$$

$$z_{2(\text{offset})} = y_{2(\text{total})} \, \tan \alpha_1$$

$$z_{2(\text{total})} = z_{2(\text{ref})} + z_{2(\text{offset})}$$

$$r_3 = \frac{z_{2(\text{total})}}{\cos(\alpha_1 + \beta_{2b})}$$

$$y_{3(\text{total})} = r_3 \, \sin(\alpha_1 + \beta_{2b}) + y_{2(\text{total})}$$

$$(3.28)$$

The OPLs for this propagation element of the prism optics system are described by the expression, $n_3 r_3$.

3.6.4 Fourth bulk media propagation.   Propagation through the third media of the prism, which is the second actual bulk media stage of the prism. The aft surface for this stage of propagation is set at an angle α_3 with respect to the optic axis of the system, also giving the appearance of a bevelled prism face. Treat the propagation of the wavefront for each wavelength as a collimated beam propagating at an angle to the optic axis of the system.

$$r_4 = \frac{z_3}{\cos(\alpha_3 + \beta_{3b})} = \frac{z_{3(\text{ref})} + z_{3(\text{offset})}}{\cos(\alpha_3 + \beta_{3b})} \qquad (3.29)$$

An expression for computing $z_{3(\text{offset})}$ directly could not be determined, so an alternate approach using the geometry of the direct vision prism was developed to compute the length of propagation r_4. The equation list described at equation 3.30 reveals the detail of computation required to obtain r_4 and the cumulative vertical displacement of the simulated electromagnetic radiation wavefront $y_{4(\text{total})}$ after completing this stage of propagation.

Figure 3.11:   Paths of propagation through the aft section of the prism optics system

$$z_{3(ref)} = \tfrac{1}{2} \, dia_{prism} \, \tan \alpha_3 \; + \; z_{3(min)}$$

$$r_{4(ref)} = \frac{\cos \beta_{3b}}{z_{3(ref)}}$$

$$y_{4(ref)} = r_{4(ref)} \, \sin \beta_{3b} + y_{3(total)}$$

$$r_{4(offset)} = \frac{y_{4(ref)} \, \sin \alpha_3}{\sin\left(\frac{\pi}{2} - \alpha_3 + \beta_{3b}\right)}$$

$$r_4 = r_{4(ref)} - r_{4(offset)}$$

$$y_{4(total)} = r_4 \, \sin \beta_{3b} + y_{3(total)}$$

$$(3.30)$$

The OPLs for this propagation element of the prism optics system are described by the expression, $n_4 r_4$.

3.6.5 *Fifth bulk media propagation.* Propagation from the aft surface of the prism to the focussing lens of the Infrared detector. Treat the propagation of the wavefront for each wavelength as a collimated beam propagating at an angle to the optic axis of the system.

The equation list described at equation 3.31 reveals the detail of computation used to obtain the length of propagation r_5 and the cumulative vertical displacement of the simulated electromagnetic radiation wavefront $y_{5(total)}$ after completing this stage of propagation.

$$z_{5(\text{offset})} = y_{4(\text{total})} \, \tan \alpha_3$$

$$z_{5(\text{total})} = z_{5(\text{ref})} + z_{5(\text{offset})}$$

$$r_5 = \frac{z_{5(\text{total})}}{\cos(\alpha_3 + \beta_{4\text{b}})}$$

$$y_{5(\text{total})} = r_5 \, \sin(\alpha_3 + \beta_{4\text{b}}) + y_{3(\text{total})}$$

$$(3.31)$$

The OPLs for this propagation element of the prism optics system are described by the expression, $n_5 r_5$.

Need to evaluate the phase across the transverse plane to the optic axis, and modify the exit angle of the propagation so that this phase is constant across the wavefront lying in the transverse plane. To modify the exit angle of the propagation, the angles between optic axis and the respective entry and exit faces of the prism along the direction of dispersion can be modified to tune the propagation through the prism for the centre wavelength.

The physical appearance of wedge shaped prism optical components was used for the design of the software model to represent the construct of the direct vision prism bulk media. To simulate the electromagnetic field that propagates through each different bulk media, the software model utilises the design expectations that the wedge shaped bulk media has a certain diameter, and is located in the sensor optics system so that the centre axis of the bulk media is located with the optics axis. The wedge shaped optical components are specified typically by the angle that the face of the wedge subtends with the transverse plane to the centre axis, and the minimum length dimension of bulk media parallel to the optic axis, described as $z_{\min}$ in the software model. The parameters are physical constraints of geometry with the bulk media that must be considered when evaluating the propagation of the electromagnetic radiation. These parameters are used in the software model to evaluate the actual path lengths of propagation for all samples of each spectral field. The actual

lengths of propagation are used to compute the optical path length for the respective samples of each spectral field.

3.6.6   Prism rotation.   Rotating the direct vision prism should result in circular translation of the spectral real image of the remote scene, based on the spectral wavelength electromagnetic radiation specific to the spectral real image.

Sampling of the spectral field wavefronts of electromagnetic radiation from the aft lens is used as the input spectral field wavefronts for the prism optics system. As the angular position of the direct vision prism changes due to rotation, these wavefronts incident on the prism entry surface aperture remain unchanged. The characteristics of these wavefronts are modified by the different orientations of the prism entry surface aperture due to Snell's Law of Refraction, for each angular position of rotation. Material properties of the index of refraction and transmission for bulk media used in the direct vision prism, the incident angles of the spectral field wavefronts with each respective prism bulk media interface are treated in the wave optics software model to model the rotation of the direct vision prism.

This is done by using a separate coordinate system, referred to as prism coordinates, for the propagation of the spectral field wavefronts of electromagnetic radiation. With the direct vision prism oriented in the upright angular position, the prism coordinates align with the system coordinates.

3.7   Detector Optics System

The design of the detector optics system as a software model is represented as a simple block diagram at Figure 3.12.

The detector optics system includes a focussing lens and a focal plane array. The simulated field of electromagnetic radiation developed by the software model only represents the field incident on the transverse plane where the focal plane array is situated. The focal plane array used for the
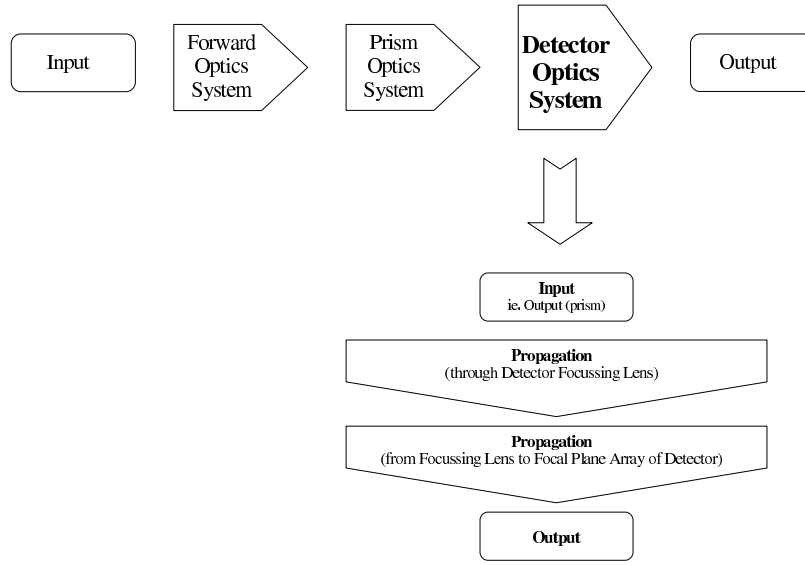
Figure 3.12:   Detector Optics System description for software model

physical system must have responsivity properties suited to detecting photons at infrared spectral wavelengths of electromagnetic radiation.

The software model is designed to simulate the point spread function for each spectral wavelength band. Thus modelling the detector optics system must include a process for locating where the point spread functions must be in the focal plane array transverse plane. Without an implementation in the software model that performs this task, assembling all spectral wavelength point spread functions as a chromotomographic real image would be very difficult to achieve.

The task of locating the point spread function is further challenged by the sampling phenomenon identified from the Whittaker-Shannon sampling theorem for representing continuous aperiodic signals as discrete signals [16: 22-26]. Representing the continuous fields of the point spread functions as discretely sampled simulated fields, the software model duplicates the point spread functions of the discrete fields in the transverse plane of the focal plane array.

The software model of the detector optics system is required to locate the discrete point spread function for each spectral wavelength that represents the continuous field point spread

function from these duplicate discrete point spread functions. Using the principles of Fourier optics that relate the fields in the transverse planes of the detector focussing lens and focal plane array respectively, the centre of the point spread function for each spectral wavelength can be determined which closely match the realistic physical locations expected from analysing the continuous fields of the point spread functions.

3.7.1 Real image locations. The time delay Fourier Transform relationship is analogous to the relationship between these transverse planes using Fourier optics. The time delay Fourier Transform identity is stated in equation 3.32,

$$g(t - \alpha) \Rightarrow e^{-j\omega\alpha}G(\omega) \tag{3.32}$$

where $G(\omega) = F\{g(t)\} = \int_{-\infty}^{+\infty} g(t)e^{-j\omega t}dt$, is the expression for the Fourier Transform used in the equation. This equation states that a delay in time, α, of the signal, g(t), relates to a constant gradient of phase change over the frequency content of the signal.

Using Fourier optics to describe the relationship of the electromagnetic fields between both transverse planes, the time delay Fourier Transform relationship is modified to describe the relationship between these fields, as described at equation 3.33.

$$g(x - \alpha_u, y - \alpha_v) \Rightarrow e^{-j(\omega_u\alpha_u + \omega_v\alpha_v)}G(\omega_u, \omega_v) = e^{-j\frac{2\pi}{\lambda z}(u\alpha_u + v\alpha_v)}G(\omega_u, \omega_v) \tag{3.33}$$

For the detector optics system, this expression indicates that a constant gradient of phase introduced to the field that characterising the spatial frequency content for the remote scene (right side of equation 3.33), is related to the position offset location from the central location (left side of equation 3.33) for the image of the remote scene. The expression $g(x - \alpha_u, y - \alpha_v)$ represents the field present in the transverse plane for the the detector focal plane array. The expression

56

$e^{-j(\omega_u \alpha_u + \omega_v \alpha_v)} G(\omega_u, \omega_v)$ represents the field present in the transverse plane at the detector focussing lens, prior to propagating through the lens.

The prism optics system has been described to introduce a phase tilt to the electromagnetic fields, based on the angular direction change in propagation from on-axis propagation along the optic axis. The prism optics system can be approximated as a collection of phase tilts on the collimated wavefront entering the prism optics system, where these phase tilts are established according to the angle of dispersion calculated using Snell's Law of refraction at equation 2.5. Relating each phase tilt to a position in the detector focal plane array where the real image of the remote scene is formed, serves the purpose for approximating the prism optics system.

3.7.2 Direct vision prism approximation. The angular change in direction of propagation for the electromagnetic field propagating through the direct vision prism due to dispersion of each spectral field, can be represented as a constant gradient of phase (phase tilt) across the collimated wavefront in the direction of dispersion.

Commencing with the electromagnetic field at the detector focussing lens U_5. This field can be represented as the Fourier Transform of the electromagnetic field at the detector focal plane array that forms an upright and minified real image of the remote scene. The field at the detector focussing lens, leaving the prism optics system, U_5 can be described by equation 3.34.

$$U_5(u, v) = G(u, v) = F\{g(x, y)\} \tag{3.34}$$

The two-dimensional Fourier Transform of an arbitrary image as a two-dimensional signal $g(x, y)$, representing the real image at the focal plane array for a specific wavelength of electromagnetic radiation, is described at equation 3.35,

$$F\{g(x, y)\} = \iint_{-\infty}^{+\infty} g(x, y) e^{-j(\omega_u x + \omega_v y)} dx dy \tag{3.35}$$

where the angular spatial frequency expressions ω_u and ω_v represent the spectrum of electromagnetic radiation in terms of spatial frequencies, f_u and f_v, as, $\omega_u = 2\pi f_u$ and $\omega_v = 2\pi f_v$. The two-dimensional Fourier Transform expression, described at equation 3.36 with the use of these expressions becomes,

$$F\{g(x,y)\} = \iint_{-\infty}^{+\infty} g(x,y)e^{-j2\pi(f_u x + f_v y)}dxdy \tag{3.36}$$

and the expressions for these spatial frequencies respectively are, $f_u = \frac{u}{\lambda z}$ and $f_v = \frac{v}{\lambda z}$. Substituting for these expressions, the two-dimensional Fourier Transform expression described at equation 3.37 becomes,

$$F\{g(x,y)\} = \iint_{-\infty}^{+\infty} g(x,y)e^{-j\frac{2\pi}{\lambda z}(ux+vy)}dxdy \tag{3.37}$$

Examine the electromagnetic field of the same real image, now offset a displacement $x = a$ and $y = b$ from the previous position in the focal plane array transverse plane. The two-dimensional Fourier Transform of this offset real image is described at equation 3.38.

$$G_{pt}(u,v) = F\{g(x-a,y-b)\} = \iint_{-\infty}^{+\infty} g(x-a,y-b)e^{-j\frac{2\pi}{\lambda z}(ux+vy)}dxdy \tag{3.38}$$

Grouping the system ordinates variables and the offset displacements as new variables, where $x - a = x_a$ and $y - b = y_b$, and the derivative with respect to the system ordinates variables as, $dx = dx_a$ and $dy = dy_b$, substituting the new variables for the system ordinate variables in the expression is described at equation 3.39.

$$F\{g(x-a,y-b)\} = F\{g(x_a,y_b)\} = \iint_{-\infty}^{+\infty} g(x_a,y_b)e^{-j\frac{2\pi}{\lambda z}\{u(x_a+a) + v(y_b+b)\}}dx_a dy_b \tag{3.39}$$

58

Rationalising terms from the integration expression leads to the two-dimensional Fourier Transform expression as described at equation 3.40.

$$F\{g(x-a, y-b)\} \;=\; e^{-j\frac{2\pi}{\lambda z}(au+bv)} \iint_{-\infty}^{+\infty} g(x_a, y_b) e^{-j\frac{2\pi}{\lambda z}(ux_a+vy_b)} dx_a dy_b \qquad (3.40)$$

Recognising the expression contained within the integral to be similar to the expression at equation 3.35, changing the notation of variables within this integral where $x = x_a$, $y = y_b$ and $dx = dx_a$, $dy = dy_b$, the two-dimensional Fourier Transform expression of the real image offset in position, as described at equation 3.41 becomes,

$$F\{g(x-a, y-b)\} \;=\; e^{-j\frac{2\pi}{\lambda z}(au+bv)} \iint_{-\infty}^{+\infty} g(x, y) e^{-j\frac{2\pi}{\lambda z}(ux+vy)} dx dy \qquad (3.41)$$

Expressing the Fourier Transform in terms of the original real image, as described by equation 3.42,

$$G_{pt}(u, v) \;=\; F\{g(x-a, y-b)\} \;=\; e^{-j\frac{2\pi}{\lambda z}(au+bv)} F\{g(x, y)\} \;=\; e^{-j\frac{2\pi}{\lambda z}(au+bv)} G(u, v) \qquad (3.42)$$

the Fourier Transform for the offset real image can be expressed in terms the Fourier Transform of the image at the original location with a constant phase gradient included, as described at equation 3.43, where the phase gradient is related to the displacement offset between the images.

$$U_6(x-a, y-b) \;=\; g(x-a, y-b) \;\implies\; e^{-j\frac{2\pi}{\lambda z}(au+bv)} U_5(u, v) \;=\; e^{-j(a\omega_u+b\omega_v)} U_5(u, v) \quad (3.43)$$

3.7.3 Phase tilts for prism rotation. The expressions derived earlier use the principles of Fourier Transforms to relate the two-dimension electromagnetic field between the focussing lens and the focal plane array in the detector optics system. The software model was designed to use composite phase tilts of the electromagnetic wavefront as the reference for predetermining the

location of the centre for each point spread function. The composite phase tilts exhibited by the simulated electromagnetic field wavefronts along the x-axis and y-axis directions with respect to the system coordinates are required for every angular position of rotation for the direct vision prism. Predetermining these locations with the software model allows the electromagnetic field wavefronts to be realistically simulated to form real images of the remote scene in the transverse plane of the detector focal plane array.

The angular direction of propagation with respect to the optic axis ϵ_{4b}, for each wavefront of electromagnetic field can be expressed in physical dimensions as described from equation 3.44 to equation 3.46.

$$\sin \epsilon_{4b} = \frac{a}{c} \tag{3.44}$$

$$\cos \epsilon_{4b} = \frac{b}{c} \tag{3.45}$$

$$\tan \epsilon_{4b} = \frac{a}{b} \tag{3.46}$$

Representing these angular directions or trajectory angles for each wavefront as composite trajectory angles ϵ_{4bX} and ϵ_{4bY} and relate to the phase tilt for each wavefront with respect to x-axis and y-axis of system coordinates.

As the prism rotates, the composite trajectory angles ϵ_{4bX} and ϵ_{4bY} are related to the dispersion trajectory angle ϵ_{4b} as described in equations 3.47 to equation 3.54 as follows.

$$\tan \theta = \frac{d_1}{b} \tag{3.47}$$

$$\tan(\frac{\pi}{2} - \theta) = \frac{d_2}{b} \tag{3.48}$$

Using the Sine rule.

$$\frac{\sin \theta}{d_1} = \frac{\sin \frac{\pi}{2}}{e_1} = \frac{1}{e_1} \tag{3.49}$$

$$\frac{\sin(\frac{\pi}{2} - \theta)}{d_2} = \frac{\sin \frac{\pi}{2}}{e_2} = \frac{1}{e_2} \tag{3.50}$$

Noting the composite angles ϵ_{4bX} and ϵ_{4bY} respectively.

$$\tan \epsilon_{4bX} = \frac{a}{e_2} = \frac{a \sin(\frac{\pi}{2} - \theta)}{d_2} = \frac{a \sin(\frac{\pi}{2} - \theta)}{b \tan(\frac{\pi}{2} - \theta)} = \frac{a}{b} \cos(\frac{\pi}{2} - \theta) \tag{3.51}$$

$$\tan \epsilon_{4bY} = \frac{a}{e_1} = \frac{a \sin \theta}{d_1} = \frac{a \sin \theta}{b \tan \theta} = \frac{a}{b} \cos \theta \tag{3.52}$$

Observing the relationship, $\cos(\frac{\pi}{2} - \theta) = -\sin \theta$, and revisiting the expression for the dispersion trajectory angle, $\tan \epsilon_{4b} = \frac{a}{b}$, the composite trajectory angles ϵ_{4bX} and ϵ_{4bY} can be expressed as follows,

$$\epsilon_{4bX} = \arctan\{-\sin \theta \tan \epsilon_{4b}\} \tag{3.53}$$

$$\epsilon_{4bY} = \arctan\{\cos \theta \tan \epsilon_{4b}\} \tag{3.54}$$

Apply these expressions to specifically determine the location of the real image in the focal plane array transverse plane of the object according to the Dispersion for each wavelength of optical EM radiation.

The optical EM radiation is always examined across a transverse plane to the optic axis. Examining the dispersion of optical EM radiation resulting from propagation through the prism across a transverse plane leaves a constant change in phase (phase tilt) in the direction of dispersion, encoded across the entire wavefront of optical EM radiation.

Examining the phase tilt in terms of the composite trajectory angles, the phase tilt across the transverse plane along the x-axis direction in system coordinates is described at equation 3.55, and the phase tilt across the transverse plane along the y-axis direction in system coordinates is described at equation 3.56.

$$e^{j\frac{2\pi}{\lambda}r_x} = e^{j\frac{2\pi}{\lambda}u\sin\epsilon_{4bX}} \tag{3.55}$$

$$e^{j\frac{2\pi}{\lambda}r_y} = e^{j\frac{2\pi}{\lambda}v\sin\epsilon_{4bY}} \tag{3.56}$$

Using these expressions to represent the composite phase tilts evident on the electromagnetic field wavefront at the detector focussing lens, after propagating through the prism optics system, the expression for the fields at the focussing lens U_5 and the focal plane array U_6, are described from equation 3.57 to equation 3.64.

$$U_5(u,v) = e^{j\frac{2\pi}{\lambda}u\sin\epsilon_{4bX}}e^{j\frac{2\pi}{\lambda}v\sin\epsilon_{4bY}}F\{U_6(x,y)\} \tag{3.57}$$

$$U_5(u,v) = e^{-j\left(-\frac{2\pi}{\lambda}u\sin\epsilon_{4bX}\right)}e^{-j\left(-\frac{2\pi}{\lambda}v\sin\epsilon_{4bY}\right)}F\{U_6(x,y)\} \tag{3.58}$$

$$U_5(u,v) = e^{-j\left(-\frac{2\pi}{\lambda}u\sin\epsilon_{4bX}\right)}e^{-j\left(-\frac{2\pi}{\lambda}v\sin\epsilon_{4bY}\right)}\iint_{-\infty}^{+\infty}U_6(x,y)e^{-j(\omega_u x+\omega_v y)dxdy} \qquad (3.59)$$

$$U_5(u,v) = e^{-j\left(-\frac{2\pi}{\lambda}u\sin\epsilon_{4bX}\right)}e^{-j\left(-\frac{2\pi}{\lambda}v\sin\epsilon_{4bY}\right)}\iint_{-\infty}^{+\infty}U_6(x,y)e^{-j2\pi(f_u x+f_v y)}dxdy \qquad (3.60)$$

$$U_5(u,v) = e^{-j\left(-\frac{2\pi}{\lambda}u\sin\epsilon_{4bX}\right)}e^{-j\left(-\frac{2\pi}{\lambda}v\sin\epsilon_{4bY}\right)}\iint_{-\infty}^{+\infty}U_6(x,y)e^{-j2\pi\left(\frac{u}{\lambda z}x+\frac{v}{\lambda z}y\right)}dxdy \qquad (3.61)$$

$$U_5(u,v) = \iint_{-\infty}^{+\infty}U_6(x,y)e^{-j\frac{2\pi u}{\lambda z}(x-z\sin\epsilon_{4bX})}e^{-j\frac{2\pi v}{\lambda z}(y-z\sin\epsilon_{4bY})}dxdy \qquad (3.62)$$

Using new variables, $s = x - z\sin\epsilon_{4bX}$ and $t = y - z\sin\epsilon_{4bY}$, together with the respective derivatives, $ds = dx$ and $dt = dy$, the expression becomes,

$$U_5(u,v) = \iint_{-\infty}^{+\infty}U_6(s+z\sin\epsilon_{4bX},t+z\sin\epsilon_{4bY})e^{-j2\pi\left(\frac{u}{\lambda z}s+\frac{v}{\lambda z}t\right)}dsdt \qquad (3.63)$$

$$U_5(u,v) = F\{U_6(s+z\sin\epsilon_{4bX},t+z\sin\epsilon_{4bY})\} \qquad (3.64)$$

The expression at equation 3.64 offers the ability to locate the real image of the point spread functions in the focal plane array, due to the angle of propagation due to dispersion through the prism. This expression together with equation 3.53 and equation 3.54 provide a mathematical

outcome that was used for the software model to commence locating the centres of the real images

for the point spread functions.

IV. Analysis

This chapter describes the main considerations encountered with designing the software model to simulate the sensor optics system. Considerations with the area of each aperture, at section 4.1, the optical component parameters, at section 4.2, and numerically simulating wave optics propagation, at section 4.3 are discussed. Manipulation of the MatLab® functions and program scripts comprising the suite of software developed during this research is presented at section 4.5 to demonstrate the design of a software model that simulates a particular configuration of the sensor optics system.

4.1   Apertures

The spatial extent of the apertures throughout the sensor optics system should be validated before using these dimensions for each respective aperture in the construct of the simulated sensor optics system software model. An explanation of the sequence of apertures selected for validating the software model, each numbered to enable the reader to keep track of the dependencies between certain apertures, appears in the following paragraphs.

Based on the area of the direct vision prism entry aperture (1), the area of the aft lens aperture (2) was established for some spatial freedom to accommodate the spectral fields of electromagnetic radiation dispersing through the prism. Validating the area of the direct vision prism exit aperture (3) was based on the range of spectral wavelengths of electromagnetic radiation dispersed through the direct vision prism. Each spectral field in the software model represents the respective wavelength band of electromagnetic radiation collected by the physical sensor optics system. Validating the area of the detector focussing lens aperture (4) was based on the distance of separation along the optic axis between the direct vision prism exit surface and the detector focussing lens. The angular directions propagation for every spectral wavefront field of electromagnetic radiation must be collected within the spatial extent of the focussing lens aperture.

To simulate the sensor optics system these dependencies between system parameters required validation before a software model configuration could be used. Validation of the system parameters to be used in the software model was based on the collective influence of the respective areas of each aperture, the separation between the direct vision prism and detector focussing lens, the choice of undeviated spectral wavelength of electromagnetic radiation, the finite spectral range of electromagnetic radiation of interest for the design of the sensor optics system. Geometric optics was used in the software model to discern the spatial extent requirements for each aperture and validate the system parameters used for the simulated sensor optics system.

4.1.1 Forward Optics System. The spatial extent of the forward aperture and lens should be selected to allow the collection of sufficient electromagnetic radiation from the remote scene for hyperspectral imaging. The forward aperture collects (sampling) the radiant energy incident on the sensor optic system from the remote scene, represented as spectral electromagnetic field wavefronts in the software model, and the forward lens focusses focusses this radiant energy to form a real image of the remote scene in the field stop. Spatial sampling criteria is important for the software model to ensure continuous spectral fields are represented accurately as discrete spectral fields with the software model. Spatial sampling at the forward lens establishes the representation of the spectral fields of electromagnetic radiation used through the remaining simulated propagation of these fields.

The spatial extent of the aft aperture and lens is required to be smaller than the spatial extent of the direct vision prism entry aperture. The spatial extent of the aperture, and F# number characteristics of the aft lens are established in the software model so the radiant energy collected by the forward aperture also propagates through the aft aperture.

To reduce the wavefront error resulting from the propagation of the electromagnetic radiation through both lenses, the software model represents both lenses with the same F# number characteristics.

4.1.2 Prism Optics System. The spatial extent of the direct vision prism exit aperture must be sufficient to accommodate for dispersing all spectral wavefront fields of electromagnetic radiation from the remote scene to be used in the hyperspectral real image data set. The spatial offset in the transverse plane and angular direction of propagation, both with respect to the optic axis for each spectral wavefront differs according to Snell's Law of Refraction and the bulk media configurations used in the direct vision prism for each stage of propagation in the prism optics system. Each spectral wavelength no longer propagates symmetrically along the optic axis, instead each spectral wavelength has some distinct angular direction of propagation with respect to the optic axis. In the software model, the presence of electromagnetic radiation at the outermost locations with respect to the optic axis, in the transverse plane of the exit surface of the direct vision prism defines the minimum aperture area required for the direct vision prism.

The spatial extent of the detector focussing lens must be sufficient to collect the incident fields of electromagnetic radiation dispersed from propagation through the direct vision prism. The separation along the optic axis between the exit surface of the direct vision prism and the detector focussing lens influences the required spatial extent of the detector focussing lens. In the software model, the presence of electromagnetic radiation at the outermost locations with respect to the optic axis, in the transverse plane of the focussing lens defines the minimum aperture area required for the focussing lens.

4.1.3 Detector Optics System. The detector focussing lens used in the software model to focus the electromagnetic radiation collected through the focussing lens aperture on the detector focal plane array, is configured with the same F# number characteristics as the previous lenses in the forward optics system.

The parameters used in the software model to represent the optical components of the sensor optics system were selected to enable use of equations based on the theory of optics stemming from geometric optics, Fourier optics and the Rayleigh-Sommerfield diffraction formula. The system components represented in the software model were the forward lens, the aft lens, the direct vision prism, and the detector focussing lens. All intrinsic characteristics of the detector focal plane array such as material sensivities, non-uniformities, responsivity, are not represented in the software model. The spectral fields of electromagnetic radiation incident on the detector focal plane array are computed in the software model.

4.2.1   Lenses.   All lenses in the sensor optics system were represented with the Lens Maker's equation in the software model. These lenses are approximated as thin lenses with this equation also known as the Gauss thin lens formula, and using this formula implies the constraint with choice of F# numbers to characterise the lenses. The maximum thickness and the focal length of each lens are two parameters used in the Lens Maker's equation, where the maximum thickness was arbitrarily chosen for each lens, and the focal length defined so the same F# number was used. The choice of F# number used for all lenses in the software model obeying the criteria of F# number $\geq$ 10.

The software model simulates the point spread function of the sensor optics system for a point source located at some distance from the forward lens of the system emitting spectral wavefront fields as spherical wavefronts of electromagnetic radiation. Each incident spectral wavefront has a different phase curvature across the aperture of the forward lens, resulting with the real image of the point spread function for each spectral wavefront located at different locations along the optic axis. If these spectral wavefronts appeared planar (hence no phase curvature) across the aperture of the forward lens, the real image of the point spread functions of each spectral wavefront would be located at the focal point of the lens.
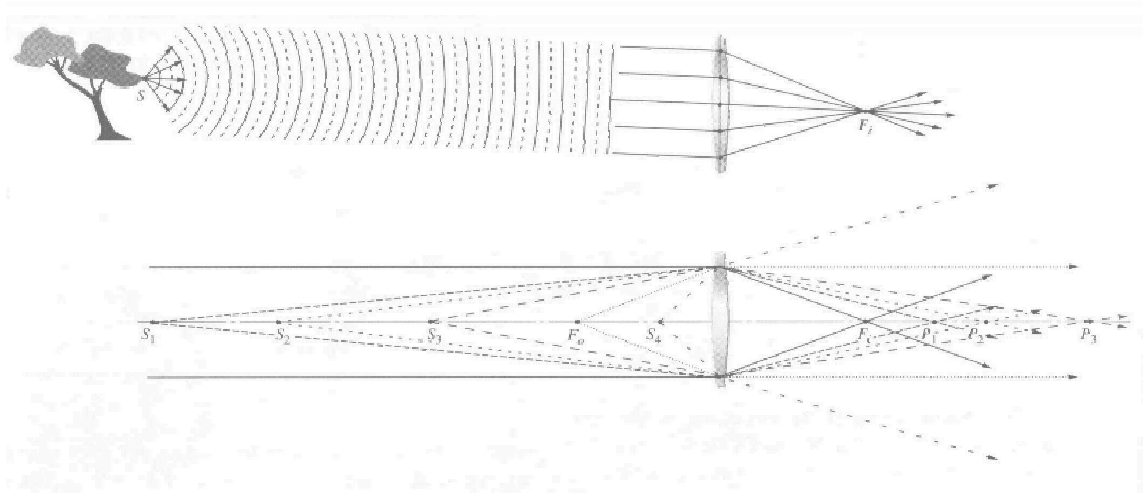
Figure 4.1: Spherical wavefront propagation through a lens [2: 164]. The point source location along the optic axis from the lens influences where on the optic axis the spherical wavefront converges to form a real image of the point source.

The forward lens aperture would be arbitrarily chosen to collect sufficient radiant electromagnetic energy and enable recording of spectral real image data from the remote scene. The aft lens aperture would be chosen to ensure this energy is permitted to propagate and disperse through the prism optics system. The distance between the remote scene and the forward aperture influences the angular extent of the emitted spherical wavefront incident on the forward aperture, and further influences the focal distance of the real image for the point source at the field stop. So the location of the remote scene cannot be within the focal length of the forward lens. Figure 4.1 illustrates the location of the point source at various distances from the forward aperture and lens that result in real images being formed. Observe from this figure the location of the remote scene cannot be within the focal length of the forward lens in order for a real image of the remote scene to be formed in the field stop.

Choosing the same F# number for all lenses offers an inherent attribute of minimising the wavefront error encountered on the spectral wavefront fields of electromagnetic radiation with propagating through lenses. Near complementary magnitude and phase errors due to propagation through the forward optics system are introduced to the spectral wavefront fields when the same F# number is used for the forward and aft lenses, thereby minimising wavefront error. Figure 4.2
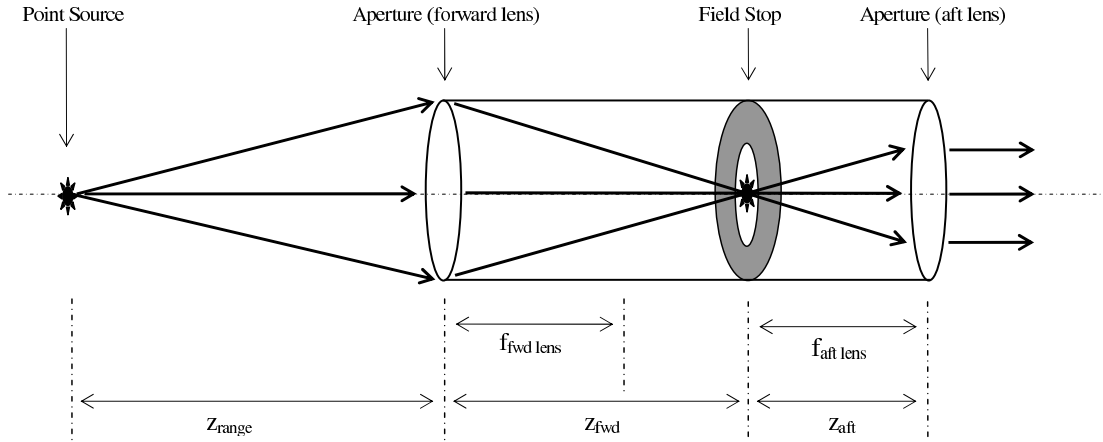
Figure 4.2:   Point source location along the optic axis of the sensor optics system. The location of the remote scene is defined by the location of the point source in the software model. The location of the forward lens with respect to the field stop is related to the location of the point source along the optic axis.

illustrates the arrangement of the forward and aft lenses used in the software model to obtain a real image of the point source in the field stop, and propagate the spectral wavefront fields to the aft lens.

4.2.2 Direct Vision Prism.   Optical materials chosen to represent the bulk media and thin coating stages of propagation through the direct vision prism were selected because they exhibited high transmissive properties over the medium wave infrared (MWIR) spectral range of electromagnetic radiation. The indexes of refraction for these materials at specific spectral wavelengths were obtained and linear interpolation between each specified spectral wavelength was used in the software model to develop index of refraction data for these materials in one nanometre increments. Indexes of refraction characteristics of these optical materials suited to the MWIR spectral range of electromagnetic radiation and available in the software model are detailed at Appendix B. Any birefringent properties with these materials were treated in the software model only for the fast axis indexes of refraction.

70

4.3   Wave Optics Propagation

The propagation of each spectral field wavefront of electromagnetic radiation through the lenses and direct vision prism was represented as changes in phase to each piecewise sample of these wavefronts in the software model. These optical components were treated with transmissive properties of 100% transmission for the MWIR spectrum of electromagnetic radiation.

All spectral fields of electromagnetic radiation from the multispectral point source were represented as spherical wavefronts with the Rayleigh-Sommerfield Diffraction theory. Equation 2.7 describe this theory required some manipulation to represent the discrete samples of the spectral fields of electromagnetic radiation through each stage of spherical wavefront propagation in the software model of the sensor optics system. The stages of spherical wavefront propagation evident in the software model were: (1) from the multispectral point source location to the forward lens as a spatial diverging wavefront; (2) from the forward lens to the field stop as a spatial converging wavefront; (3) from the field stop to the aft lens as a spatial diverging wavefront; and (4) from the focussing lens to the focal plane array within the detector as a spatial converging wavefront.

The numeric form of the Rayleigh-Sommerfield Diffraction formula used to represent the effects of diffraction across the wavefront each spectral field wavefront due to spherical wavefront propagation, developed further from equation 3.16, is described at equation 4.1,

$$U_1(x_1, y_1, \lambda) = A_1(x_1, y_1, \lambda) \sum_{n_x = -\frac{1}{2}(N_x - 1)}^{\frac{1}{2}(N_x - 1)} \sum_{n_y = -\frac{1}{2}(N_y - 1)}^{\frac{1}{2}(N_y - 1)} \frac{U_0(x_{n_x}, y_{n_y}, \lambda)}{r^2} e^{j \frac{2\pi}{\lambda} r} t_{lens}(x_{n_x}, y_{n_y}, \lambda) \quad (4.1)$$

where the discrete amplitude function, $A_1(x_1, y_1, \lambda)$, is described in equation 4.2, the discrete path length of propagation function, $r = r(x_1, y_1, x_{n_x}, y_{n_y})$, is described in equation 4.3, the lens transformation function, $t_{lens}(x_{n_x}, y_{n_y}, \lambda)$, and lens thickness function, $\triangle(x_{n_x}, y_{n_y})$, are described in equation 4.4.

$$A_1(x_1, y_1, \lambda) = \frac{z}{j\lambda} \text{sinc}\left(\frac{\pi x_1}{z\lambda} dx_0\right) \text{sinc}\left(\frac{\pi y_1}{z\lambda} dy_0\right) \quad (4.2)$$

$$r = r(x_1, y_1, x_{n_x}, y_{n_y}) = \sqrt{z^2 + (x_{n_x} - x_1)^2 + (y_{n_y} - y_1)^2} \tag{4.3}$$

$$t_{lens}(x_{n_x}, y_{n_y}, \lambda) \;=\; e^{\;j\;\frac{2\pi}{\lambda}(n_{lens}-1)\triangle(x_{n_x},y_{n_y})} \;=\; e^{\;j\;\frac{2\pi}{\lambda}(n_{lens}-1)\left[\triangle_0 - \left(x_0{}^2 + y_0{}^2\right)\left(\frac{1}{2R_1} - \frac{1}{2R_2}\right)\right]} \tag{4.4}$$

4.4 Design the Sensor Optics System

The software suite used for developing the software model of the simulated sensor optics system is listed at Appendix C. Knowing certain parameters about the optical components to be used for the sensor optics system is only the start for developing the software model. Other parameters such as spatial sampling intervals, separation distances along the optic axis between components, validation of aperture sizes are derived from the optical components characteristics to form the software model and simulate the design of the sensor optics system. One program script was used as the software model to simulate the wave optics propagation of a point source of electromagnetic radiation through the sensor optics system appears at Appendix C.

4.4.1 System parameters. The parameters of the software model are defined and evaluated using the MatLab® function *parameters.m.* The spectrum of electromagnetic radiation used for representing the remote scene is represented an array of discrete wavelengths, where each wavelength is the centre wavelength for a specific spectral wavelength band of electromagnetic radiation. Parameters that are specified for the system design are represented in the MatLab® function *parameters_02_define.m,* and based on these parameters, other system parameters computed for the system design are evaluated with the MatLab® function *parameters_03_compute.m.* The distances along the optic axis between the forward lens and the field stop, and between the field stop and the aft lens, plus the spatial sampling intervals for each principal transverse plane in the simulated sensor optics system are computed based on the defined system parameters.

4.4.2 Undeviated spectral wavelength. Two pivotal parameters in the system design are the undeviated spectral wavelength and the spectral range of electromagnetic radiation around this

wavelength required to represent the spectral detail of radiant energy collected from the remote scene. Both parameters are specified by the system designer, and both contribute to the dispersion characteristics for the system. From the specified diameter of the direct vision prism, the dispersion characteristics influence the aperture sizes required at the aft lens (forward optics system) and the focussing lens (detector optics system).

The design of the direct vision prism must be tailored for the undeviated spectral wavelength, since the spectral real images of the remote scene are spatially distributed along a radial line (representing the direction of dispersion) in the transverse plane at the detector focal plane array. The undeviated spectral wavelength spectral real image is formed with the centre of the image on the optic axis. Spectral real images for spectral wavelength bands below the undeviated spectral wavelength are formed with centres along the radial line located away from the optic axis in one direction, and the images for spectral wavelength bands above the undeviated spectral wavelength are formed in the opposite direction along the radial line. The spatial separation between each spectral real image is derived from the dispersion attained with the direct vision prism for each corresponding spectral wavelength band.

Using Snell's Law of Refraction, the undeviated spectral wavelength of electromagnetic radiation is evaluated using geometric optics through each stage of propagation through the prism optics system, to arrive at the detector focussing lens with an angular direction of propagation with respect to the optic axis of zero. The parameter $\epsilon_{4\mathrm{b}}$ is used in the software model to describe this angular direction. Based on the index of refraction characteristics of the bulk media materials used for the direct vision prism, the parameters of the direct vision prism available for tailoring the system design are the separate prism surface angles. By retaining one prism surface angle constant, and thus a specified parameter, the other prism surface angle can be evaluated iteratively by testing against the angular direction of propagation criterion, so the prism surface angle solution achieves an angular direction of propagation with respect to the optic axis of zero.

The entry prism surface angle, defined as α_1, can be evaluated by using the MatLab® function *evaluate_alpha_1.m*, with the exit prism surface angle predefined. The exit prism surface angle, defined as α_3, can be evaluated by using the MatLab® function *evaluate_alpha_3.m*, with the entry prism surface angle predefined.

4.4.3 Spatial extent of apertures. With the surface angles of the direct vision prism established so the prism optics system is tailored for the specified undeviated spectral wavelength, the next task in designing the software model is to validate the spatial extent of all apertures in the prism optics system. These apertures are: (1) the prism entry surface; (2) the prism exit surface; (3) the aft lens; and (4) the detector focussing lens.

The direction of dispersion encountered by the spectral wavefront fields of electromagnetic radiation occurs along the vertical orientation in prism coordinates. Using an upright orientation of the direct vision prism, the direction of dispersion for these spectral wavefront fields also occurs in the vertical orientation in system coordinates.

Geometric optics and Snell's Law of Refraction are used to evaluate the propagation path distances through each stage of propagation in the prism optics system. The minimum lengths parallel to the optic axis of the direct vision prism, defined z_{2min} for the entry surface and z_{3min} for the exit surface, plus the diameter of the direct vision prism, are system parameters defined by the system designer. Working with these parameters, sensible propagation path distances can be determined. By testing: (1) the propagation distances with the minimum lengths parallel to the optic axis; and (2) the vertical position of each spatial sample of the spectral wavefront fields as these positions change due to dispersion with the radius of the direct vision prism, sensible spatial extent sizes for the entry surface and exit surface apertures of the direct vision prism can be determined by the system designer. Once sensible minimum spatial extent sizes for the direct vision prism apertures are determined, the sensible minimum spatial extent size for the detector focussing lens aperture can be determined.

Should the tests for propagation distances or vertical positions fail during these evaluations, the system designer has the option of changing the defined system parameters of: (1) direct vision prism diameter, to effect a change in entry surface and exit surface apertures; (2) minimum lengths of each bulk media component of the direct vision prism diameter, to effect changes in propagation distance and vertical position to accommodate for the available spatial extent of the entry surface and exit surface apertures; (3) separation between the direct vision prism exit aperture and the detector focussing lens along the optic axis, defined $z_{5\mathrm{ref}}$, to effect a change in the spatial extent for all dispersed spectral wavefront fields collected at the focussing lens aperture; (4) diameters of the aft lens and focussing lens, to effect adjustments in the spatial extent of the spectral wavefront fields commencing propagation through the prism optics system (with the aft lens) or effect adjustments in the spatial extent available at the detector for collecting these fields (focussing lens).

Deciding how these defined system parameters should be varied is left to the system designer, since each parameter is not entirely independent from influencing the design requirements with another of these parameters. Each design change made needs to be tested against the propagation distances and vertical position criteria so that a sensible arrangement of apertures in the prism optics system is found for the software model.

Propagation of the spectral wavefront fields of electromagnetic radiation through the prism optics system, is simulated with the MatLab® function *propagate_04_prism.m*. The *prism* group of metrics obtained from this function deliver values for each stage of propagation as: propagation distances, defined prism.r_1, prism.r_2, prism.r_3, prism.r_4, prism.r_5 respectively; and vertical position, defined prism.y1_total; prism.y2_total; prism.y3_total; prism.y4_total; prism.y5_total respectively. These metrics are available for the system designer to determine the appropriate choices in system parameters for achieving a sensible arrangement of apertures in the system design. The MatLab® function *propagate_04_prism.m* can be used with manipulation from the system designer to evaluate different choices of defined system parameters.

Table 4.1:   Software Model Design Parameters used to simulate the CTIS Sensor Optics System

Description of Design Parameter	Values
Number of spectral wavelength bands	31
Centre wavelengths of spectral wavelength bands	2.0 μm to 5.0 μm in 100 nm intervals
Undeviated spectral wavelength	3.6 μm
Number of spatial samples across the remote scene	66
Power, emitted for each spectral wavelength band	1 Watt
Range, distance between remote scene and forward lens	1000 m
Forward Lens Aperture	0.1 m
Forward Lens Diameter	0.1 m
Forward Lens Focal Length	1.0 m
Aft Lens Aperture	0.022 m
Aft Lens Diameter	0.022 m
Aft Lens Focal Length	0.220 m
Focussing Lens Aperture	0.050 m
Focussing Lens Diameter	0.050 m
Focussing Lens Focal Length	0.500 m
Prism Diameter	0.030 m
Prism Entry Surface Angle, α_1	30° 00′ 00″
Prism Exit Surface Angle, α_3	23° 56′ 00″
Prism Entry Bulk Media, n_3	Lithium Fluoride (LiF)
Prism Exit Bulk Media, n_4	Barium Fluoride (BaF$_2$)

4.5   Simulate the Sensor Optics System

Once a sensible arrangement for propagation distances and vertical offsets were obtained for a set of system parameters, these parameters were retained to define the sensor optics system design configuration to be represented through simulation with the software model. The software model was used to propagate a multispectral point source through the system and obtain the point spread functions for the specific system design configuration using wave optics propagation theory. From the linear systems viewpoint these point spread functions represent the impulse response of the simulated sensor optics system. The system design configuration parameters used for the software model presented in the following discussion are listed at Table 4.1. A limited extent of the output parameters available from the software model are presented in the following discussion, as a means of providing some insight on the extent of metrics computed in simulating the sensor optics system.
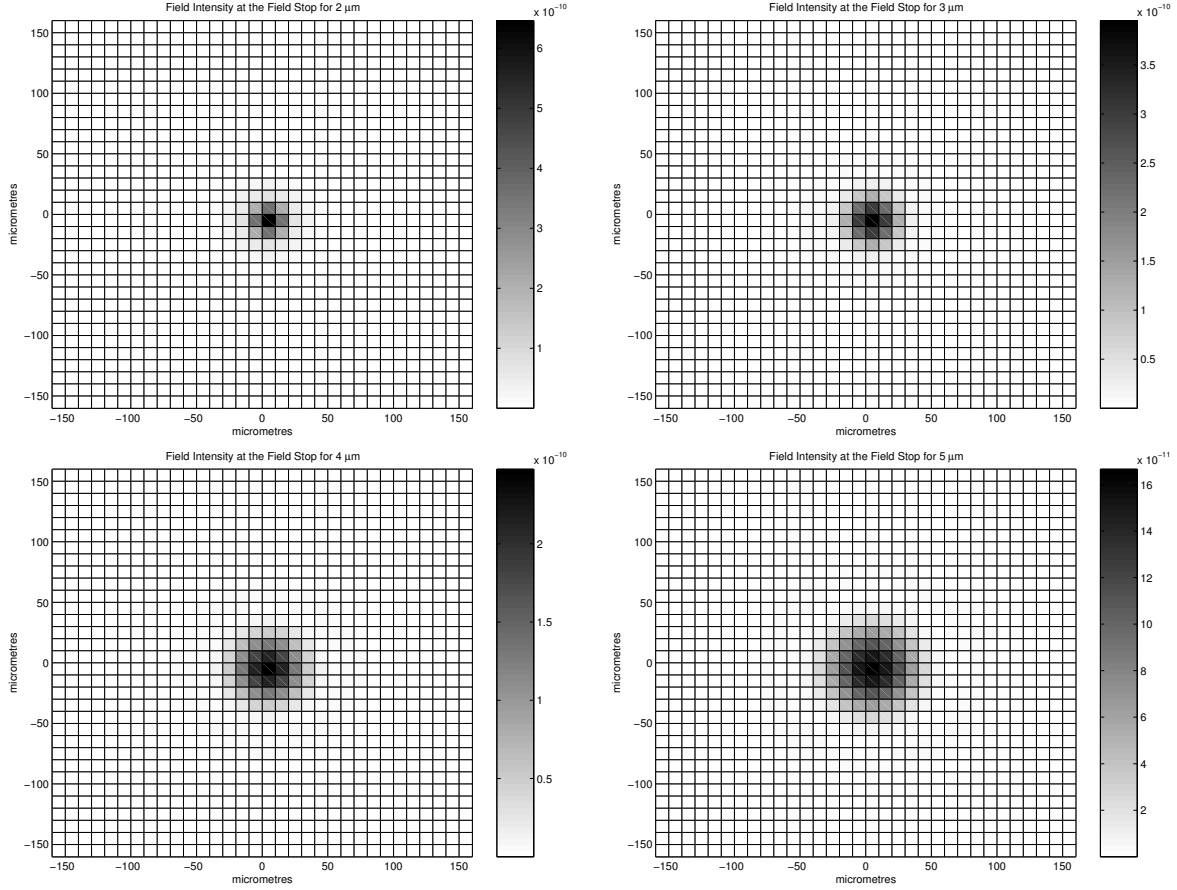
Figure 4.3:   Point Spread Functions for 2.0 μm, 3.0 μm, 4.0 μm, 5.0 μm at the Field Stop Aperture. An increase in spectral wavelength is coupled with an increase in spatial area and a decrease in peak intensity for the Point Spread Functions

4.5.1   Field Stop Aperture (Forward Optics System).   The intensity of electromagnetic radiation at each spatial sample in the field stop transverse plane of the forward optics system is represented at Figure 4.3. The point spread functions at the field stop increase in area across the transverse plane for increased spectral wavelength. Since the power for each spectral wavelength band emitted from the multispectral point source is the same, the trend of a decrease in peak intensity for increased spectral wavelength. These complementary relationships reveal the total energy for each spectral wavelength band from the point source is conserved, thus demonstrating the software model also obeys the laws of conservation of energy.

77

The cross-section cut-away through the centre of the point spread functions for the 2.0 μm, 3.0 μm, 4.0 μm, and 5.0 μm spectral wavefront fields of electromagnetic radiation are superimposed on the same diagram for comparison at Figure 4.4. The ability to view the spatial profile of individual spectral point spread functions at the field stop is available with the software model, however this observation would not be possible with the actual system. Observing the spatial profile of the sum of all spectral point spread functions at the field stop would only be possible with the actual system since the centres of these spectral point spread functions are collocated in the field stop.

4.5.2   Aft Lens Aperture (Forward Optics System).   The phase curvature of the spectral wavefront fields of electromagnetic radiation after propagating through the aft lens are displayed at Figure 4.5. Each spectral wavefront field has less than half a wavelength of phase deviation across the aft lens aperture. These spectral wavefront fields form the inputs to the prism optics system. The wavefront propagation from the aft lens aperture is simulated as a collimate wavefront. The low variation in phase across the wavefront simulated through wave optics propagation theory supports this next stage of propagation for the spectral wavefront fields.

4.5.3   Focussing Lens Aperture (Prism Optics System).   Results from the software model for simulating the wave optics propagation through the direct vision prism for 3.6 μm and 3.8 μm spectral wavefront fields of electromagnetic radiation are shown at Figure 4.6. The phase tilt evident on each spectral wavefront, for the prism angular position of rotation oriented in the upright position. The 3.8 μm spectral field shows noticeable phase tilt across the wavefront along the direction of dispersion, which is vertical due to the angular orientation of the prism. The 3.6 μm spectral field shows no significant phase tilt, demonstrating this spectral wavelength is the undeviated wavelength of the simulated sensor optics system.

Results from the software model for simulating rotation of the 3.8 μm wavelength band of spectral wavefront field at the detector focussing lens aperture are shown in Figure 4.7. These
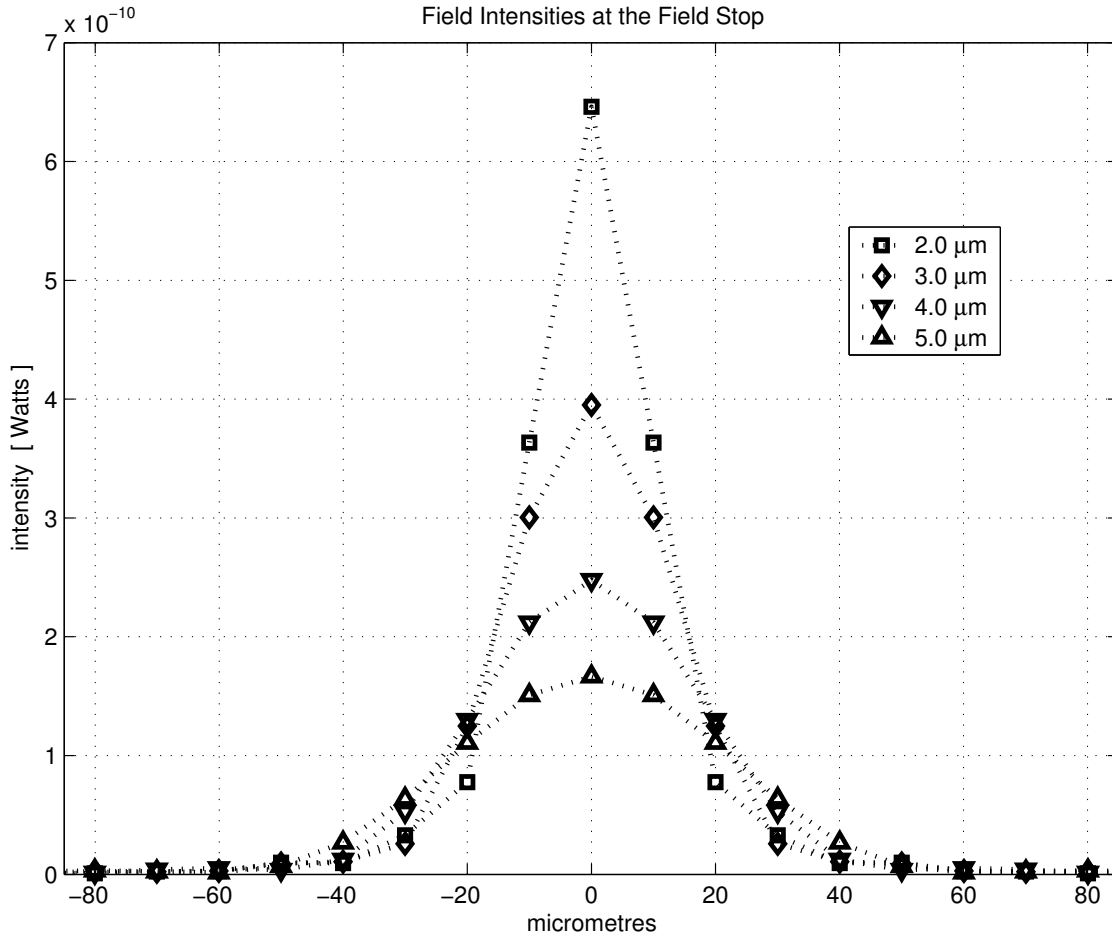
Figure 4.4: Point Spread Function cross sections for 2.0 μm, 3.0 μm, 4.0 μm, 5.0 μm at the Field Stop. Shows the relationship between peak intensity and the spatial cross section coverage (spatial area) for different spectral wavelengths, where 2.0 μm has maximum peak intensity and 5.0 μm has most spatial cross section coverage.

results show the sampled phases obtained through simulated wave optics propagation using the software model. The trend of phase variation reveals the phase tilt across the wavefront aligns with the angular orientation of the direct vision prism with respect to the system coordinates. Note the change location at the detector focussing lens aperture of each sampled element of the wavefront with different angular orientations of the direct vision prism. The phase tilts across the wavefront, the angular orientation of the wavefront with respect to the system coordinates, and the change in spatial location of the wavefront with different angular orientations of the prism, are results that demonstrate the use of wave optics propagation theory in the software model.
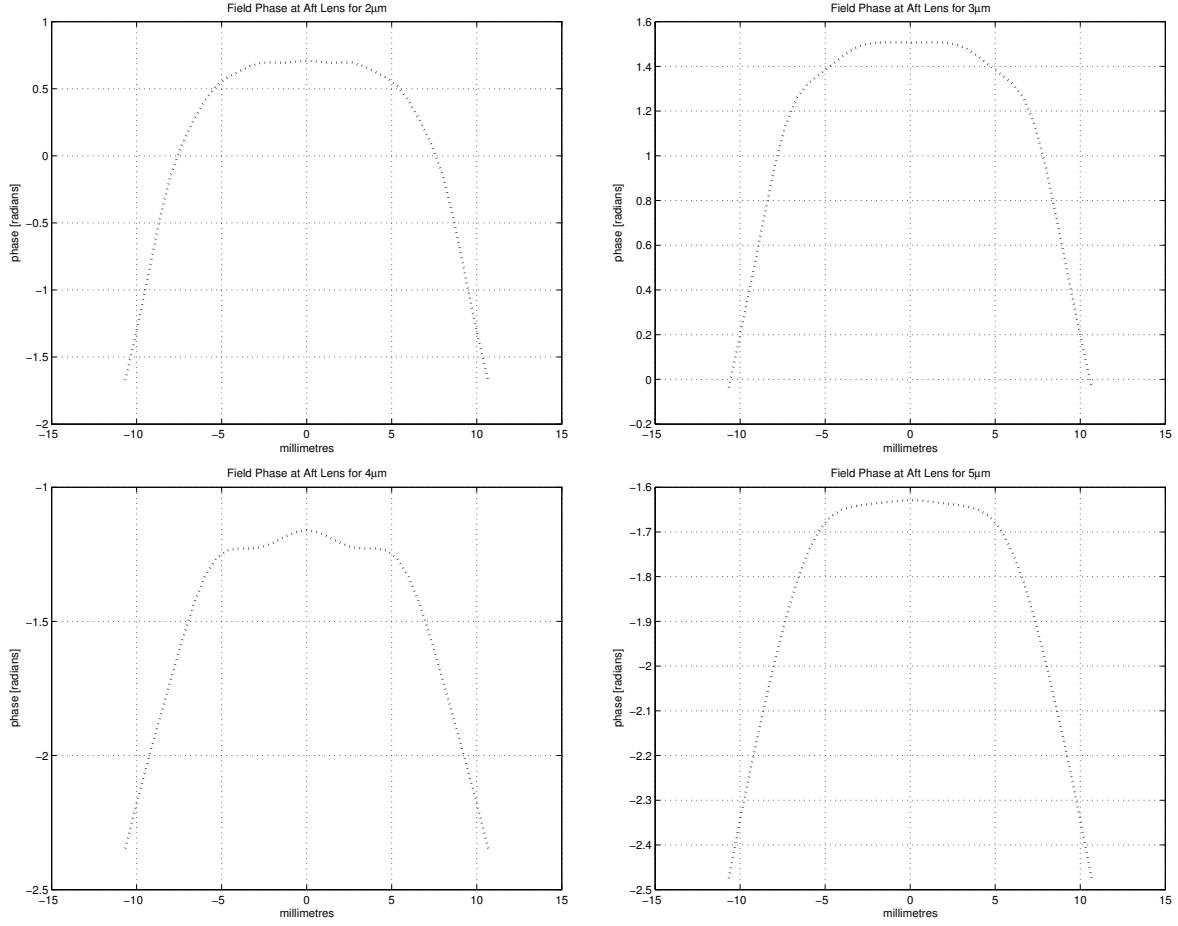
Figure 4.5:   Phase of the spectral wavefront fields for 2.0 μm, 3.0 μm, 4.0 μm, 5.0 μm at the Aft Lens. Each spectral wavefront field has less than half a wavelength of phase deviation across the aft lens aperture.

4.5.4   Focal Plane Array (Detector Optics System).   Obtaining the point spread functions

for each spectral wavelength of electromagnetic radiation at the focal plane array was achieved

at first for a stationary upright oriented direct vision prism configuration of the simulated sensor

optics system. Propagation theory based on Fourier optics was used to identify locations in the

transverse plane at the focal plane array where the centres of every spectral point spread function

were anticipated. A spatial area of arbitrary size around the location of these spectral point spread

function centres was chosen to simulate the wave optics propagation to the focal plane array for each

respective spectral field. The outcome from performing this simulation is shown in Figure 4.8 (a)

80
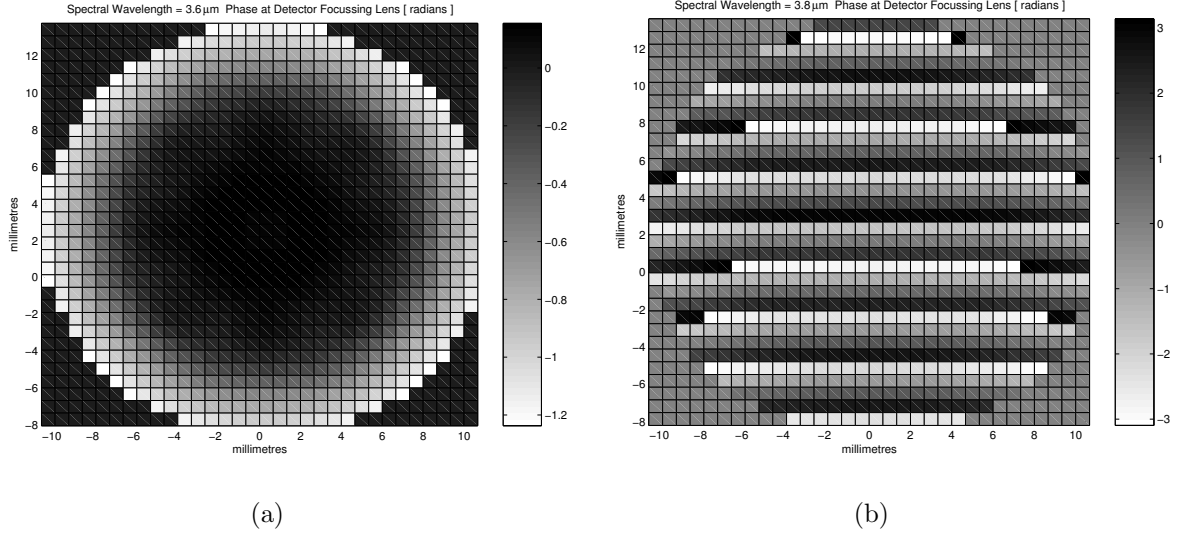
Figure 4.6: Phase of the spectral wavefront field for wavelengths (a) 3.6 μm and (b) 3.8 μm, with the prism oriented in the upright position with respect to the system coordinates of the software model. These results from the software model show noticeable phase tilt across the wavefront for 3.8 μm spectral field, and no noticeable phase tilt across the wavefront for 3.6 μm spectral field. The 3.6 μm spectral wavefront field corresponds to the undeviated spectral wavelength for this configuration of the simulated sensor optics system.

with a spectral point spread function formed according to the propagation of the corresponding spectral field. The spectral fields of infrared electromagnetic radiation were uniformly distributed over the finite spectral range between 2.0 μm and 5.0 μm in 100 nm increments. The spatial separation between the respective spectral point spread functions in the focal plane array was not uniform along the radial line aligned in the direction of dispersion and indicating the angular orientation of the direct vision prism. This non-uniform spatial separation between spectral point spread functions is a testament to the trigonometric expressions at equation 3.53 and equation 3.54.

Incorporating the rotating direct vision prism feature in simulating the sensor optics system was the next step in designing the software model. Fourier optics propagation theory was used to identify the spectral point spread function centre locations for an upright orientation of the prism commensurate with each angular orientation of the direct vision prism. With a rotational transform relationship from linear algebra for every discretely sampled angular position of prism rotation, these spectral point spread function centre locations were used to compute the anticipated
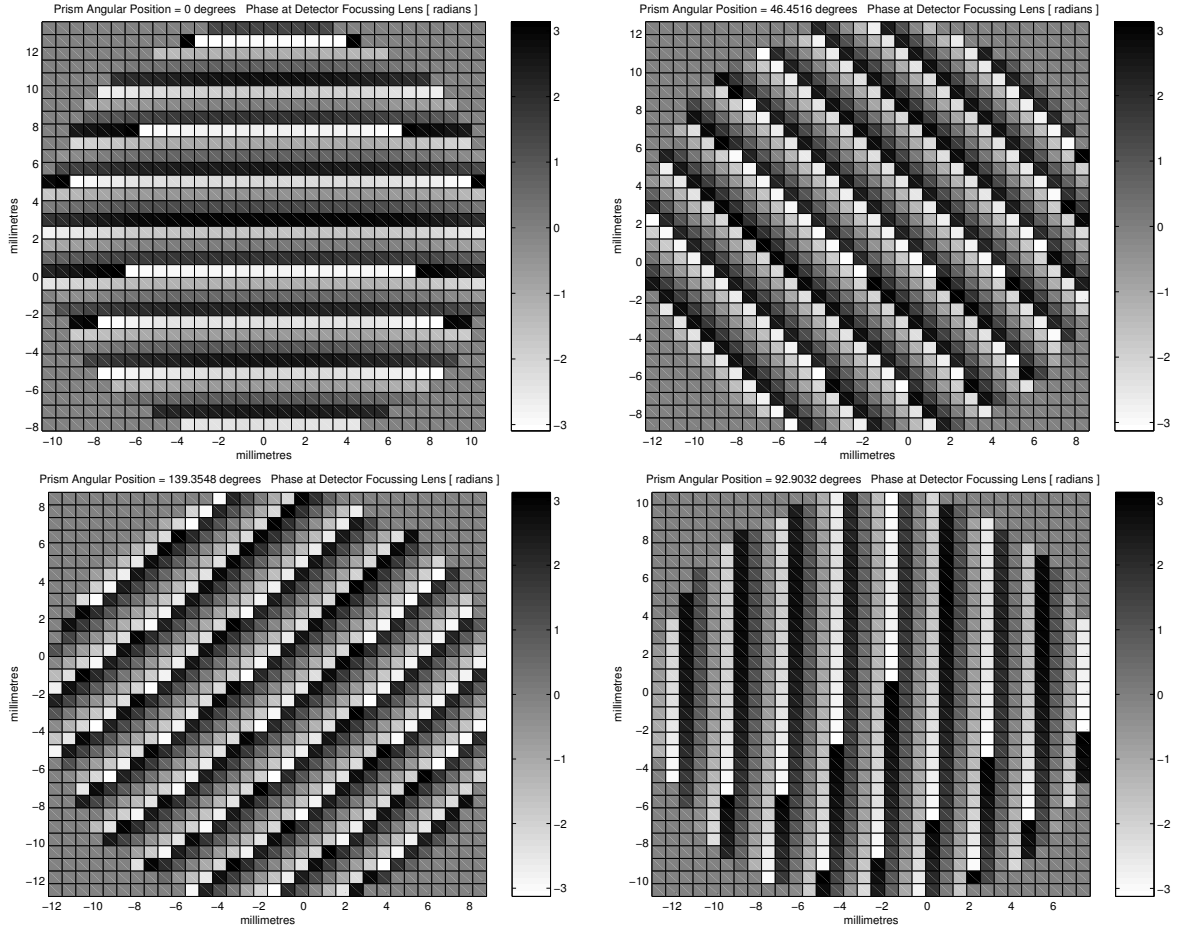
Figure 4.7: Phase of the 3.8 μm spectral wavefront field at the detector focussing lens aperture. Four angular orientations of the 3.8 μm spectral wavefront field are shown corresponding to direct vision prism angular positions of rotation. This example is representative of the angular orientation with respect to the optic axis simulated for all spectral wavefront fields in the software model.

spectral point spread function centre locations in the focal plane array transverse plane resulting from direct vision prism rotation.

Performing the wave optics propagation using solely this process revealed favourable outcomes for prism angular orientations that situated the directions of dispersion tending along a vertical orientation and unfavourable outcomes for prism angular orientations that situated the directions of dispersion tending along a horizontal orientation. Favourable outcomes correspond to prism angular orientations near 0 degrees and 180 degrees, while unfavourable outcomes correspond to prism angular orientations near 90 degrees and 270 degrees.
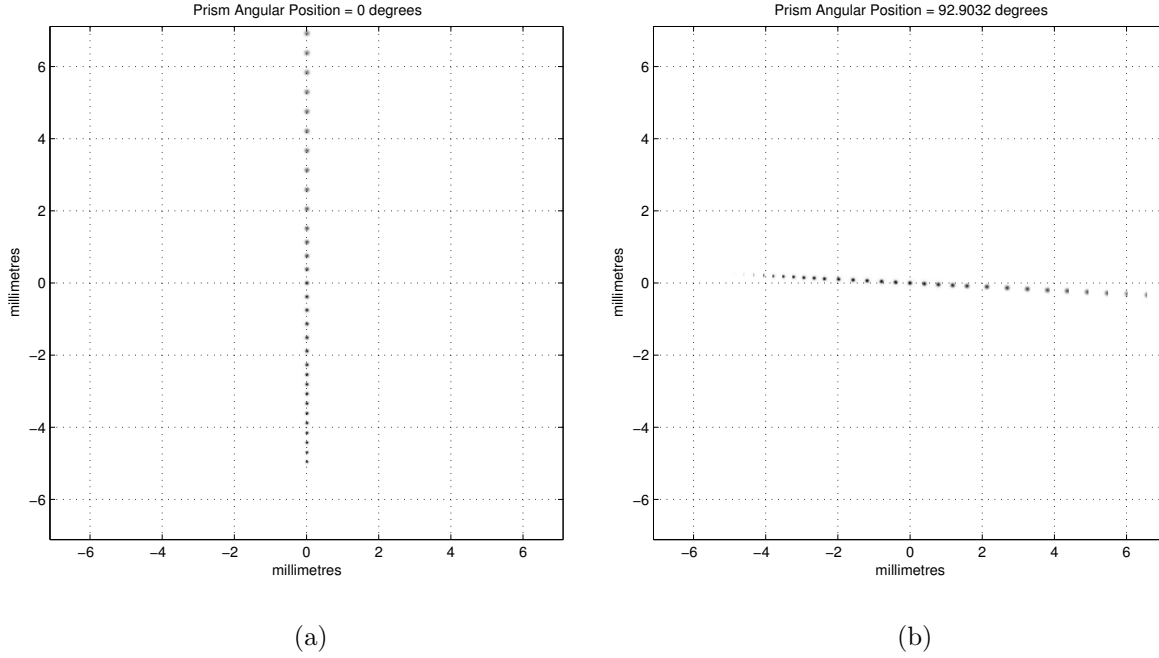
Figure 4.8:   Point Spread Functions for all spectral wavelengths as a Chromotomographic real image for Prism Angular Position at (a) 0 degrees, and (b) 92.9032 degrees from upright orientation. Locations for the Point Spread Functions in the Detector Focal Plane Array were determined using Fourier optics principles only.

The outcome obtained for the 90 degrees case of angular prism orientation is shown in Figure 4.8 (b). The spectral point spread functions for electromagnetic fields at spectral wavelengths to either side of and near the undeviated spectral wavelength appear favourable, while the spectral point spread functions for fields at spectral wavelengths further from the undeviated spectral wavelength appear unfavourable. An attempt to display the unfavourable outcomes for both extremes of the finite spectral range of wavelengths appear at Figure 4.9 (a) for electromagnetic fields at spectral wavelengths between 2.0 μm and 3.2 μm, and Figure 4.9 (b) for fields at spectral wavelengths between 3.8 μm and 5.0 μm.

In simulating the dispersed spectral wavefront fields of electromagnetic radiation at the detector focussing lens, the vertical and horizontal intervals between discrete samples of the spectral wavefront fields no longer remains constant. These intervals vary according to (1) spectral wavelength as a result of non-uniform dispersion in the prism, indicated along the radial line of spectral
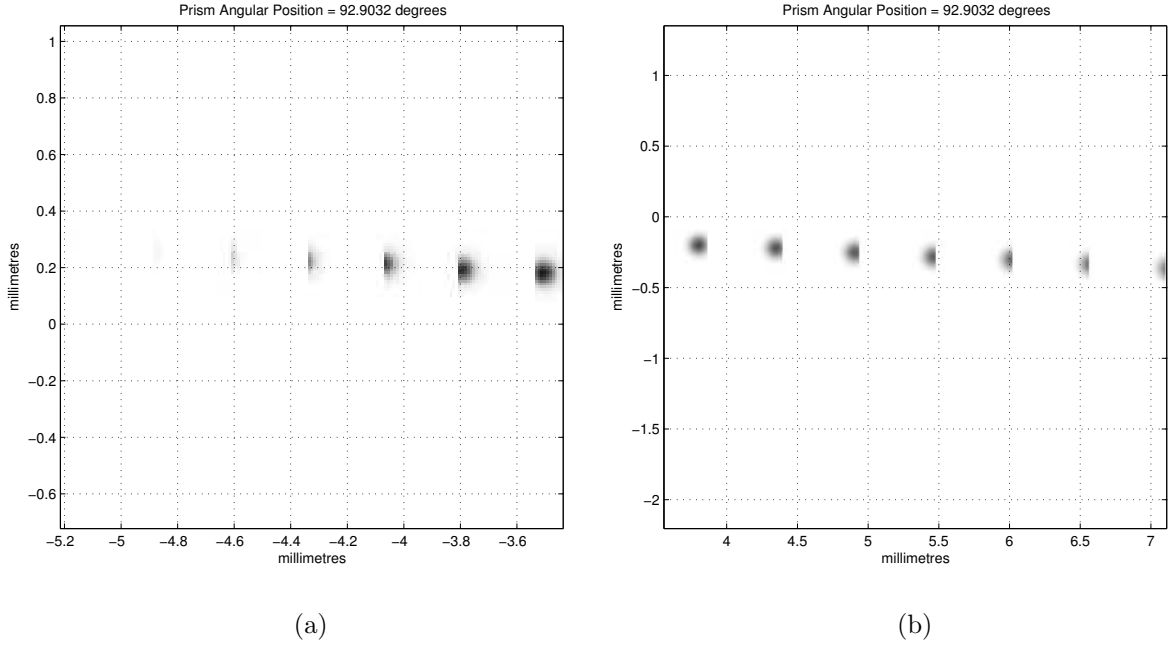
Figure 4.9: Magnified view of Point Spread Functions for spectral wavelengths as a Chromotomographic real image for Prism Angular Position at 92.9032 degrees from upright orientation. Locations for the Point Spread Functions in the Detector Focal Plane Array were determined using Fourier optics principles only where, (a) represents spectral wavelengths between 2.0 μm and 3.2 μm, and (b) represents spectral wavelengths between 3.8 μm and 5.0 μm.

point spread functions at the detector focal plane array, and (2) angular orientation of the direct vision prism, where prism angular orientations deviating from an upright or vertical position introduce non-uniform dispersion along the x-axis in system coordinates. For the upright prism orientation the x-axis was simulated with spatial sampling intervals that were uniform across spectral wavefront fields. Introducing non-uniform variation in spatial sampling intervals along the x-axis, due to (1) simulating the angular rotation of the direct vision prism and (2) different angular directions of propagation with respect to the optic axis for spectral wavefront fields at the detector focussing lens, alters the accuracy of determining the spectral point spread function centre locations using the rotational transform relationship. Remember the centre locations for spectral point spread functions were obtained for an upright angular orientation of the direct vision prism using Fourier optics propagation theory only.

Some approach was required to locate the spectral point spread function centres successfully for all discretely sampled prism angular orientations. A radial search function was developed and incorporated in the software model to perform the task of accurately pin-pointing the respective spectral point spread function centre locations for every prism angular orientation. The radial search function employs Fourier optics propagation theory with the rotational transform linear algebra relationship to identify the vicinity of the respective spectral point spread function centre locations in the focal plane array transverse plane, then assembles a finite length radial line of spatial sample intensity points aligned with the prism angular orientation. Wave optics propagation is then used to obtain the intensity profile along this radial line. Searching along the radial line of spatial sample points for the peak intensity, and identifying the location of the spatial sample point with the peak intensity completes the task of defining the favourable location of all spectral point spread function centres for all prism angular orientations. These spectral point spread function centre locations were used as the centres for the spatial areas defined to simulate the wave optics propagation of the spectral wavefront fields from the detector focussing lens to the focal plane array.

Incorporating the radial search function in the software model resulted in a dramatic improvement with accurately simulating the spectral point spread functions across the finite spectral range of electromagnetic radiation at the focal plane array. Figure 4.10 displays the improvement in the spectral point spread functions for the 90 degree angular orientation of prism rotation. Figure 4.11 offers a comparison to assess the improvement made with respect to the unfavourable results shown in Figure 4.9 for both spectral extremes of spectral point spread functions.

To appreciate the impact this anomaly had on the accuracy of simulated power for samples in the spectral point spread function, Figure 4.12 shows the power for each sample computed over the spatial inaccurately define areas used for simulating the 2.0 μm, 3.0 μm, 4.0 μm, 5.0 μm spectral point spread functions. After incorporating the radial search method to locate the centres of the spectral point spread functions, the wave optics propagation resulted in significantly superior
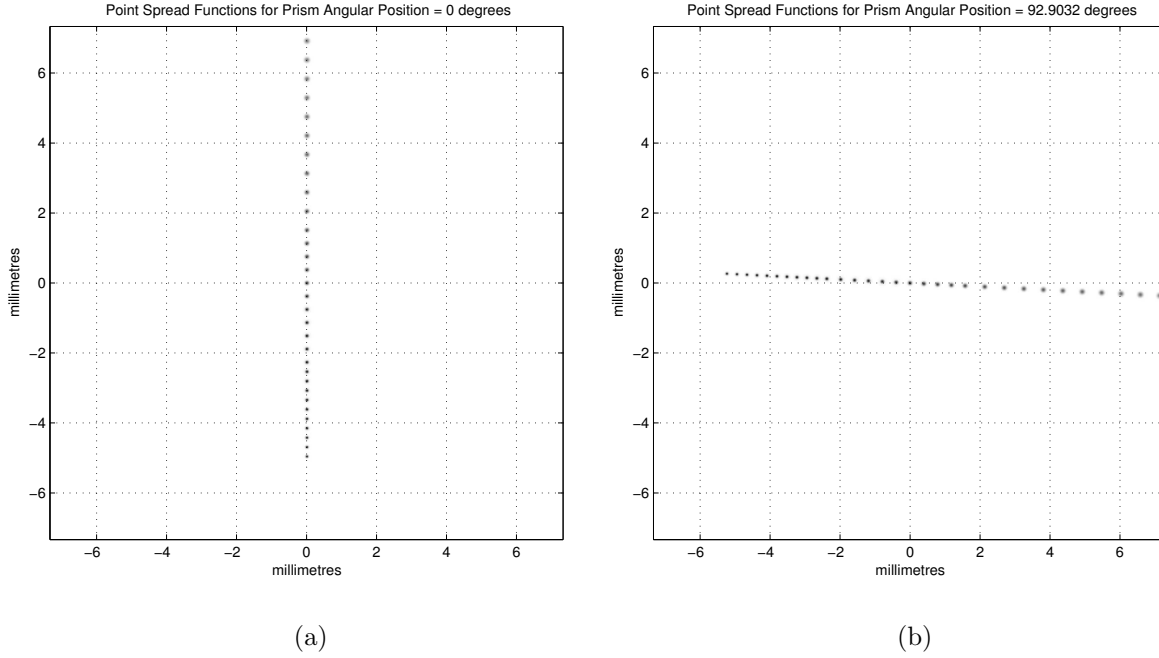
Figure 4.10:   Point Spread Functions for all spectral wavelengths as a Chromotomographic real image for Prism Angular Position at (a) 0 degrees, and (b) 92.9032 degrees from upright orientation. Locations for the Point Spread Functions in the Detector Focal Plane Array were determined by combining Fourier optics principles with the radial search technique.

outcomes for the simulated spectral point spread functions. These outcomes for the the 2.0 μm, 3.0 μm, 4.0 μm, 5.0 μm spectral point spread functions are shown in Figure 4.13 with the peak intensity of the spectral point spread functions located in the centre of each spatial area, and coinciding with the off-centre locations where peak intensity would be expected in Figure 4.12.

The spectral point spread function for the undeviated wavelength remained unaffected from these anomalies, as evidenced in Figure 4.14 showing the spectral point spread function for a 90 degrees angular orientation of the direct vision prism.

4.5.5 Energy Distribution under the Point Spread Functions.   Look at the shape of the point spread function for each spectral wavelength of electromagnetic radiation. The intensity profile between spectral wavelengths of electromagnetic radiation at the focal plane array.
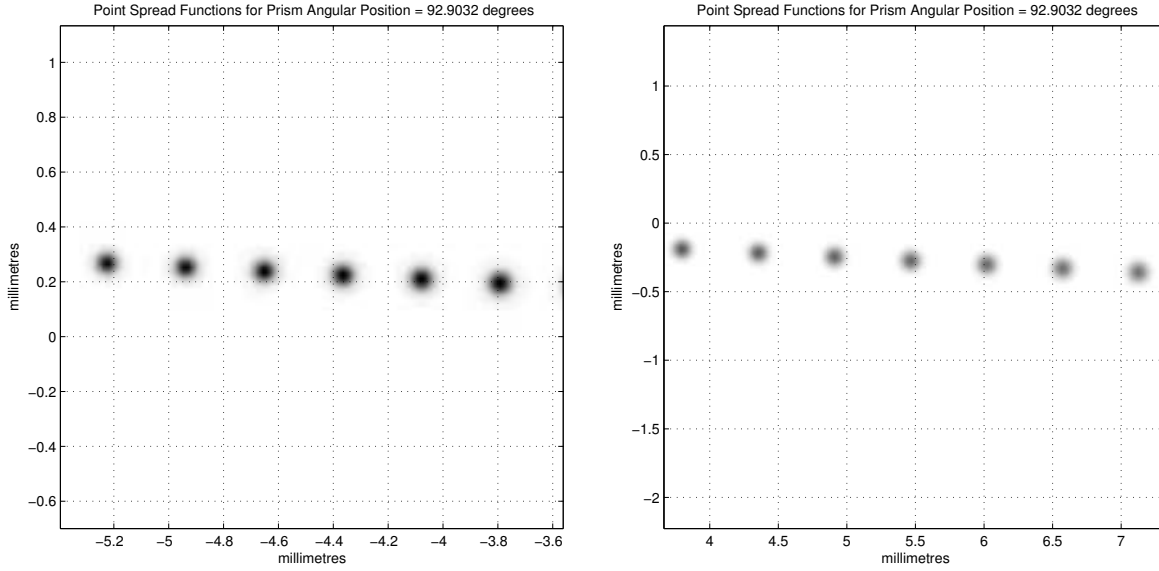
Figure 4.11: Magnified view of Point Spread Functions for spectral wavelengths as a Chromo-tomographic real image for Prism Angular Position at 92.9032 degrees from upright orientation. Locations for the Point Spread Functions in the Detector Focal Plane Array were determined by combining Fourier optics principles with the radial search technique. Note the centres of each Point Spread Function are accurately located, enabling the imaging area to capture the entire spread of spectral wavelength intensity.

The point spread functions for the spectral fields of electromagnetic radiation located at the detector focal plane array can be compared with the point spread functions for these spectral fields located at the field stop. Viewing the spectral point spread functions at the field stop in Figure 4.3, and comparing these with the point spread functions at the focal plane array in Figure 4.13 for spectral wavelengths 2.0 μm, 3.0 μm, 4.0 μm and 5.0 μm, the peak intensities at the focal plane array are approximately one order of magnitude below the peak intensities at the focal plane array. The decrease in peak intensity between the field stop and the focal plane array is also coupled with an increase in spatial coverage of the distribution of intensity for each spectral point spread function, demonstrating the conservation of energy for each spectral point spread function. The effects of diffraction on each spectral wavefront field of electromagnetic radiation due to propagation through the aft lens, direct vision prism, and focussing lens optical components are also evident by viewing the differences between these spectral point spread functions.
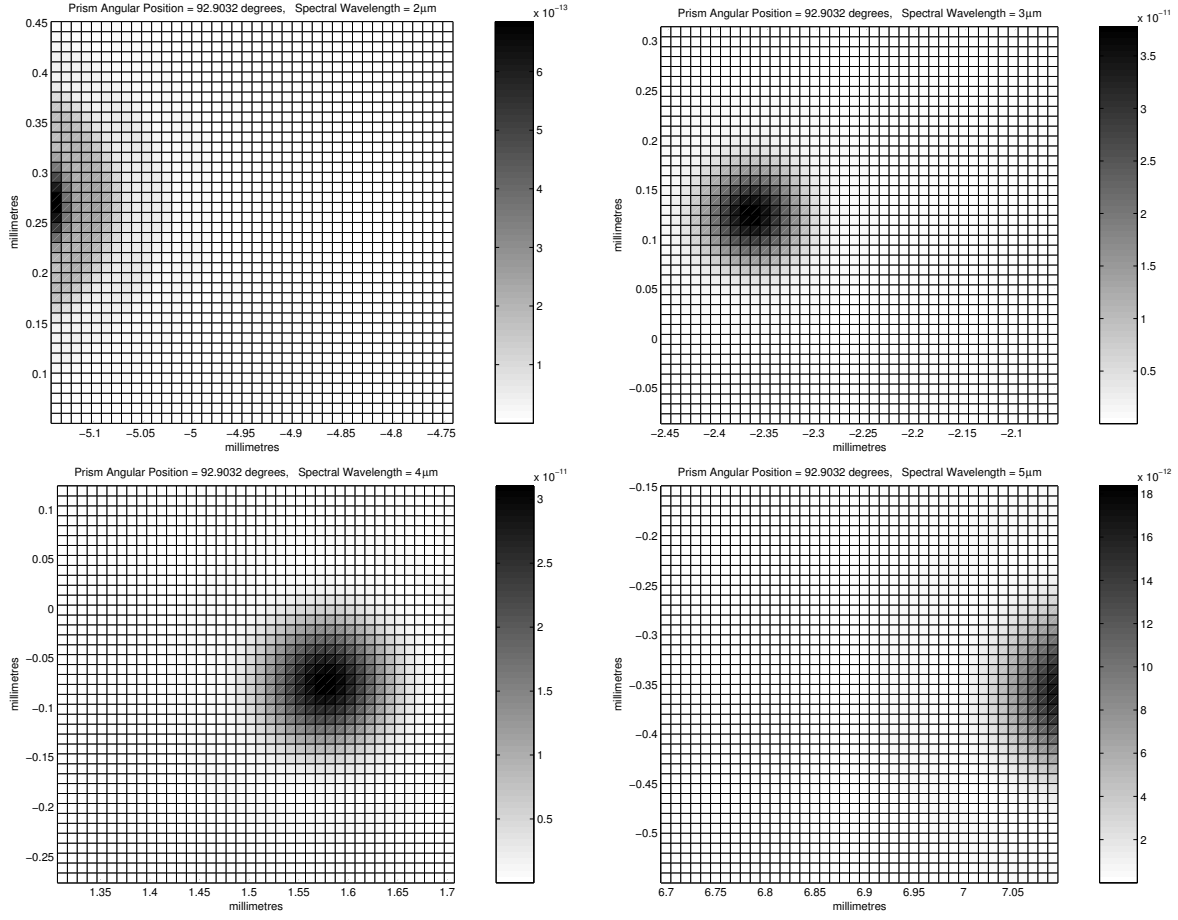
Figure 4.12: Point Spread Functions for 2.0 μm, 3.0 μm, 4.0 μm, 5.0 μm, with Prism Angular Position at 92.9032 degrees from upright orientation. Locations for each Point Spread Function in the Detector Focal Plane Array were determined using Fourier optics principles only. The centre of each imaging area does not accurately locate the centres for every spectral point spread function. Further evaluation of the centre locations for every spectral point spread function is required from the software model.

4.6 Summary of Assumptions

The development of the software model to simulate the sensor optics system of the chromotomographic imaging system has involved a number of assumptions. Some assumptions have been disclosed during discussion of the software model while others have not been mentioned. This section is an attempt to identify the assumptions that made a contribution to the development of the software model.
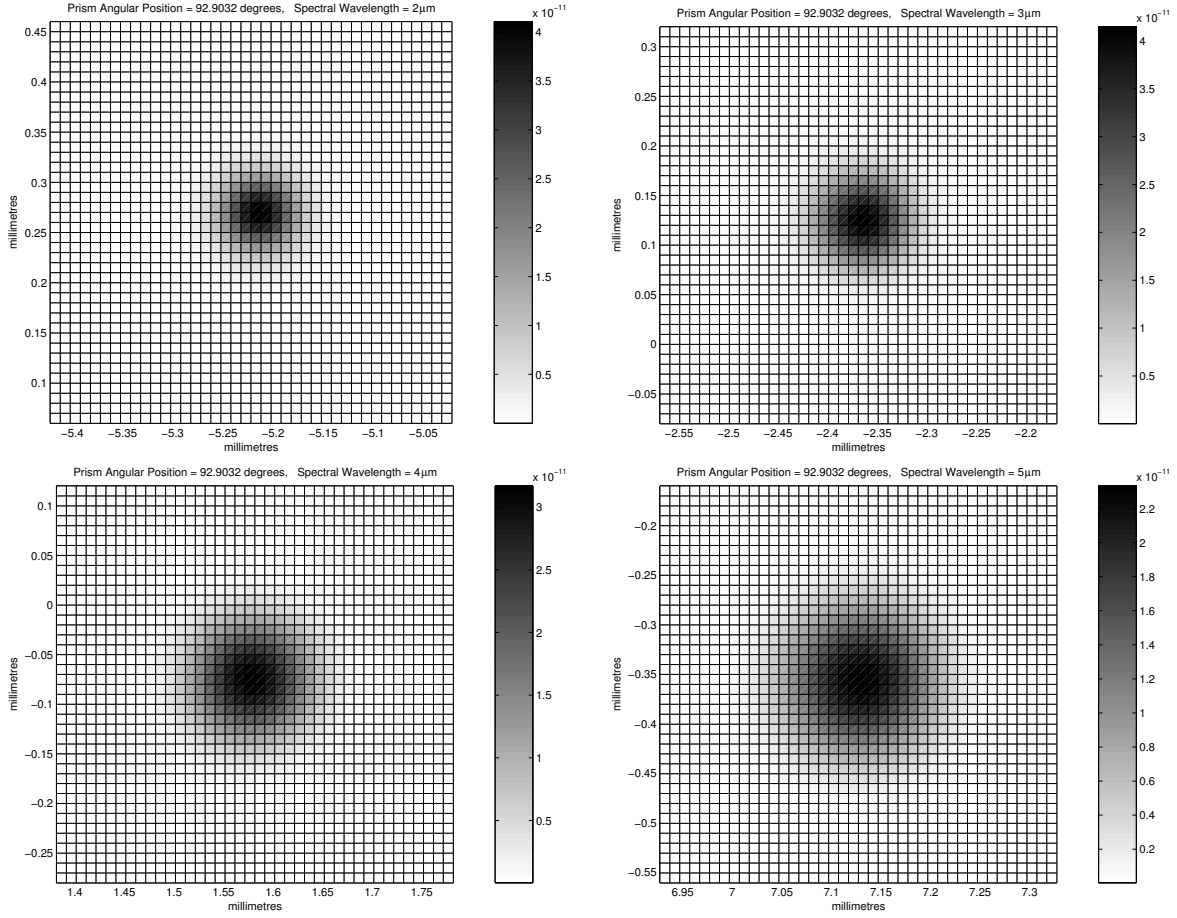
Figure 4.13: Point Spread Functions for 2.0 μm, 3.0 μm, 4.0 μm, 5.0 μm, with Prism Angular Position at 92.9032 degrees from upright orientation. Locations for each Point Spread Function in the Detector Focal Plane Array were determined by combining Fourier optics principles with the radial search technique. The centre of each imaging area accurately locates the centres for every spectral point spread function.

Lenses are modelled as thin lenses only, using the paraxial approximation for the surface contour of each lens as parabolic in curvature instead of a spherical curvature. Another design constraint was imposed using the thin lens representation regarding the F#number criteria for each lens. Demonstration of the software model presented in this thesis obeyed the constraint F# number $\geq$ 10.

All intrinsic characteristics of the detector focal plane array such as material sensities, non-uniformities, responsivity, are not represented in the software model. The simulated intensity at
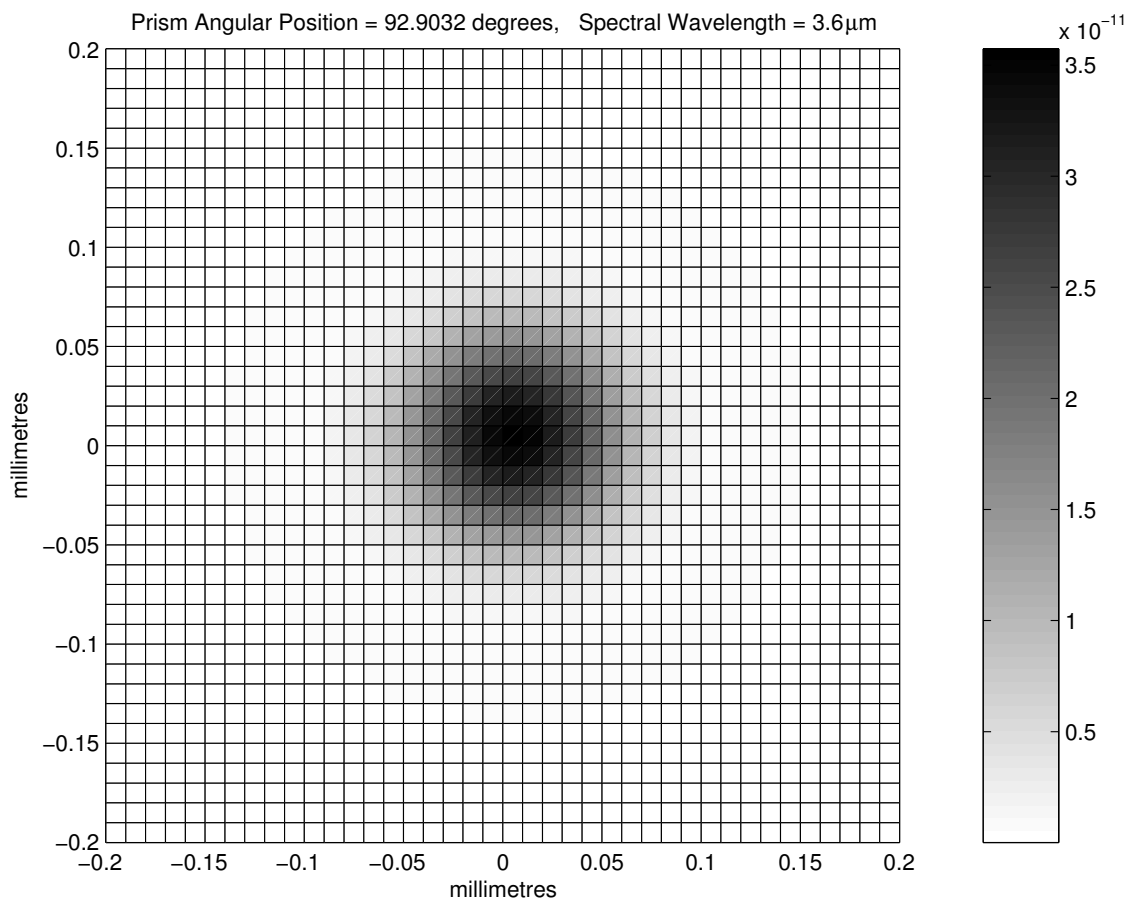
Figure 4.14:   Point Spread Function for 3.6 μm with Prism Angular Position at 92.9032 degrees from upright orientation. Location for the imaging area centre Point Spread Function in the Detector Focal Plane Array was determined using Fourier optics principles only.

the focal plane array available for detection with a focal plane array has been represented in the software model.

Transmission influences of optical materials used for the lenses and bulk media for the direct vision prism were only considered from an influencing phase perspective. Attenuation effects were not considered.

Atmospheric transmission characteristics related to extinction of electromagnetic radiation due to atmospheric absorption and scattering were not considered.
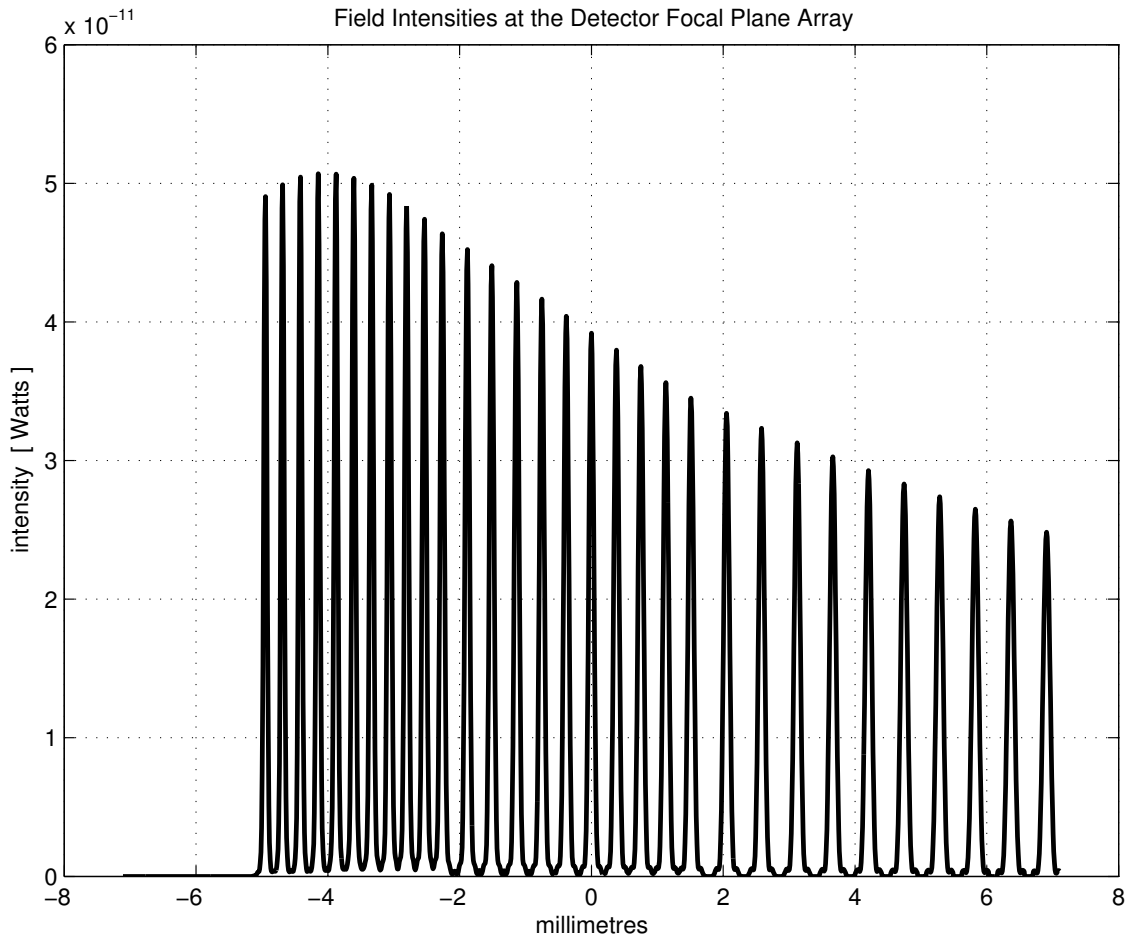
Figure 4.15:   Intensity profiles of the Point Spread Functions for all spectral wavelength bands of electromagnetic radiation between 2.0 μm and 5.0 μm.

The effects of a random atmosphere influencing the wavefront of electromagnetic radiation during the initial stage of propagation was not considered.

The remote scene scenario was simulated without the presence of background electromagnetic radiation.

The wave optics propagation was simulated for a stationary direct vision prism for each angular orientation of the prism. In collecting the spectral point spread functions through simulating wave optics propagation for one entire rotation cycle of the prism, a stationary direct vision prism was simulated at each different angular orientation of the prism. The collection of wave optics prop-

agations through the system for different angular orientations simulated the wave optics simulation of the system for a rotating prism.

V. Conclusions

Hyperspectral imaging systems passively sense radiant electromagnetic energy from a remote scene to form a three dimension profile of the remote scene. The data contained in this profile describes real images of the remote scene (two spatial dimensions) for a certain number of spectral wavelength bands across a finite spectral range of electromagnetic radiation (one spectral dimension). Typical grating type hyperspectral imaging systems collect spectral electromagnetic radiation in the visible and near infrared spectral range, by incrementally scanning across the spatial extent of the remote scene. Due to the very low optical throughput used in these systems, a legacy of the optical techniques employed to scan for spectral and spatial information, adapting these systems for spectral ranges extending into the mid wave and long wave infrared is difficult. Since features in the remote scene at infrared spectral wavelengths have characteristically low contrast between radiant energy levels emitted from remote features, hyperspectral imaging in the infrared demands higher optical throughput techniques to overcome the low contrast challenges with existing hyperspectral imaging systems.

The chromotomographic imaging system was developed by Jonathon M. Mooney and colleagues of AFRL/SNHI at Hanscom Air Force Base [4–6], utilising an optical system that angularly multiplexes the spatial electromagnetic radiation collected from a remote scene onto a focal plane array detector, to provide significantly greater optical throughput for collecting radiant electromagnetic energy from remote scenes. A rotating prism disperses the collected electromagnetic radiation according to the finite spectral range of wavelength bands to be used with obtaining spectral real images as a hyperspectral real image data set of the remote scene. The CTIS has been reported to demonstrate reasonable quality hyperspectral images for finite spectral ranges in the mid wave and long wave infrared.

This thesis investigates the design for a software model that emulates the attributes of the optics system loosely detailed in reports of the CTIS. Using optics principles and wave optics

propagation theory, the software model has been designed to simulate the point spread function characteristics of the optics system in the chromotomographic real image plane. The software model can be used as an aid to develop and test the characteristics of an optics system through simulation, or simulate acquiring actual chromotomographic real image based on spectral information about a remote scene, or explore certain hyperspectral image reconstruction techniques suited to the chromotomograhic imaging system.

5.1 Software Model

The software model developed in this research simulates the spectral point spread functions and chromotomographic point spread functions characterising the chromotomographic sensor for the chromotomographic imaging system. The design of the software model was founded on the optics principles related by geometric optics, Fourier optics, and wave optics propagation.

Geometric optics principles were used to examine the propagation of the electromagnetic radiation using ray tracing principles. These principles enabled an appreciation of the aperture sizes, focussing lengths for real imaging, and dispersion angles through the sensor optics system to be evaluated. Use of Snell's Law of Refraction and the Lensmaker's formula also aided with gaining an appreciation of the system.

Fourier optics principles were used to guide the expectation of wavefront behaviour at certain apertures throughout the software model design, plus serve as the foundation to establish the spatial sampling requirements for each significant aperture in the sensor optics system. In establishing the spatial sampling requirements, general optics principles describing: where real images at the remote scene would be expected, at the field stop and the focal plane array; the differences between coherent and incoherent imaging systems, where the cut-off spatial frequency for an incoherent imaging system is double the cut-off frequency for a coherent imaging system, results in the number of spatial samples required to sample the electromagnetic field across the forward lens evaluated as

half the number of spatial samples evident in the remote scene. This outcome achieved a noticeable reduction in computation workload for wave optic propagation using the Rayleigh Sommerfield diffraction formula.

Fourier optics principles proved useful only as a start for obtaining the true relationship between the detector focussing lens and the focal plane array. The software model delivered a wave optics simulated wavefront with characteristics that deviated sufficiently from Fourier optics principles to required further processing of spatial data with the radial search technique to locate each spectral point spread function accurately.

Wave optics principles were used to represent the simulated wavefront propagation through all stages of the simulated chromotomographic sensor, characterised by Rayleigh-Sommerfield diffraction theory. The Rayleigh-Sommerfield diffraction formula was modified to a numeric expression that aligned with the discrete sampling requirements adopted for each significant aperture in the sensor optics system.

The algorithms used in the MatLab® functions for the software model are explained in Chapter III. A step-by-step process for using the MatLab® functions to develop the system parameters for a simulated software model of the chromotomographic sensor has been detailed in Chapter IV. Results for a simulated sensor optics system are also presented in Chapter IV, including the requirement to improve the accuracy of the algorithms used to simulate the final wave optics stage of propagation in the detector optics system.

The software suite can be adapted to simulate a sensor optics system suited for hyperspectral imaging over a different finite spectral range of electromagnetic radiation from the remote scene. This would only require the use of different optical material characteristics, say index of refraction parameters, and other system parameters discussed in Chapter IV to achieve a different system configuration with the same software suite.

The software suite developed during this research is intended to be a versatile baseline for developing simulated point spread functions results for chromotomographic sensor designs. Use of the software suite presented in this thesis used system parameters suited for the MWIR spectral range to simulate the design configuration of the chromotomographic sensor. The versatility of the software suite enables different optical material characteristics, say index of refraction parameters, and other system parameters discussed in Chapter IV to be used to tailor the simulated chromotomographic sensor design for different spectral ranges of electromagnetic radiation from the MWIR.

The baseline reached during this research for the software suite also enables the software model design to be adapted for further investigation into design attributes of the chromotomographic sensor, or possibly allow the option for progressively more complex additions to be incorporated in further revisions of the software model with further research.

5.2   *Research Motivation*

Motivation for improving upon the MASINT understanding of the radiant energy phenomenology in the fireball resulting from an explosion or explosions in the remote scene is the foundation of interest behind this research of the chromotomographic sensor. To capture the spectral and spatial details from transient events in the remote scene, such as explosions, in the context of hyperspectral imagery, a sensor with the optical throughput characteristics of the chromotomographic sensor is needed. Some questions of that foster the motivation behind this research are included in the following paragraph.

Is the size of the fireball, as a time resolved hyperspectral real image data set, have a spectral wavelength dependence ? What is the spectral and spatial profile of the detonation wavefront from the explosion creating the fireball ? Other research efforts at AFIT reveal from observations of explosions in the visible spectrum that radiant energy decay rates do not follow a Planckian trend.

What does the infrared spectrum reveal about the radiant energy decay rates from similar types of explosions ? Can the radial temperature gradient profile of the fireball be obtained from the spectral two dimension real images of the remote scene constructed from the radiant energy data collected at the detector focal plane array of the chromotomographic sensor ?

The chromotomographic sensor's high optical throughput feature offers the ability to collect the spectral electromagnetic radiation content from the remote scene to form a hyperspectral real image data set representing the remote scene in a significantly lower duration of time (seconds) compared with other grating type conventional scanning hyperspectral imaging systems (hours). This lower time duration with the staring chromotomographic sensor allows for speedier sequential collection over time of radiant energy from the remote scene to obtain a time resolved series of hyperspectral real image data sets representing the remote scene. Achieving time-resolved hyperspectral imagery of transient events elevates the dimensionality of for this type of imagery with the inclusion of time as a dimension to a four dimension real image data set.

The software model simulates the unit impulse response of the chromotomographic sensor as spectral point spread functions and chromotomographic point spread functions. In the context of modelling the radiant energy from explosions in the remote scene, collected by the chromotomographic sensor, the software model may be used to simulate an explosion (input) with unity magnitude across the spectral profile for detonation, the initial time period, of the explosion in the remote scene. This context of modelling would also rely on the radiant energy from the explosion being the significantly dominant source of radiant energy in the remote scene.

With its significantly greater optical throughput feature the chromotomographic sensor appears well suited for collecting the spectral content of radiant energy from explosions. Furthermore the software suite developed during this research is a useable software tool to simulate and evaluate different configurations for a chromotomographic sensor design.

Analysis of chromotomographic sensor system designs simulated with the software model is readily possible. A case in point is the intensity profile of spectral point spread functions between 2.0 μm and 5.0 μm shown in Figure 4.15, also shown at Figure 5.1 (a). An expectation of spectral point spread function spatial profiles is for the peak intensity to follow an increasing trend as the spectral wavelength of the point spread functions follows a decreasing trend. The conservation of energy collected at the focal plane array is the basis of this relationship, since the total energy (or total intensity) available for every spectral point spread function at the focal plane array should be the same (or very close).

The peak intensity relationship evident from the spatial profile slice of the simulated chromotomographic point spread function is the trend of increasing peak intensity does occur for spectral point spread functions above 3.6 μm. This spectral wavelength also coincided with the undeviated wavelength for the simulated chromotomographic sensor design. For spectral wavelengths below 3.6 μm the trend revealed from the software model shows the trend of peak intensity rolling off and tending to decrease with decreasing spectral point spread functions. This change in trend for the peak intensity of spectral point spread functions counters the intuitive relationship based on the conservation of energy. A possible conclusion assessed from this information may link this change in trend for the peak intensity to the undeviated wavelength of the simulated chromotomographic sensor.

Further information available from the software model, specifically the total intensities for every spectral wavefront of electromagnetic radiation as spectral point spread functions at the field stop and the focal plane array, allowed a comparison of the total intensity throughput between the field stop and the focal plane array based on the spectral content of electromagnetic radiation to be made. Figure 5.2 reveals the results of this comparison, where Figure 5.2 (a) shows the total spectral intensity at the field stop and focal plane array, and Figure 5.2 (b) shows the percentage
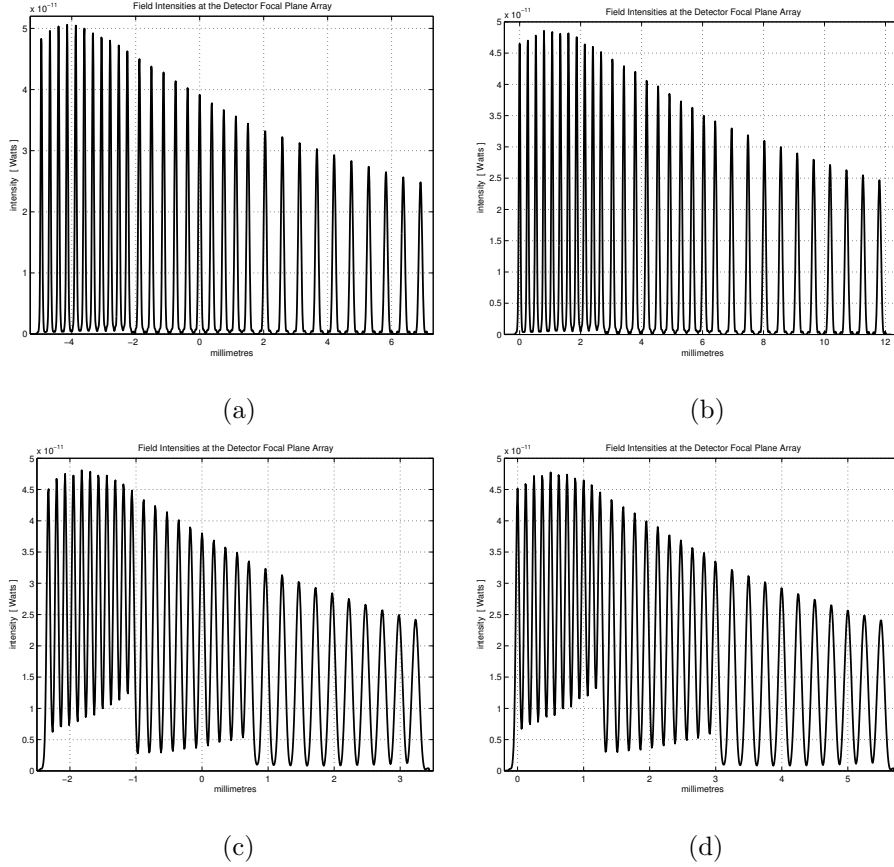
Figure 5.1:   Spectral Point Spread Function spatial profiles at the focal plane array between spectral wavelengths 2.0 μm and 5.0 μm for different simulated direct vision prism configurations, where (a) represents 3.6 μm undeviated spectral wavelength, prism entry surface angle of 30° 00′ 00″, prism exit surface angle of 23° 56′ 00″, (b) represents 2.0 μm undeviated spectral wavelength, prism entry surface angle of 30° 00′ 00″, prism exit surface angle of 24° 58′ 47″, (c) represents 3.6 μm undeviated spectral wavelength, prism entry surface angle of 15° 00′ 00″, prism exit surface angle of 11° 44′ 32″, and (d) represents 2.0 μm undeviated spectral wavelength, prism entry surface angle of 15° 00′ 00″, prism exit surface angle of 12° 17′ 41″.

loss in total spectral intensity between the field stop and focal plane array. Clearly a trend of declining percentage in total intensity throughput between the field stop and the focal plane array as the spectral point spread functions follow a trend of decreasing spectral wavelength. Furthermore this decrease gets more dramatic, losing from 22% to 58% of total intensity in the spectral point spread functions as the spectral wavelength decreases from 5.0 μm to 2.0 μm respectively.

Total spectral intensities are more revealing than following the trend of peak intensity for spectral point spread functions because the total spectral intensities revealed a definite trend of
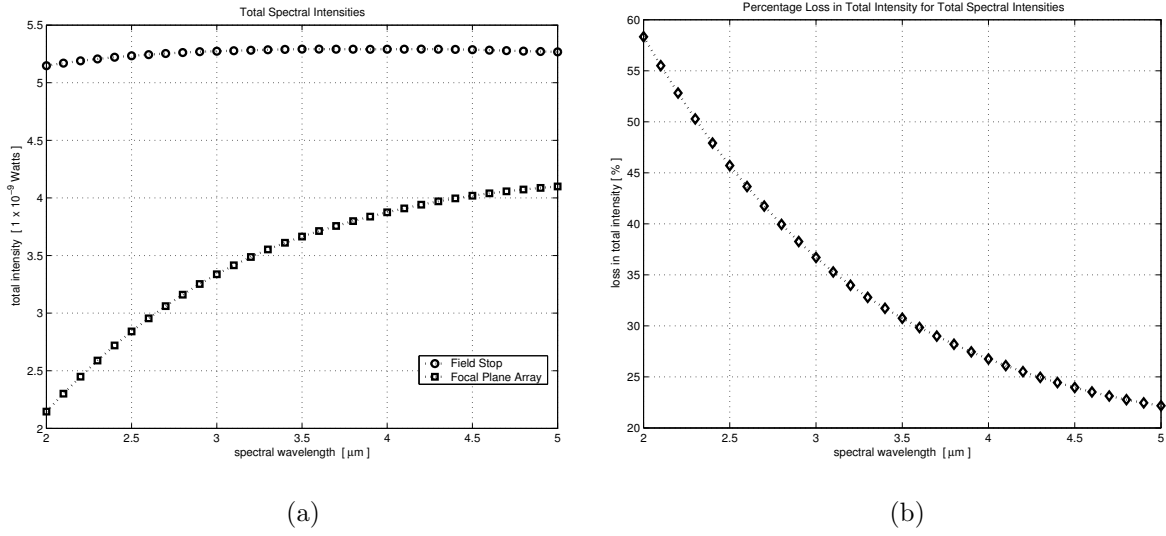
Figure 5.2:   Total spectral intensities between spectral wavelengths 2.0 μm and 5.0 μm at the field stop and the focal plane array (a), and (b) loss in total spectral intensity throughput between the field stop and the focal plane array for spectral point spread functions between spectral wavelengths 2.0 μm and 5.0 μm

spectral intensity throughput loss between the field stop and the focal plane array. Understanding whether design aspects of the simulated chromotomographic sensor influence the degree of total spectral intensity throughput loss forms the motivation for the following notes with investigating to a limited extent certain attributes of the sensor design between the field stop and the focal plane array.

Investigating the phenomenon of total spectral intensity throughput loss further, subtle changes to the simulated chromotomographic sensor design were made by varying the direct vision prism entry surface angle and exit surface angle systematically, and note the differences in the chromotomographic point spread function, spectral point spread functions and the total intensity available at the focal plane array. Figure 5.1 (b) through (d) are the chromotomographic point spread functions obtained for different simulated chromotomographic sensor design configurations. The simulated sensor design represented at Figure 5.1 (b) has the same direct vision prism aperture size and same prism entry surface angle of 30° from Figure 5.1 (a), however a different prism exit surface angle to accommodate an undeviated spectral wavelength of 2.0 μm. The simulated

sensor design represented at Figure 5.1 (c) has the same direct vision prism aperture size and same undeviated spectral wavelength of 3.6 μm from Figure 5.1 (a), however the prism entry surface angle was changed to 15° and the prism exit surface angle changed accordingly to accommodate the undeviated spectral wavelength. The simulated sensor design represented at Figure 5.1 (d) has the same direct vision prism aperture size and same prism entry surface angle from Figure 5.1 (c), however a different prism exit surface angle to accommodate an undeviated spectral wavelength of 2.0 μm.

Analysis of the total intensities for every spectral wavefront of electromagnetic radiation as spectral point spread functions at the field stop and the focal plane array revealed no discernible differences in total intensity values and percentage loss in total intensity throughput between the field stop and the focal plane array trends shown at Figure 5.2. This outcome suggests that varying the geometries of the direct vision prism entry and exit surfaces has no discernible influence on the total intensity throughput between the field stop and the focal plane array, however does influence the spatial profile of the spectral point spread functions and the chromotomographic point spread function.

The purpose for exploring the different configurations of the direct vision prism related to investigating whether these sensor design changes influenced the proportion of total spectral intensity throughput loss observed from analysis of the simulated chromotomographic sensor. The spectral wavefront fields simulated using wave optics propagation theory have some measure of wavefront error and establishing system design choices that influence the wavefront error may assist with some level of mitigating the loss in spectral total intensity throughput between the field stop and the focal plane array.

The aft lens aperture was the next system parameter evaluated as a candidate for potentially influencing the total spectral intensity throughput loss in the simulated chromotomographic sensor design. Two sensor design configurations were assessed through simulation, the only distinguishable
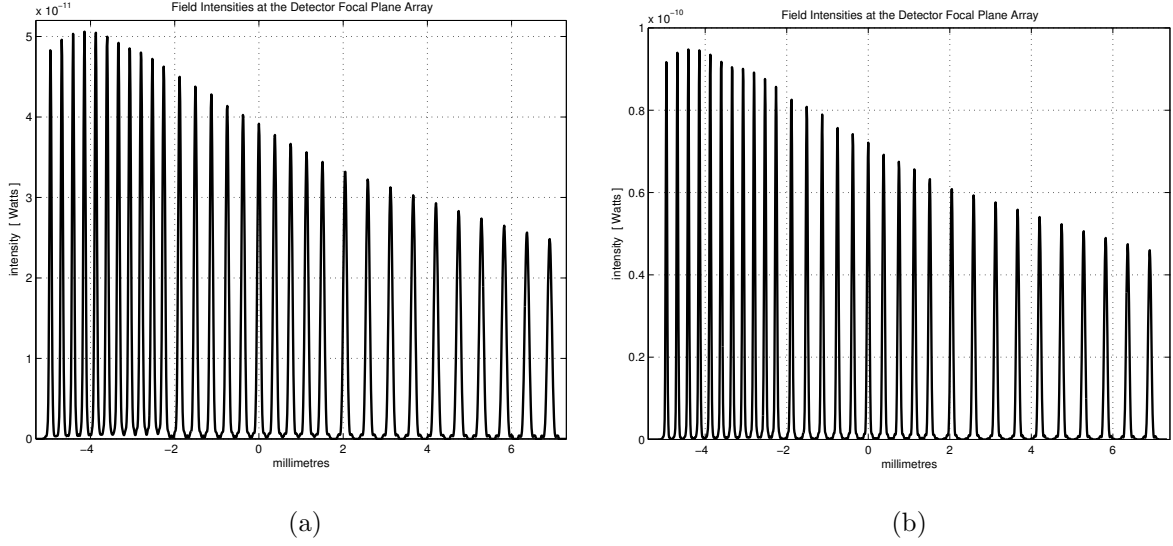
Figure 5.3: Spectral Point Spread Function spatial intensity profiles for, (a) the 22 mm diameter, and (b) the 30 mm diameter, aft lens aperture sensor design configurations between spectral wavelengths 2.0 μm and 5.0 μm

difference between these configurations being the diameter for the aft lens aperture. Figure 5.3 shows the simulated spatial profile of the chromotomographic point spread functions for each sensor design configuration where Figure 5.3 (a) simulates the sensor design with an aft lens diameter of 22 mm and direct vision prism diameter of 30 mm, and Figure 5.3 (b) simulates the sensor design with an aft lens diameter of 30 mm and direct vision prism diameter of 38 mm. The values used for the aft lens diameter were arbitrarily chosen, however the direct vision prism diameter values used were evaluated using the software suite to ensure a sensible software model was used to simulate the sensor design configurations.

Figure 5.3 (b) clearly reveals an increase in the peak intensities for every spectral point spread function and an increase in the peak intensities across the spatial profile of the chromotomographic point spread function at the focal plane array. Viewing the total spectral intensities for the spectral point spread functions at the field stop and the focal plane array respectively for the 30 mm aft lens diameter sensor design configuration at Figure 5.4 (a), and the previous chart at Figure 5.2 (a) for the 22 mm aft lens diameter sensor design configuration, these charts show a similar trend for
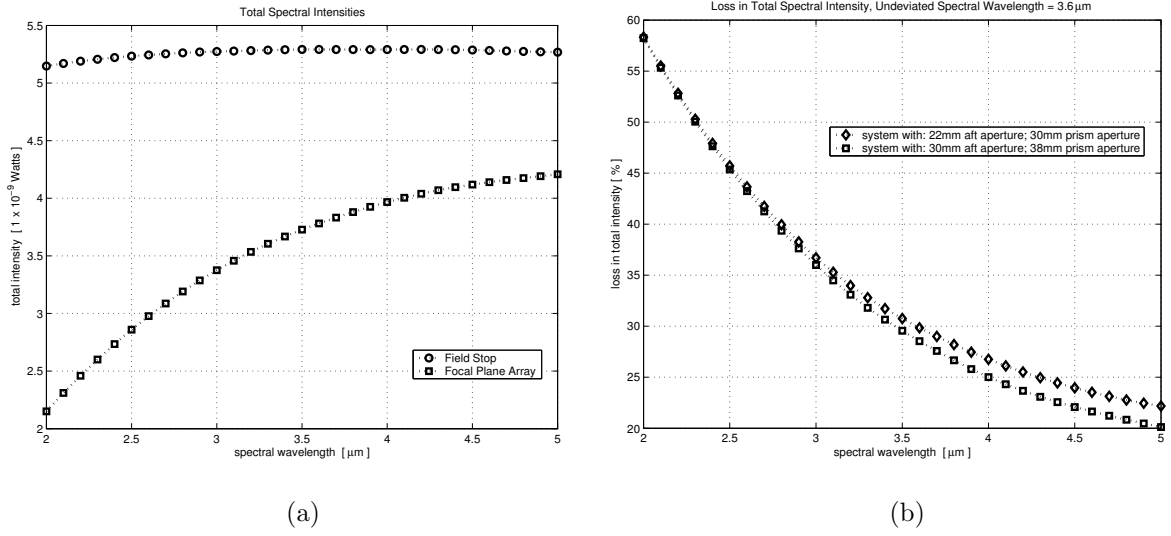
Figure 5.4: Total spectral intensities between spectral wavelengths 2.0 μm and 5.0 μm at the field stop and the focal plane array for, (a) the 30 mm diameter aft lens aperture sensor design configuration, and (b) comparison of loss in total spectral intensity throughput between the field stop and the focal plane array for spectral point spread functions between spectral wavelengths 2.0 μm and 5.0 μm for the 22 mm diameter and 30 mm diameter aft lens aperture sensor design configurations

total spectral intensities. Comparing the percentage loss in total spectral intensity throughput from the field stop to the focal plane array for both sensor design configurations, shown in the chart at Figure 5.4 (b), a noticeable reduction in total spectral intensity throughput loss is apparent for increasing spectral wavelengths. However, for spectral point spread functions tending toward the minimum spectral wavelength there is no appreciable difference in total spectral intensity throughput between the simulated sensor design configurations. This outcome is counter intuitive to the expected results from a physical sensor design with similar changes in design configuration.

Thorough analysis of the simulated sensor design configurations represented with the software model was not accomplished. Items worth investigating in the software model include the treatment of wavefront error in the wave optics propagation for the prism optics system and detector optics system, plus the spatial sampling criteria with respect to the aperture sizes presented in the various simulated sensor design configurations. The sampling criteria used in the software model seems to sufficiently sample all spectral wavefront fields nominated for simulation purposes, however

103

considering the spatial variation of the point spread functions for lower spectral wavelengths may dictate greater spatial sampling is required to improve the sampled spatial profile for these spectral wavelengths.

Aside from extending or investigating the software model design more thoroughly, there are other areas of further research related to the research effort reported in this thesis worthy of consideration and introduced in the following paragraphs.

5.4   Further Research

The software model developed in this research simulates the point spread functions characterising the sensor optics system for the chromotomographic imaging system. The design maturity of the software model would enable an optics technician or engineer to simulate a design configuration for the sensor optics system, and evaluate the spectral real imaging and chromotomographic real imaging aspects of this system design. Further research may be undertaken using this baseline of the software model to explore other aspects with simulating the design configuration for a sensor optic system, or evaluating digital post-processing techniques for the chromotomographic imaging system. Some areas of further research are mentioned and may contain far greater scope than the few lines allocated in the following paragraphs.

5.4.1   Chromotomographic Real Images.   Using the spectral radiant energy characteristics for an arbitrary remote scene, spectral real images in the chromotomographic real image plane can be obtained using the software model.

The spatial details of the remote scene for each spectral wavelength of incident electromagnetic radiation represents a different system input to the sensor optics system. The point spread function for each spectral wavelength of electromagnetic radiation represents a different system impulse response characterising the sensor optics system. Using linear system theory, a two dimension

convolution between each system input and each system impulse response may be used to obtain the system output for the respective system input.

Using the software model to simulate the system impulse response for each spectral wavelength of electromagnetic radiation at each angular position of rotation for the direct vision prism, a simulated system output can be obtained. The system outputs being the real image of the remote scene for each spectral wavelength of electromagnetic radiation at the detector focal plane array transverse plane. The collection of spectral real images for each angular position of rotation for the direct vision prism represents the chromotomographic real image of the remote scene.

The remote scene of interest is approximated as a two dimension spatial image even though the scene is actually three-dimensional event over time. Point spread functions characterising the simulated sensor optics system for different ranges from the forward lens can be developed with the software model (system impulse response) and convolved with the associated features from the remote scene (system inputs) to obtain a simulated representation of the chromotomographic real image of the remote scene (system output).

5.4.2 Physical System Parameters. The software model developed with this research does not have many of the practical influences evident with a physical sensor optics system included in the simulated system. Transmission characteristics of optical components, attenuation parameters characterising the extinction of radiant energy in the propagating spectral wavefronts due to atmospheric absorption and scattering, the presence of background radiant energy surrounding the remote scene and evident from the optical components used for the sensor optics system, collectively contribute as some of the added influences evident in a physical system. Other features of physical components in the sensor optics system that may warrant further research include the optical properties of the bulk media used in the direct vision prism varying due to temperatures, pressures, and operating environment. Similarly, influences with focal plane array non-uniformities in detecting the radiant intensity may be worth further study.

Developing versions of the software model that contain these influences would offer a closer simulation of the physical sensor optics system.

5.4.3   Maximum Acceptance Angle.   The size of the field stop aperture will influence the maximum acceptance angle subtended at the forward lens, between the optic axis and the location of a source of radiant electromagnetic energy in the remote scene. The size of the field stop aperture, the range distance of the remote scene from the forward lens, are aspects with the sensor optics system that can be evaluated with the software model to simulate the collection of radiant electromagnetic energy for different angular locations of remote scene sources. An evaluation of the maximum acceptance angle for the sensor optics system, based on the scenario of range and spatial extent used to represent the remote scene. Mean square error of the intensity profiles between point spread functions obtained for the simulated system for point sources located on the optic axis compared with point sources located some angular location from the optic axis, may be used to evaluate the maximum acceptance angle.

5.4.4   Radiometry.   The software model represents the wavefront propagation for spectral fields of electromagnetic radiation as point spread functions. The radiant energy used for these spectral fields is a 1 watt source emitting spherical wavefronts of electromagnetic radiation spatially across a complete spherical surface. Whatever fraction of this radiant energy incident on the forward lens is represented as an electromagnetic field in the software model. Photon energy emission is the source of this radiant energy, so characterising the radiometric aspects of this radiant energy for an arbitrary remote scene would provide a connection with the photon phenomena occurring in the remote scene.

The spectral fields of electromagnetic radiation collected by the sensor optics system originate from the radiant energy emissions from features in the remote scene. This radiant energy occurs from photon emissions in the remote scene, where each photon emission is a quantised amount of

energy according to spectral wavelength ν characterising the photon energy emission, as described by equation 5.1.

$$E = h\nu = h\left(\frac{c}{n\lambda}\right) \tag{5.1}$$

From the spectral real images of the remote scene. the phenomena of photon emissions may be derived from the fields of spectral electromagnetic radiation represented in the software model. Photons with low oscillation have low energy and high spectral wavelength, whereas photons with high oscillation have high energy and low spectral wavelength.

5.4.5 Digital Post-Processing Techniques. A further research area extending from developing chromotomographic real images mentioned in section 5.4.1 would be exploring different digital post-processing techniques like the pseudo inverse method [5,6] for assembling a hyperspectral data set of spectral real images of the remote scene from the collection of chromotomographic real images available at the detector focal plane array.

Appendix A.   Alternate Interpretations of the Sensor Optics System

A.1   Linear System Interpretation
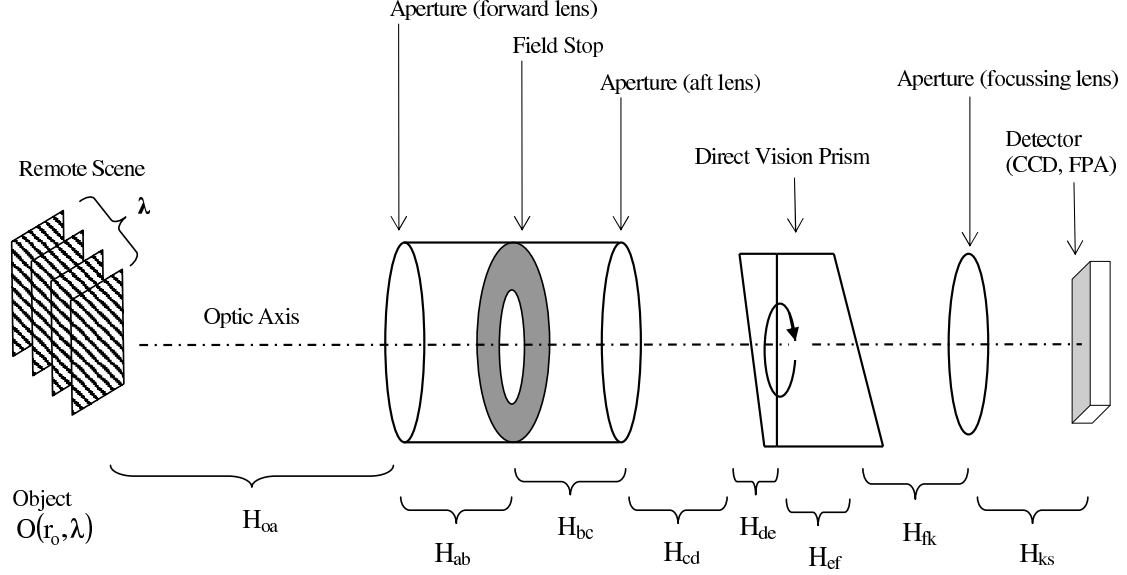
Figure A.1:   Linear Systems Interpretation of Sensor Optics System

The following stages of propagation. The symbols used, O represents the spectral wavelength electromagnetic field as spatial information for objects or subjects of interest observed in the remote scene, B represents the background spectral wavelength electromagnetic field propagating from the surrounding environment for the stage of propagation, τ represents the extinction function for the stage of propagation, r represents the position reference as a radial distance from the optic axis for locations in the spectral wavelength electromagnetic field for stages of propagation, λ represents the spectral wavelengths under examination with the sensor optics system, g represents the output electromagnetic field for a stage of propagation and the input electromagnetic field for the following stage of propagation.

Implementing a simple version of the model with these expressions can be done with considering the background radiation parameter B set to zero, thereby removing any background radiation effects in the model, and the extinction function parameter τ set to unity, thereby operating the

system in an atmospheric environment with no magnitude attenuation of electromagnetic radiation from propagating through the atmosphere. Results of this simple model are presented for different transverse planes along the optic axis that represent different stages of the radiation (broadband signal) propagation through the forward optics system. The general notation for each distinct transfer function between stages of propagation, H_{12}, subscript (1) represents the commencing system transverse plane and subscript (2) represents the concluding system transverse plane through the distinct stage of propagation characterised by the transfer function H_{12}.

A.1.1 Remote Scene.

$$B_o(r_o, \lambda) + O(r_o, \lambda)$$

A.1.2 Forward Optics (after Forward Lens).

$$g_a(r_a, \lambda) \; = \; H_{oa}(r_o \longrightarrow r_a, \lambda) \; \{ \; \tau_o(r_o, \lambda) \; [\; B_o(r_o, \lambda) + O(r_o, \lambda) \;] \; \}$$

A.1.3 Forward Optics (Field Stop).

$$g_b(r_b, \lambda) \; = \; H_{ab}(r_a \longrightarrow r_b, \lambda) \; \{ \; \tau_a(r_a, \lambda) \; [\; B_a(r_a, \lambda) + g(r_a, \lambda) \;] \; \}$$

A.1.4 Forward Optics (after Aft Lens).

$$g_c(r_c, \lambda) \; = \; H_{bc}(r_b \longrightarrow r_c, \lambda) \; \{ \; \tau_b(r_b, \lambda) \; [\; B_b(r_b, \lambda) + g(r_b, \lambda) \;] \; \}$$

A.1.5 Prism Optics (Entry Surface).

$$g_d(r_d, \lambda) \; = \; H_{cd}(r_d \longrightarrow r_c, \lambda) \; \{ \; \tau_c(r_c, \lambda) \; [\; B_c(r_c, \lambda) + g(r_c, \lambda) \;] \; \}$$

A.1.6 Prism Optics (Centre Surface).

$$g_e(r_e, \lambda) \; = \; H_{de}(r_d \longrightarrow r_e, \lambda) \; \{ \; \tau_d(r_d, \lambda) \; [\; B_d(r_d, \lambda) + g(r_d, \lambda) \;] \; \}$$

A.1.7   Prism Optics (Exit Surface).

$$g_f(r_f, \lambda) \; = \; H_{ef}(r_e \longrightarrow r_f, \lambda) \; \{ \; \tau_e(r_e, \lambda) \; [\; B_e(r_e, \lambda) + g(r_e, \lambda) \;] \; \}$$

A.1.8   Detector Optics (after Focussing Lens).

$$g_k(r_k, \lambda) \; = \; H_{fk}(r_f \longrightarrow r_k, \lambda) \; \{ \; \tau_f(r_f, \lambda) \; [\; B_f(r_f, \lambda) + g(r_f, \lambda) \;] \; \}$$

A.1.9   Detector Optics (Focal Plane Array).

$$g_s(r_s, \lambda) \; = \; H_{ks}(r_k \longrightarrow r_s, \lambda) \; \{ \; \tau_k(r_k, \lambda) \; [\; B_k(r_k, \lambda) + g(r_k, \lambda) \;] \; \}$$

Figure A.2:   Geometric Optics Interpretation of Sensor Optics System

Table A.1:   Matrices for Forward Section of the Sensor Optics System

Matrix	Expression	Description of Propagation
M_1	$\begin{bmatrix} 1 & z_1 \\ 0 & 1 \end{bmatrix}$	1st stage of propagation
M_2	$\begin{bmatrix} 1 & 0 \\ -\frac{1}{f_1} & 1 \end{bmatrix}$	2nd stage of propagation
M_3	$\begin{bmatrix} 1 & z_2 \\ 0 & 1 \end{bmatrix}$	3rd stage of propagation
M_4	$\begin{bmatrix} 1 & z_3 \\ 0 & 1 \end{bmatrix}$	4th stage of propagation
M_5	$\begin{bmatrix} 1 & 0 \\ -\frac{1}{f_2} & 1 \end{bmatrix}$	5th stage of propagation

Table A.2:   Matrices for Prism Section of the Sensor Optics System

Matrix	Expression	Description of Propagation
M_6	$\begin{bmatrix} 1 & z_4 \\ 0 & 1 \end{bmatrix}$	6th stage of propagation
M_7	$\begin{bmatrix} 1 & 0 \\ 0 & \frac{n_1}{n_2} \end{bmatrix}$	7th stage of propagation
M_8	$\begin{bmatrix} 1 & z_5 \\ 0 & 1 \end{bmatrix}$	8th stage of propagation
M_9	$\begin{bmatrix} 1 & 0 \\ 0 & \frac{n_2}{n_3} \end{bmatrix}$	9th stage of propagation
M_{10}	$\begin{bmatrix} 1 & z_6 \\ 0 & 1 \end{bmatrix}$	10th stage of propagation
M_{11}	$\begin{bmatrix} 1 & 0 \\ 0 & \frac{n_3}{n_4} \end{bmatrix}$	11th stage of propagation
M_{12}	$\begin{bmatrix} 1 & z_7 \\ 0 & 1 \end{bmatrix}$	12th stage of propagation

Table A.3:   Matrices for Aft Section of the Sensor Optics System

Matrix	Expression	Description of Propagation
M_{13}	$\begin{bmatrix} 1 & 0 \\ -\frac{1}{f_3} & 1 \end{bmatrix}$	13th stage of propagation
M_{14}	$\begin{bmatrix} 1 & z_8 \\ 0 & 1 \end{bmatrix}$	14th stage of propagation

Appendix B. Indexes of Refraction for Optical Materials in the Infrared

Indexes of refraction for optical materials that have relatively high transmission properties for the infrared spectrum of electromagnetic radiation have been collected. The properties of optical materials according to their respective indexes of refraction can be modelled using MATLAB®.

The tables below contain the spectral indexes of refraction for Lithium Fluoride (LiF), Barium Fluoride (BaF_2), Sodium Chloride (NaCl), Calcium Fluoride (CaF_2), and Sapphire (Al_2O_3), as optical materials of interest.

Table B.1:   Spectral Indexes of Refraction for Lithium Fluoride (LiF)

index of refraction	wavelength (λ) in μm
1.38711	1
1.37875	2
1.36660	3
1.34942	4
1.32661	5

Table B.2:   Spectral Indexes of Refraction for Barium Fluoride (BaF_2)

index of refraction	wavelength (λ) in μm
1.46856	1
1.46460	2
1.46115	3
1.45102	5
1.43566	7

Table B.3:   Spectral Indexes of Refraction for Sodium Chloride (NaCl)

index of refraction	wavelength (λ) in μm
1.5303	1.1786
1.5231	3.5359
1.51356	6.4825

Table B.4:   Spectral Indexes of Refraction for Calcium Fluoride (CaF$_2$)

index of refraction	wavelength (λ) in μm
1.42888	1
1.42385	2
1.41785	3
1.40963	4
1.39895	5
1.38559	6

Table B.5:   Spectral Indexes of Refraction for Sapphire (Al$_2$O$_3$)

index of refraction	wavelength (λ) in μm
1.74618	1.550
1.73748	2.010
1.73232	2.249
1.719	2.703
1.712	2.941
1.701	3.333
1.687	3.704
1.674	4.000
1.658	4.348
1.636	4.762
1.623	5.000
1.607	5.263

Appendix C. Software Suite

C.1 Simulated Chromotomographic Sensor

C.1.1 Sensor Optics System MatLab® Function.

```
% ----------------------------------------------------------------
% CTHIS_type_11c_prism_02.m
% ----------------------------------------------------------------
% -  computes the propagation of the electric field (denoted U),
%       starting at the transverse plane where the electric field
%       is denoted U_start, and ending at the transverse plane where
%       the electric field is denoted U_end.
% ----------------------------------------------------------------
% EENG799 (Independent Study)   Hyperspectral Chromotomography
% Date:  12 February 2004
% FLTLT Anthony J. Dearinger
% Royal Australian Air Force
% GE-04M
% ----------------------------------------------------------------


% ----------------------------------------------------------------
% START
% ----------------------------------------------------------------


% ----------------------------------------------------------------
clear all
% ----------------------------------------------------------------
prm = parameters;
% ----------------------------------------------------------------


% ----------------------------------------------------------------
sprintf('Computation for propagation to the FORWARD APERTURE PLANE has commenced')
% ----------------------------------------------------------------
[U_2a prm] = propagate_01_fwd_aperture(prm);
% ----------------------------------------------------------------
sprintf('Computation for propagation to the FORWARD APERTURE PLANE has completed')
% ----------------------------------------------------------------


% ----------------------------------------------------------------
sprintf('Computation for the FORWARD APERTURE has commenced')
% ----------------------------------------------------------------
[U_2b prm] = fwd_aperture(prm, U_2a);
% ----------------------------------------------------------------
sprintf('Computation for the FORWARD APERTURE has completed')
% ----------------------------------------------------------------


% ----------------------------------------------------------------
sprintf('Computation for propagation to the FIELD STOP PLANE has commenced')
% ----------------------------------------------------------------
[U_3a prm] = propagate_02_field_stop(prm, U_2b);
U_3b = U_3a;
% ----------------------------------------------------------------
sprintf('Computation for propagation to the FIELD STOP PLANE has completed')
% ----------------------------------------------------------------


% % ----------------------------------------------------------------
% sprintf('Computation for the FIELD STOP APERTURE has commenced')
% % ----------------------------------------------------------------
% [U_3b prm] = field_stop_aperture(prm, U_3a);
% % ----------------------------------------------------------------
% sprintf('Computation for the FIELD STOP APERTURE has completed')
% % ----------------------------------------------------------------
```

```
% ----------------------------------------------------------------
sprintf('Computation for propagation to the AFT APERTURE PLANE has commenced')
% ----------------------------------------------------------------
[U_4a prm] = propagate_03_aft_aperture(prm, U_3b);
% ----------------------------------------------------------------
sprintf('Computation for propagation to the AFT APERTURE PLANE has completed')
% ----------------------------------------------------------------


% ----------------------------------------------------------------
sprintf('Computation for the AFT APERTURE has commenced')
% ----------------------------------------------------------------
[U_4b prm] = aft_aperture(prm, U_4a);
% ----------------------------------------------------------------
sprintf('Computation for the AFT APERTURE has completed')
% ----------------------------------------------------------------


% ----------------------------------------------------------------
save  data_test_10a_prm  prm
clear  ans  prm
save  data_test_10a_field_optics
% ----------------------------------------------------------------
clear all
load  data_test_10a_prm
load  data_test_10a_field_optics
% ----------------------------------------------------------------


% ----------------------------------------------------------------
sprintf('Computation for propagation through the DIRECT VISION PRISM has commenced')
% ----------------------------------------------------------------
[U_5  prm  prism] = propagate_04_prism(prm, U_4b);
% ----------------------------------------------------------------
sprintf('Computation for propagation through the DIRECT VISION PRISM has completed')
% ----------------------------------------------------------------


% ----------------------------------------------------------------
save  data_test_10a_prm  prm
save  data_test_10a_field_prism  U_5
save  data_test_10a_field_prism_prm  prism
% ----------------------------------------------------------------
clear all
load  data_test_10a_prm
load  data_test_10a_field_prism
% ----------------------------------------------------------------


% ----------------------------------------------------------------
sprintf('Computation for propagation to the INFRA-RED DETECTOR has commenced')
% ----------------------------------------------------------------
U_6_search_1 = [];
U_6_search_2 = [];
U_6 = [];
% ----------------------------------------------------------------
[U_6_search_1, prm] = propagate_05_IR_array_01_search(prm, U_5);
% ----------------------------------------------------------------
% [U_6_search_2, prm] = propagate_05_IR_array_02_search(prm, U_5);
% ----------------------------------------------------------------
[U_6, prm] = propagate_05_IR_array_03_image(prm, U_5);
% ----------------------------------------------------------------
sprintf('Computation for propagation to the INFRA-RED DETECTOR has completed')
% ----------------------------------------------------------------


% ----------------------------------------------------------------
save  data_test_10a_prm  prm
save  data_test_10a_field_detector  U_6
% ----------------------------------------------------------------
```

```
clear all
load  data_test_10a_prm
load  data_test_10a_field_detector
%  ----------------------------------------------------------------

%  ----------------------------------------------------------------
sprintf(['Computation for assembling the Point Spread Functions '  ...
    'on the INFRA-RED DETECTOR ARRAY has commenced'])
%  ----------------------------------------------------------------
prm = assemble_PSF_on_IR_array(prm, U_6);
%  ----------------------------------------------------------------
sprintf(['Computation for assembling the Point Spread Functions '  ...
    'on the INFRA-RED DETECTOR ARRAY has completed'])
%  ----------------------------------------------------------------

%  ----------------------------------------------------------------
save  data_test_10a_prm  prm
%  ----------------------------------------------------------------

%  ----------------------------------------------------------------
%  END
%  ----------------------------------------------------------------
```

C.2 Wave Optics Propagation MatLab® Functions

C.2.1 Propagate from Remote Scene to Forward Lens Aperture.

```
function[U_end, prm] = propagate_01_fwd_aperture(prm);
% ----------------------------------------------------------------
%  propagate_01_fwd_aperture
% ----------------------------------------------------------------
%  -  computes the propagation of the electric field from the OBJECT PLANE (ie. INPUT SCENE)
%         to the FORWARD APERTURE PLANE.
%  -  computes the propagation of the electric field (denoted U), starting at the transverse plane
%         where the electric field is denoted U_start, and ending at the transverse plane where the
%         electric field is denoted U_end.
%  -  this function employs the Rayleigh-Sommerfield diffraction formula to describe the
%         propagation of a diverging EM radiation wavefront
% ----------------------------------------------------------------
%  EENG799 (Independent Study)   Hyperspectral Chromotomography
%  Date:  17 November 2003
%  FLTLT Anthony J. Dearinger
%  Royal Australian Air Force
%  GE-04M
% ----------------------------------------------------------------


% ----------------------------------------------------------------
%  START
% ----------------------------------------------------------------
sprintf('----------------------------------------------------------------')
sprintf('Propagation from the POINT SOURCE to the FORWARD APERTURE PLANE')
sprintf('----------------------------------------------------------------')
sprintf('Computation has commenced for all wavelengths')
% ----------------------------------------------------------------
prop_dist = [];
tempX  =  prm.pt_source_x_loc - prm.system.x2_index;
tempY  =  prm.pt_source_y_loc - prm.system.y2_index;
tempZ  =  prm.z1_range;
prop_dist = sqrt(tempX.^2  +  tempY.^2  +  tempZ.^2);
% ----------------------------------------------------------------


% ----------------------------------------------------------------
radiant_intensity = prm.amplitude / (4 * pi);   %  [watts per steradian]
% ----------------------------------------------------------------
%  solid angle - use small angle approximation for computing the solid angle
%  solid angle - use rectangular aperture to help with computing the distribution
%     of incident radiant flux across the aperture
% ----------------------------------------------------------------
%  solid angle - circular aperture
% solid_angle = (pi / 4) * (prm.dia_aperture_fwd^2 / prm.z1_range^2);   %  [steradians]
% ----------------------------------------------------------------
%  solid angle - rectangular aperture
solid_angle = prm.dia_aperture_fwd^2 / prm.z1_range^2;   %  [steradians]
% ----------------------------------------------------------------
incident_flux = radiant_intensity * solid_angle;   %  [watts]
% ----------------------------------------------------------------
%  sampled_incident_flux - use small angle approximation, therefore assume flux is
%     uniformly distributed across the forward aperture
% ----------------------------------------------------------------
sampled_incident_flux = incident_flux / (prm.pts * prm.pts) *  ...
    prm.system.dx1 * prm.system.dy1;
% ----------------------------------------------------------------
c = 299792458;   %  [metre / sec], speed of light
permitivity_free_space = 8.85e-12;   %  [sec^2 Coulombs^2 / (metre^3 - kilogram)]
% ----------------------------------------------------------------
sampled_field_amplitude = sqrt(sampled_incident_flux / c / permitivity_free_space);
% ----------------------------------------------------------------
```

```
% -----------------------------------------------------------------
for s1 = 1 : prm.lambda_bands
    U_end(:,:,s1) = sampled_field_amplitude(:,s1) .* exp(j * prm.k(s1) .* prop_dist);
end
% -----------------------------------------------------------------
sprintf('Computation has completed for all wavelengths')
sprintf('-------------------------------------------------------------')
% -----------------------------------------------------------------


% -----------------------------------------------------------------
return
% -----------------------------------------------------------------
%   END
% -----------------------------------------------------------------
```

```
function[U_end, prm] = propagate_02_field_stop(prm, U_start);
% ----------------------------------------------------------------
%  propagate_02_field_stop.m
% ----------------------------------------------------------------
%  -  computes the propagation of the electric field from the FORWARD APERTURE PLANE
%         to the FIELD STOP PLANE.
%  -  computes the propagation of the electric field (denoted U), starting at the transverse plane
%         where the electric field is denoted U_start, and ending at the transverse plane where the
%         electric field is denoted U_end.
% ----------------------------------------------------------------
%  EENG799 (Independent Study)   Hyperspectral Chromotomography
%  Date:  11 February 2004
%  FLTLT Anthony J. Dearinger
%  Royal Australian Air Force
%  GE-04M
% ----------------------------------------------------------------


% ----------------------------------------------------------------
%  START
% ----------------------------------------------------------------


% ----------------------------------------------------------------
sprintf('----------------------------------------------------------------')
sprintf('Propagation from the FORWARD APERTURE PLANE to the FIELD STOP PLANE')
sprintf('----------------------------------------------------------------')
sprintf('Computation has commenced for all wavelengths')
% ----------------------------------------------------------------


% ----------------------------------------------------------------
clear  temp*
% ----------------------------------------------------------------


% ----------------------------------------------------------------
lens_thick_fwd = [];
% ----------------------------------------------------------------
tempX = prm.system.x2_index;
tempY = prm.system.y2_index;
% ----------------------------------------------------------------
lens_thick_fwd = prm.delta_0_fwd  -  (tempX.^2 + tempY.^2 ) *  ...
    ( (prm.R1_fwd) / (2*(prm.R1_fwd)^2) - (prm.R2_fwd) / (2*(prm.R2_fwd)^2) );
% ----------------------------------------------------------------
prm.lens_thick_fwd = lens_thick_fwd;
% ----------------------------------------------------------------


% ----------------------------------------------------------------
%  expression A2 - lens thickness function
% ----------------------------------------------------------------
%  apply the lens thickness function to the phase of the electric field of the optical
%     electromagnetic radiation
% ----------------------------------------------------------------
for s1 = 1 : length(prm.lambda)
    U_start(:,:,s1) = U_start(:,:,s1) .*  ...
        exp(j * prm.k(s1) .* (lens_thick_fwd)*(prm.n_fwd - 1));
end
% ----------------------------------------------------------------


% ----------------------------------------------------------------
U_start = reshape(U_start, prm.pts, (prm.pts)*(prm.lambda_bands));
% ----------------------------------------------------------------
clear  temp*
% ----------------------------------------------------------------
temp_lambda = kron(prm.lambda, ones(prm.pts));
temp_K = kron(prm.k, ones(prm.pts));
```

```
% ------------------------------------------------------------------

% ------------------------------------------------------------------
for sX = 1 : prm.pts
    % --------------------------------------------------------------
    for sY = 1 : prm.pts
        % ----------------------------------------------------------
        tempX = prm.system.x2_index - prm.system.x3_index(sY,sX);
        tempY = prm.system.y2_index - prm.system.y3_index(sY,sX);
        tempZ = (prm.z2_fwd_focal)*(ones(prm.pts));
        % ----------------------------------------------------------
        prop_dist = [];
        prop_dist = sqrt( tempX.^2  +  tempY.^2  +  tempZ.^2 );
        % ----------------------------------------------------------

        % ----------------------------------------------------------
        % for s1 = 1 : length(prm.lambda)
        %     U_end(sY,sX,s1) = sum( sum( squeeze(U_start(:,:,s1)) .*  ...
        %         (exp(j * prm.k(s1) * dist_phase)) ) );
        % end
        % ----------------------------------------------------------
        %  comments
        %  -  U_start must not undergo the reshape at line 056 for this loop to work
        %  ----------------------------------------------------------

        % ----------------------------------------------------------
        %  expression A1 - approximated Rayleigh-Sommerfield diffraction propagation
        %  expression A1 - was originally used with lens thickness function
        %     (expression A2)
        %  ----------------------------------------------------------
        % temp_U  =  U_start ./ repmat(prop_dist, 1, prm.lambda_bands) .*  ...
        %     exp( j * kron(prm.k, ones(prm.pts)) .* repmat(prop_dist, 1, prm.lambda_bands) );
        %  ----------------------------------------------------------

        % ----------------------------------------------------------
        %  expression B1 - approximated Rayleigh-Sommerfield diffraction propagation
        %  expression B1 - more accurate numerical approximation compared to
        %     propagation using expression A1
        %  ----------------------------------------------------------
        temp_U_amplitude = sinc( repmat((prm.system.x3_index(sY,sX) * pi * prm.system.dx2),  ...
            prm.pts, prm.pts * prm.lambda_bands) ./ repmat(tempZ, 1, prm.lambda_bands) ./  ...
            temp_lambda ) .* ...
            sinc( repmat((prm.system.y3_index(sY,sX) * pi * prm.system.dy2),  ...
            prm.pts, prm.pts * prm.lambda_bands) ./ repmat(tempZ, 1, prm.lambda_bands) ./  ...
            temp_lambda ) .* ...
            prm.system.dy2 .* prm.system.dy2 .* repmat(tempZ, 1, prm.lambda_bands) ./  ...
            j ./ temp_lambda;
        % ----------------------------------------------------------
        temp_U  =  U_start .* temp_U_amplitude ./  ...
            repmat(prop_dist.^2, 1, prm.lambda_bands) .*  ...
            exp( j * temp_K .* repmat(prop_dist, 1, prm.lambda_bands) );
        % ----------------------------------------------------------
        temp_U = sum(temp_U);
        temp_U = sum( reshape(temp_U, prm.pts, prm.lambda_bands) );
        % ----------------------------------------------------------
        U_end(sY,sX,:) = temp_U;
        % ----------------------------------------------------------
        clear  temp_U*
        % ----------------------------------------------------------
    end
    % --------------------------------------------------------------
    sprintf('sX = %d', sX)
    % --------------------------------------------------------------
end
% ------------------------------------------------------------------
```

```
sprintf('Computation has completed for all wavelengths')
sprintf('------------------------------------------------------------------')
%   -------------------------------------------------------------


%   -------------------------------------------------------------
return
%   -------------------------------------------------------------
%   END
%   -------------------------------------------------------------
```

C.2.3 Propagate from Field Stop Aperture to Aft Lens Aperture.

```
function[U_end, prm] = propagate_03_aft_aperture(prm, U_start);
% ------------------------------------------------------------------
%  propagate_03_aft_aperture
% ------------------------------------------------------------------
%  -  computes the propagation of the electric field from the FIELD STOP PLANE
%         to the AFT APERTURE PLANE.
%  -  computes the propagation of the electric field (denoted U), starting at the transverse plane
%         where the electric field is denoted U_start, and ending at the transverse plane where the
%         electric field is denoted U_end.
% ------------------------------------------------------------------
%  EENG799 (Independent Study)   Hyperspectral Chromotomography
%  Date:  11 February 2004
%  FLTLT Anthony J. Dearinger
%  Royal Australian Air Force
%  GE-04M
%  ------------------------------------------------------------------


%  ------------------------------------------------------------------
%  START
%  ------------------------------------------------------------------


%  ------------------------------------------------------------------
sprintf('----------------------------------------------------------------')
sprintf('Propagation from the FIELD STOP PLANE to the AFT APERTURE PLANE')
sprintf('----------------------------------------------------------------')
sprintf('Computation has commenced for all wavelengths')
%  ------------------------------------------------------------------


%  ------------------------------------------------------------------
clear  temp*
%  ------------------------------------------------------------------


%  ------------------------------------------------------------------
U_start = reshape(U_start, prm.pts, (prm.pts)*(prm.lambda_bands));
%  ------------------------------------------------------------------
temp_lambda = kron(prm.lambda, ones(prm.pts));
temp_K = kron(prm.k, ones(prm.pts));
%  ------------------------------------------------------------------


%  ------------------------------------------------------------------
for sX = 1 : prm.pts
    %  --------------------------------------------------------------
    for sY = 1 : prm.pts
        %  ----------------------------------------------------------
        tempX = prm.system.x3_index - prm.system.x4_index(sY,sX);
        tempY = prm.system.y3_index - prm.system.y4_index(sY,sX);
        tempZ = (prm.z3_aft_focal)*(ones(prm.pts));
        %  ----------------------------------------------------------
        prop_dist = [];
        prop_dist = sqrt( tempX.^2  +  tempY.^2  +  tempZ.^2 );
        %  ----------------------------------------------------------


        %  ----------------------------------------------------------
        % for s1 = 1 : length(prm.lambda)
        %     U_end(sY,sX,s1) = sum( sum( squeeze(U_start(:,:,s1)) .*  ...
        %         (exp(j * prm.k(s1) * dist_phase)) ) );
        % end
        %  ----------------------------------------------------------
        %  comments
        %  -  U_start must not undergo the reshape at line 034 for this loop to work
        %  ----------------------------------------------------------


        %  ----------------------------------------------------------
```

```
%  expression A1 - approximated Rayleigh-Sommerfield diffraction propagation
        %  expression A1 - was originally used with lens thickness function
        %     (expression A2)
        %  --------------------------------------------------------------
% temp_U  = U_start ./ repmat(prop_dist, 1, prm.lambda_bands) .*  ...
%     exp( j * kron(prm.k, ones(prm.pts)) .* repmat(prop_dist, 1, prm.lambda_bands) );
%  --------------------------------------------------------------


        %  --------------------------------------------------------------
%  expression B1 - approximated Rayleigh-Sommerfield diffraction propagation
%  expression B1 - more accurate numerical approximation compared to
        %     propagation using expression A1
        %  --------------------------------------------------------------
        temp_U_amplitude = sinc( repmat((prm.system.x4_index(sY,sX) * pi * prm.system.dx3),  ...
            prm.pts, prm.pts * prm.lambda_bands) ./ repmat(tempZ, 1, prm.lambda_bands) ./  ...
            temp_lambda ) .* ...
            sinc( repmat((prm.system.y4_index(sY,sX) * pi * prm.system.dy3),  ...
            prm.pts, prm.pts * prm.lambda_bands) ./ repmat(tempZ, 1, prm.lambda_bands) ./  ...
            temp_lambda ) .* ...
            prm.system.dx3 .* prm.system.dy3 .* repmat(tempZ, 1, prm.lambda_bands) ./  ...
            j ./ temp_lambda;
        %  --------------------------------------------------------------
        temp_U  =  U_start .* temp_U_amplitude ./  ...
            repmat(prop_dist.^2, 1, prm.lambda_bands) .*  ...
            exp( j * temp_K .* repmat(prop_dist, 1, prm.lambda_bands) );
        %  --------------------------------------------------------------


        %  --------------------------------------------------------------
        temp_U = sum(temp_U);
        temp_U = sum( reshape(temp_U, prm.pts, prm.lambda_bands) );
        %  --------------------------------------------------------------
        U_end(sY,sX,:) = temp_U;
        %  --------------------------------------------------------------
        clear  temp_U*
        %  --------------------------------------------------------------
    end
    %  --------------------------------------------------------------
    sprintf('sX = %d', sX)
    %  --------------------------------------------------------------
end
%  --------------------------------------------------------------


%  --------------------------------------------------------------
lens_thick_aft = [];
%  --------------------------------------------------------------
tempX = prm.system.x4_index;
tempY = prm.system.y4_index;
%  --------------------------------------------------------------
lens_thick_aft  =  prm.delta_0_aft  -  (tempX.^2 + tempY.^2 ) *  ...
    ( (prm.R1_aft)/(2*(prm.R1_aft)^2) - (prm.R2_aft)/(2*(prm.R2_aft)^2) );
%  --------------------------------------------------------------
prm.lens_thick_aft = lens_thick_aft;
%  --------------------------------------------------------------


%  --------------------------------------------------------------
%  expression A2 - lens thickness function
%  --------------------------------------------------------------
%  apply the lens thickness function to the phase of the electric field of the optical
%     electromagnetic radiation
%  --------------------------------------------------------------
for s1 = 1 : length(prm.lambda)
    U_end(:,:,s1) = U_end(:,:,s1) .*  ...
        exp(j * prm.k(s1) .* (lens_thick_aft)*(prm.n_aft - 1));
end
%  --------------------------------------------------------------
```

```
clear  temp*;
%  ----------------------------------------------------------------


%  ----------------------------------------------------------------
sprintf('Computation has completed for all wavelengths')
sprintf('----------------------------------------------------------------')
%  ----------------------------------------------------------------


%  ----------------------------------------------------------------
return
%  ----------------------------------------------------------------
%  END
%  ----------------------------------------------------------------
```

C.2.4   Propagate through the Direct Vision Prism to Detector Focussing Lens.

```
function[U_end, prm, prism] = propagate_04_prism(prm, U_start);
% ----------------------------------------------------------------
% propagate_04_prism.m
% ----------------------------------------------------------------
% EENG799 (Independent Study)   Hyperspectral Chromotomography
% Date:  05 January 2004
% FLTLT Anthony J. Dearinger
% Royal Australian Air Force
% GE-04M
% ----------------------------------------------------------------

% ----------------------------------------------------------------
% START
% ----------------------------------------------------------------

% ----------------------------------------------------------------
% initialise the parameters for the direct vision prism
% ----------------------------------------------------------------
prm  =  prism_01_initialise(prm);
% ----------------------------------------------------------------

% ----------------------------------------------------------------
% define the parameters for the direct vision prism
% ----------------------------------------------------------------
prm  =  prism_02_parameters(prm);
% ----------------------------------------------------------------

% ----------------------------------------------------------------
% define the index of refraction for the centre wavelength of each
%    wavelength band at each stage of propagation through the
%    direct vision prism
% ----------------------------------------------------------------
prm  =  prism_03_refractive_index(prm);
% ----------------------------------------------------------------

% ----------------------------------------------------------------
% compute the angles of dispersion for the centre wavelength of each
%    wavelength band at each stage of propagation through the
%    direct vision prism
% ----------------------------------------------------------------
prm  =  prism_04_angles(prm);
% ----------------------------------------------------------------

% ----------------------------------------------------------------
% rotation of axes
% -  for CW prism rotation, axes must rotate CCW
% -  for CCW prism rotation, axes must rotate CW
% ----------------------------------------------------------------
% -  outputs are horizontal distances, and vertical distances according to
%        the rotation of each sample point of the field with respect to the prism
%        orientation
% ----------------------------------------------------------------
prm  =  prism_05_rotate_x4y4(prm);
% ----------------------------------------------------------------

% ----------------------------------------------------------------
% theoretical angles of dispersion
% ----------------------------------------------------------------
% -  compute the theoretical angles of dispersion for the centre wavelength of
%        each wavelength band due to propagating the electromagnetic field through
%        the direct vision prism
% -  the theoretical angles computed are the x-axis and y-axis components of the
%        angles of dispersion with respect to the transverse plane for the sensor
```

```matlab
%        coordinate system
% -  the theoretical angles are also computed for each position of rotation for
%       the direct vision prism, for CCW and CW prism rotation
% -  the theoretical angles will serve to aid with determining each location in
%       the detector focal plane array of the imaging centre for the point spread
%       function associated with the centre wavelength of each wavelength band
% ----------------------------------------------------------------
prm  =  prism_06_tilt_angles(prm);
% ----------------------------------------------------------------


% ----------------------------------------------------------------
%  propagate all points in transverse plane through the 1ST stage of propagation
% ----------------------------------------------------------------
% -  propagate from aft aperture to prism 1ST surface interface
% ----------------------------------------------------------------
% -  outputs are propagation distance, and vertical displacement
% ----------------------------------------------------------------


% ----------------------------------------------------------------
y1_total = reshape(prm.prism.y4_CCW,  ...
    (prm.pts * prm.pts * prm.prism.number_angles), 1);
% ----------------------------------------------------------------
z1_offset = y1_total .* tan(prm.prism.alpha_1);
%----------------------------------------------------------------
z1_total = prm.prism.z1_ref - z1_offset;   % [metres]
temp_r_1 = z1_total;
% ----------------------------------------------------------------
% --  propagation distance through the 1ST stage of propagation, r_1
% ----------------------------------------------------------------
r_1 = reshape(temp_r_1, prm.pts, prm.pts, prm.prism.number_angles);
% ----------------------------------------------------------------
%  comments
% -  r_1  ==>  columns read from TOP = r_1(1,:,:), to BOTTOM = r_1(prm.pts,:,:)
%        for the transverse plane to the optic axis
% ----------------------------------------------------------------


% ----------------------------------------------------------------
%  refraction of all points in transverse plane at the prism 1ST surface interface
% ----------------------------------------------------------------
%  propagate all points in transverse plane through the 2ND stage of propagation
% ----------------------------------------------------------------
% -  outputs are propagation distance, and vertical displacement
% ----------------------------------------------------------------


% ----------------------------------------------------------------
% --  refraction at the 1ST surface interface
% ----------------------------------------------------------------
temp_r_2 = prm.prism.thick_surf_1 ./  ...
    repmat(cos(prm.prism.beta_1b), (prm.pts * prm.pts * prm.prism.number_angles), 1);
% ----------------------------------------------------------------
% --  propagation distance through the 2ND stage of propagation, r_2
% ----------------------------------------------------------------
r_2 = reshape(temp_r_2, prm.pts, prm.pts, prm.prism.number_angles,  ...
    prm.lambda_bands);   % [metres]
% ----------------------------------------------------------------
% --  vertical offset displacement at the 2ND interface, y2_total
%        due to refraction and dispersion through the media of the
%        2ND stage of propagation
% ----------------------------------------------------------------
y2_total  =  temp_r_2 .*  ...
    repmat(sin(prm.prism.alpha_1 + prm.prism.beta_1b),  ...
    (prm.pts * prm.pts * prm.prism.number_angles), 1) + ...
    repmat(y1_total, 1, prm.lambda_bands);   % [metres]
% ----------------------------------------------------------------
```

```
% ----------------------------------------------------------------
% refraction of all points in transverse plane at the prism 2ND surface interface
% ----------------------------------------------------------------
% propagate all points in transverse plane through the 3RD stage of propagation
% ----------------------------------------------------------------
% -  outputs are propagation distance, and vertical displacement
% ----------------------------------------------------------------


% ----------------------------------------------------------------
% --  refraction at the 2ND surface interface
% ----------------------------------------------------------------
z2_ref = (prm.prism.height/2) * tan(prm.prism.alpha_1) + prm.prism.z2_min;   % [metres]
z2_offset = y2_total .* tan(prm.prism.alpha_1);   % [metres]
z2_total = z2_ref + z2_offset;   % [metres]
% ----------------------------------------------------------------
temp_r_3 = z2_total ./ repmat(cos(prm.prism.alpha_1 + prm.prism.beta_2b),  ...
    (prm.pts * prm.pts * prm.prism.number_angles), 1);   % [metres]
% ----------------------------------------------------------------
% --  propagation distance through the 3RD stage of propagation, r_3
% ----------------------------------------------------------------
r_3 = reshape(temp_r_3, prm.pts, prm.pts, prm.prism.number_angles,  ...
    prm.lambda_bands);   % [metres]
% ----------------------------------------------------------------
% --  vertical offset displacement at the 3RD interface, y3_total
%        due to refraction and dispersion through the media of the
%        3RD stage of propagation
% ----------------------------------------------------------------
y3_total  =  temp_r_3 .* repmat(sin(prm.prism.alpha_1 + prm.prism.beta_2b),  ...
    (prm.pts * prm.pts * prm.prism.number_angles), 1) + y2_total;   % [metres]
% ----------------------------------------------------------------
% comments
% -  r_3  ==>  columns read from TOP = r_3(1,:,:), to BOTTOM = r_3(prm.pts,:,:)
%       for the transverse plane to the optic axis
% -  y3_total  ==>  columns read from TOP = y3_total(1,:), to BOTTOM = y3_total(prm.pts,:)
%       for the transverse plane to the optic axis
% ----------------------------------------------------------------


% ----------------------------------------------------------------
% refraction of all points in transverse plane at the prism 3RD surface interface
% ----------------------------------------------------------------
% propagate all points in transverse plane through the 4TH stage of propagation
% ----------------------------------------------------------------
% -  outputs are propagation distance, and vertical displacement
% ----------------------------------------------------------------


% ----------------------------------------------------------------
% --  refraction at the 3RD surface interface
% ----------------------------------------------------------------
z3_ref = (prm.prism.height / 2) * tan(prm.prism.alpha_3) + prm.prism.z3_min;   % [metres]
r4_ref = cos(prm.prism.epsilon_3b) .\ z3_ref;   % [metres]
% ----------------------------------------------------------------
y4_ref = repmat( r4_ref .* sin(prm.prism.beta_3b),  ...
    (prm.pts * prm.pts * prm.prism.number_angles), 1) + y3_total;   % [metres]
% ----------------------------------------------------------------
r4_offset = sin(prm.prism.alpha_3) .* ( y4_ref ./  ...
    repmat(sin(pi / 2 - prm.prism.alpha_3 + prm.prism.beta_3b),  ...
    (prm.pts * prm.pts * prm.prism.number_angles), 1) );
% ----------------------------------------------------------------
temp_r_4 = repmat(r4_ref, (prm.pts * prm.pts * prm.prism.number_angles), 1) - r4_offset;
% ----------------------------------------------------------------
% --  propagation distance through the 4TH stage of propagation, r_4
% ----------------------------------------------------------------
r_4 = reshape(temp_r_4, prm.pts, prm.pts, prm.prism.number_angles,  ...
    prm.lambda_bands);   % [metres]
% ----------------------------------------------------------------
```

```
% --  vertical offset displacement at the 4TH interface, y4_total
%          due to refraction and dispersion through the media of the
%          4TH stage of propagation
% ----------------------------------------------------------------
y4_total = temp_r_4 .* repmat(sin(prm.prism.beta_3b),  ...
    (prm.pts * prm.pts * prm.prism.number_angles), 1) + y3_total;   % [metres]
% ----------------------------------------------------------------
% comments
% -  y4_ref  ==>  columns read from TOP = y4_ref(1,:), to BOTTOM = y4_ref(prm.pts,:)
%      for the transverse plane to the optic axis
% -  r4_offset  ==>  columns read from TOP = r4_offset(1,:), to BOTTOM = r4_offset(prm.pts,:)
%      for the transverse plane to the optic axis
% -  r_4  ==>  columns read from TOP = r_4(1,:), to BOTTOM = r_4(prm.pts,:)
%      for the transverse plane to the optic axis
% -  y4_total  ==>  columns read from TOP = y4_total(1,:), to BOTTOM = y4_total(prm.pts,:)
%      for the transverse plane to the optic axis
% ----------------------------------------------------------------
% comments
% -  propagation through the prism is treated as a collimated beam propagation.
% -  this means all distances computed, with respect to the refractive index of each media of
%      propagation, result is a phase translation for each point in the cross-section of the
%      beam of propagation.
% -  distance also affects the magnitude of the radiation for each point in the cross-section
%      of the beam of propagation, since distance has an inverse relation with magnitude.
% ----------------------------------------------------------------


% ----------------------------------------------------------------
% refraction of all points in transverse plane at the prism 4TH surface interface
% ----------------------------------------------------------------
% propagate all points in transverse plane through the 5TH stage of propagation
% ----------------------------------------------------------------
% -  outputs are propagation distance, and vertical displacement
% ----------------------------------------------------------------


% ----------------------------------------------------------------
% --  refraction at the 4TH surface interface
% ----------------------------------------------------------------
z5_offset = y4_total .* tan(prm.prism.alpha_3);   % [metres]
% ----------------------------------------------------------------
z5_total = prm.prism.z5_ref + z5_offset;   % [metres]
% ----------------------------------------------------------------
temp_r_5 = z5_total ./ repmat(cos(prm.prism.alpha_3 + prm.prism.beta_4b),  ...
    (prm.pts * prm.pts * prm.prism.number_angles), 1);   % [metres]
% ----------------------------------------------------------------
% --  propagation distance through the 5TH stage of propagation, r_5
%        to the focusing lens of the IR Detector
% ----------------------------------------------------------------
r_5 = reshape(temp_r_5, prm.pts, prm.pts, prm.prism.number_angles,  ...
    prm.lambda_bands);   % [metres]
% ----------------------------------------------------------------
% --  vertical offset displacement at the focussing lens of the IR detector,
%          y4_total due to refraction and dispersion through the media
%          (exiting the prism) of the 5TH stage of propagation
% ----------------------------------------------------------------
y5_total = temp_r_5 .* repmat(sin(prm.prism.alpha_3 + prm.prism.beta_4b), ...
    (prm.pts * prm.pts * prm.prism.number_angles), 1) + y4_total;   % [metres]
% ----------------------------------------------------------------


% ----------------------------------------------------------------
prism.r_1 = permute(r_1, [1  2  4  3]);
prism.r_2 = permute(r_2, [1  2  4  3]);
prism.r_3 = permute(r_3, [1  2  4  3]);
prism.r_4 = permute(r_4, [1  2  4  3]);
prism.r_5 = permute(r_5, [1  2  4  3]);
```

129

```
% -----------------------------------------------------------------
temp = [];
temp = repmat(y1_total, 1, prm.lambda_bands);
prism.y1_total = permute(temp, [1  2  4  3]);   % [metres]
% -----------------------------------------------------------------
temp = [];
temp = reshape(y2_total, prm.pts, prm.pts, prm.prism.number_angles,  ...
    prm.lambda_bands);   % [metres]
prism.y2_total = permute(temp, [1  2  4  3]);   % [metres]
% -----------------------------------------------------------------
temp = [];
temp = reshape(y3_total, prm.pts, prm.pts, prm.prism.number_angles,  ...
    prm.lambda_bands);   % [metres]
prism.y3_total = permute(temp, [1  2  4  3]);   % [metres]
% -----------------------------------------------------------------
temp = [];
temp = reshape(y4_total, prm.pts, prm.pts, prm.prism.number_angles,  ...
    prm.lambda_bands);   % [metres]
prism.y4_total = permute(temp, [1  2  4  3]);   % [metres]
% -----------------------------------------------------------------
temp = [];
temp = reshape(y5_total, prm.pts, prm.pts, prm.prism.number_angles,  ...
    prm.lambda_bands);   % [metres]
prism.y5_total = permute(temp, [1  2  4  3]);   % [metres]
% -----------------------------------------------------------------
temp = [];
temp = reshape(prm.prism.x4_CCW,  ...
    (prm.pts * prm.pts * prm.prism.number_angles), 1);   % [metres]
temp = repmat(temp, 1, prm.lambda_bands);
prism.x_total = permute(temp, [1  2  4  3]);
% -----------------------------------------------------------------


% -----------------------------------------------------------------
%  PART FIVE
% -----------------------------------------------------------------
%  PHASE effects upon the IR electromagnetic radiation
% -----------------------------------------------------------------
%  -  apply the phase effects due to propagation through the direct vision prism
% -----------------------------------------------------------------


% -----------------------------------------------------------------
clear  tempU*;
% -----------------------------------------------------------------
tempU = U_start;
% -----------------------------------------------------------------
tempU = reshape(tempU, (prm.pts * prm.pts), prm.lambda_bands);
tempU = repmat(tempU, prm.prism.number_angles, 1);
% -----------------------------------------------------------------
tempU1 = tempU .* exp( j * kron((prm.k .* prm.prism.n1),  ...
    ones((prm.pts * prm.pts * prm.prism.number_angles), 1)) .*  ...
    repmat(temp_r_1, 1, prm.lambda_bands) );
% -----------------------------------------------------------------
tempU2 = tempU1 .* exp( j * kron((prm.k .* prm.prism.n2),  ...
    ones((prm.pts * prm.pts * prm.prism.number_angles), 1)) .* temp_r_2 );
% -----------------------------------------------------------------
tempU3 = tempU2 .* exp( j * kron((prm.k .* prm.prism.n3),  ...
    ones((prm.pts * prm.pts * prm.prism.number_angles), 1)) .* temp_r_3 );
% -----------------------------------------------------------------
tempU4 = tempU3 .* exp( j * kron((prm.k .* prm.prism.n4),  ...
    ones((prm.pts * prm.pts * prm.prism.number_angles), 1)) .* temp_r_4 );
% -----------------------------------------------------------------
tempU5 = tempU4 .* exp( j * kron((prm.k .* prm.prism.n5),  ...
    ones((prm.pts * prm.pts * prm.prism.number_angles), 1)) .* temp_r_5 );
% -----------------------------------------------------------------
```

```
% -----------------------------------------------------------------
prism.U_5a = reshape(tempU1, prm.pts, prm.pts, prm.prism.number_angles,  ...
    prm.lambda_bands);
prism.U_5a = permute(prism.U_5a, [1  2  4  3]);
% -----------------------------------------------------------------
prism.U_5b = reshape(tempU2, prm.pts, prm.pts, prm.prism.number_angles,  ...
    prm.lambda_bands);
prism.U_5b = permute(prism.U_5b, [1  2  4  3]);
% -----------------------------------------------------------------
prism.U_5c = reshape(tempU3, prm.pts, prm.pts, prm.prism.number_angles,  ...
    prm.lambda_bands);
prism.U_5c = permute(prism.U_5c, [1  2  4  3]);
% -----------------------------------------------------------------
prism.U_5d = reshape(tempU4, prm.pts, prm.pts, prm.prism.number_angles,  ...
    prm.lambda_bands);
prism.U_5d = permute(prism.U_5d, [1  2  4  3]);
% -----------------------------------------------------------------
prism.U_5e = reshape(tempU5, prm.pts, prm.pts, prm.prism.number_angles,  ...
    prm.lambda_bands);
prism.U_5e = permute(prism.U_5e, [1  2  4  3]);
% -----------------------------------------------------------------
U_end = prism.U_5e;
% -----------------------------------------------------------------
clear  temp*;
% -----------------------------------------------------------------


% -----------------------------------------------------------------
%  PART SIX
% -----------------------------------------------------------------
%  TRANSLATION effects upon the IR electromagnetic radiation
% -----------------------------------------------------------------
%  -  apply the translation effects due to propagation through the direct vision prism
%  -  apply coordinate transfer from PRISM coordinates to SYSTEM coordinates
%  -  located at the focussing lens of the IR detector
% -----------------------------------------------------------------


% -----------------------------------------------------------------
%  clockwise (CW) rotation ==>
%     pol2cart( kron( -(prm.prism.rotate_angles).' + pi/2,  ...
%     ones( (prm.pts * prm.pts), prm.lambda_bands ) ), prism.y_total_offset );
%  counterclockwise (CCW) rotation ==>
%     pol2cart( kron( (prm.prism.rotate_angles).' + pi/2,  ...
%     ones( (prm.pts * prm.pts), prm.lambda_bands ) ), prism.y_total_offset );
% -----------------------------------------------------------------


% -----------------------------------------------------------------
%  compute the offset displacements for each discrete ordinate of sampled
%     electromagnetic radiation
% -----------------------------------------------------------------
prism.y_total_offset = y4_total - repmat(y1_total, 1, prm.lambda_bands);
prism.y_tilt = y5_total - y4_total;
% -----------------------------------------------------------------
temp_angles = kron( (prm.prism.rotate_angles).' + pi/2,  ...
    ones( (prm.pts * prm.pts), prm.lambda_bands ) );
[ temp_x5_offset  temp_y5_offset ] =  ...
    pol2cart(temp_angles, prism.y_total_offset + prism.y_tilt);
% -----------------------------------------------------------------


% -----------------------------------------------------------------
%  compute the ordinate transfer from prism coordinates to
%     system coordinates for each discrete ordinate of sampled
%     electromagnetic radiation
% -----------------------------------------------------------------
temp_system_x5_index = repmat( reshape(prm.system.x4_index, (prm.pts * prm.pts), 1),  ...
```

```
    prm.prism.number_angles, prm.lambda_bands );
temp_system_x5_index = temp_system_x5_index + temp_x5_offset;
% ----------------------------------------------------------------
temp_system_y5_index = repmat( reshape(prm.system.y4_index, (prm.pts * prm.pts), 1),  ...
    prm.prism.number_angles, prm.lambda_bands );
temp_system_y5_index = temp_system_y5_index + temp_y5_offset;
% ----------------------------------------------------------------
temp_system_x5_index = reshape(temp_system_x5_index, prm.pts, prm.pts,  ...
    prm.prism.number_angles, prm.lambda_bands);
prm.system.x5_index = permute(temp_system_x5_index, [1  2  4  3]);
% ----------------------------------------------------------------
temp_system_y5_index = reshape(temp_system_y5_index, prm.pts, prm.pts,  ...
    prm.prism.number_angles, prm.lambda_bands);
prm.system.y5_index = permute(temp_system_y5_index, [1  2  4  3]);
% ----------------------------------------------------------------


% ----------------------------------------------------------------
%  compute the spatial intervals between samples ordinates in
%     system coordinates for each discrete ordinate of sampled
%     electromagnetic radiation
% ----------------------------------------------------------------
%  s2 ==> angle of rotation for the direct vision prism
% ----------------------------------------------------------------
for s2 = 1 : prm.prism.number_angles;
    % ------------------------------------------------------------
    %  s1 ==> spectral wavelength bands of electromagnetic radiation
    % ------------------------------------------------------------
    for s1 = 1 : prm.lambda_bands
        % --------------------------------------------------------
        temp = [];
        temp = diff(prm.system.y5_index(:,:,s1,s2),[],1);
        prm.system.dy5(s1,s2) = abs(temp(1,1));
        % --------------------------------------------------------
        temp = [];
        temp = diff(prm.system.x5_index(:,:,s1,s2),[],2);
        prm.system.dx5(s1,s2) = abs(temp(1,1));
        % --------------------------------------------------------
    end
    % ------------------------------------------------------------
end
% ----------------------------------------------------------------

% ----------------------------------------------------------------
return
% ----------------------------------------------------------------
%  END
% ----------------------------------------------------------------
```

C.2.5.1   *Search for the actual peak intensity in vicinity of anticipated peak intensity location.*

```
function[U_end, prm] = propagate_05_IR_array_01_search(prm, U_start);
%  ----------------------------------------------------------------
%  propagate_05_IR_array_01_search.m
%  ----------------------------------------------------------------
%  -  computes the propagation of the electric field from the
%         IR DETECTOR LENS PLANE to the IR DETECTOR InSb ARRAY PLANE.
%  -  computes the propagation of the electric field (denoted U),
%         starting at the transverse plane where the electric field
%         is denoted U_start, and ending at the transverse plane where
%         the electric field is denoted U_end.
%  ----------------------------------------------------------------
%  EENG799 (Independent Study)   Hyperspectral Chromotomography
%  Date:  16 January 2004
%  FLTLT Anthony J. Dearinger
%  Royal Australian Air Force
%  GE-04M
%  ----------------------------------------------------------------


%  ----------------------------------------------------------------
%  START
%  ----------------------------------------------------------------


%  ----------------------------------------------------------------
sprintf('----------------------------------------------------------------')
sprintf('Propagation from the IR DETECTOR FOCUSSING LENS PLANE to')
sprintf('IR DETECTOR InSb ARRAY PLANE')
sprintf('----------------------------------------------------------------')
sprintf('Computation has commenced for all wavelengths and prism rotations')
%  ----------------------------------------------------------------


%  ----------------------------------------------------------------
%  establish some variables of interest
%  ----------------------------------------------------------------
clear  temp*
%  ----------------------------------------------------------------
tempX_start = reshape(prm.system.x5_index,  ...
    prm.pts, (prm.pts * prm.lambda_bands * prm.prism.number_angles));
tempY_start = reshape(prm.system.y5_index,  ...
    prm.pts, (prm.pts * prm.lambda_bands * prm.prism.number_angles));
%  ----------------------------------------------------------------


%  ----------------------------------------------------------------
%  compute the lens thickness function
%  -  thickness of the lens across the transverse plane to the
%         optic axis of the system
%  ----------------------------------------------------------------
lens_thick_detector = [];
%  ----------------------------------------------------------------
lens_thick_detector = prm.delta_0_detector  -  ...
    (tempX_start.^2 + tempY_start.^2) *  ...
    ( (prm.R1_detector) / (2*(prm.R1_detector)^2) -  ...
    (prm.R2_detector) / (2*(prm.R2_detector)^2) );
%  ----------------------------------------------------------------
prm.lens_thick_detector = lens_thick_detector;
%  ----------------------------------------------------------------


%  ----------------------------------------------------------------
%  re-establish some variables of interest
%  ----------------------------------------------------------------
```

```
clear  temp*
%  ----------------------------------------------------------------
tempX_start = prm.system.x5_index;
tempY_start = prm.system.y5_index;
tempZ = prm.focal_detector;
%  ----------------------------------------------------------------


%  ----------------------------------------------------------------
%  establish the IR radiation field, U_start, and the wavenumber parameter,
%     tempK, representing the wavenumber for each wavelength band at the
%     centre wavelength for each wavelength band
%  ----------------------------------------------------------------
U_start = reshape(U_start, prm.pts,  ...
    (prm.pts * prm.lambda_bands * prm.prism.number_angles));
%  ----------------------------------------------------------------
tempK = ones((prm.pts * prm.pts * prm.prism.number_angles), 1) * prm.k;
tempK = reshape(tempK, prm.pts, prm.pts, prm.prism.number_angles, prm.lambda_bands);
tempK = permute(tempK, [1 2 4 3]);
%  ----------------------------------------------------------------


%  ----------------------------------------------------------------
%  apply the PHASE effects introduced by the lens thickness function
%     to the optical IR radiation field propagating through the lens,
%     for each wavelength band of the optical IR electromagnetic radiation
%  ----------------------------------------------------------------
U_start = U_start .* exp( -j * (prm.n_detector - 1) * lens_thick_detector .*  ...
    reshape(tempK, prm.pts, (prm.pts * prm.lambda_bands * prm.prism.number_angles)) );
%  ----------------------------------------------------------------
U_start = reshape(U_start, prm.pts, prm.pts, prm.lambda_bands,  ...
    prm.prism.number_angles);
%  ----------------------------------------------------------------


%  ----------------------------------------------------------------
clear  lens_thick_detector  Xcentre  Ycentre
%  ----------------------------------------------------------------


%  ----------------------------------------------------------------
%  compute the centre for each location where point spread function (PSF)
%     is expected to be imaged on the IR detector focal plane array
%  ----------------------------------------------------------------
%  -  the centre for each PSF is based on:
%  ----------------------------------------------------------------
%  --   each rotation angle of the direct vision prism
%  --   each wavelength band represented by each centre wavelength
%  ----------------------------------------------------------------
Xcentre = - tempZ * sin(prm.prism.epsilon_4bX_CW);
Ycentre = - tempZ * sin(prm.prism.epsilon_4bY);
%  ----------------------------------------------------------------


%  ----------------------------------------------------------------
%  establish some variables of interest
%  ----------------------------------------------------------------
dx = prm.system.dx6;
dy = prm.system.dy6;
%  ----------------------------------------------------------------
Xsamples = 20;
Ysamples = 20;
%  ----------------------------------------------------------------
tempXsamples_total = 5 * (-Xsamples) : 5 * (Xsamples);
tempYsamples_total = 5 * (-Ysamples) : 5 * (Ysamples);
%  ----------------------------------------------------------------
tempXsamples_centre = 5 * (Xsamples) + 1;
tempYsamples_centre = 5 * (Ysamples) + 1;
%  ----------------------------------------------------------------
prm.detector.Xcentre_temp = Xcentre;
```

```
prm.detector.Ycentre_temp = Ycentre;
prm.detector.Xsamples_total = tempXsamples_total;
prm.detector.Ysamples_total = tempYsamples_total;
prm.detector.Xsample_distances = tempXsamples_total * dx;
prm.detector.Ysample_distances = tempYsamples_total * dy;
prm.detector.X_samples = length(prm.detector.Xsamples_total);
prm.detector.Y_samples = length(prm.detector.Ysamples_total);
prm.detector.Xsamples_centre = tempXsamples_centre;
prm.detector.Ysamples_centre = tempYsamples_centre;
%  ----------------------------------------------------------------


%  ----------------------------------------------------------------
%  s2 ==> angle of rotation for the direct vision prism
%  ----------------------------------------------------------------
for s2 = 1 : prm.prism.number_angles;
    %  ----------------------------------------------------------------
    %  comments
    %  -  only image points along the upright prism axis of dispersion
    %  ----------------------------------------------------------------
    %  s1 ==> spectral bands of radiation
    %  ----------------------------------------------------------------
    for s1 = 1 : prm.lambda_bands
        %  ----------------------------------------------------------------
        sX = 0;
        %  ----------------------------------------------------------------
        %  comments
        %  -  entire width of imaging area is sX = [ -Xsamples : Xsamples ]
        %  ----------------------------------------------------------------
        for sY = tempYsamples_total
            %  ----------------------------------------------------------------
            %  comments
            %  -  entire height of imaging area is sY = [ -Ysamples : Ysamples ]
            %  -  search for Ycentre is being conducted along a length that is
            %         5 times the size of the imaging area height
            %  ----------------------------------------------------------------


            %  ----------------------------------------------------------------
            %  CCW (counter-clockwise rotation)
            %  ----------------------------------------------------------------
            % temp_Xrotation = cos(prm.prism.rotate_angles(s2)) *  ...
            %     prm.detector.Xsample_distances(sX + tempXsamples_centre) -  ...
            %     sin(prm.prism.rotate_angles(s2)) *  ...
            %     prm.detector.Ysample_distances(sY + tempYsamples_centre);
            % temp_Yrotation = sin(prm.prism.rotate_angles(s2)) *  ...
            %     prm.detector.Xsample_distances(sX + tempXsamples_centre) +  ...
            %     cos(prm.prism.rotate_angles(s2)) *  ...
            %     prm.detector.Ysample_distances(sY + tempYsamples_centre);
            %  ----------------------------------------------------------------


            %  ----------------------------------------------------------------
            %  CW (clockwise rotation)
            %  ----------------------------------------------------------------
            temp_Xrotation = cos(prm.prism.rotate_angles(s2)) *  ...
                prm.detector.Xsample_distances(sX + tempXsamples_centre) +  ...
                sin(prm.prism.rotate_angles(s2)) *  ...
                prm.detector.Ysample_distances(sY + tempYsamples_centre);
            temp_Yrotation = - sin(prm.prism.rotate_angles(s2)) *  ...
                prm.detector.Xsample_distances(sX + tempXsamples_centre) +  ...
                cos(prm.prism.rotate_angles(s2)) *  ...
                prm.detector.Ysample_distances(sY + tempYsamples_centre);
            %  ----------------------------------------------------------------


            %  ----------------------------------------------------------------
            tempX_end((sY + tempYsamples_centre), s1, s2) =  ...
                temp_Xrotation + Xcentre(s1,s2);
```

```
        % ----------------------------------------------------------------
        tempY_end((sY + tempYsamples_centre), s1, s2) =  ...
            temp_Yrotation + Ycentre(s1,s2);
        % ----------------------------------------------------------------

        % ----------------------------------------------------------------
        tempX = [];
        tempX = tempX_end((sY + tempYsamples_centre), s1, s2) -  ...
            tempX_start(:,:,s1,s2);
        % ----------------------------------------------------------------
        tempY = [];
        tempY = tempY_end((sY + tempYsamples_centre), s1, s2) -  ...
            tempY_start(:,:,s1,s2);
        % ----------------------------------------------------------------
        prop_dist = [];
        prop_dist = sqrt( tempX.^2  +  tempY.^2  +  tempZ.^2 );
        % ----------------------------------------------------------------

        % ----------------------------------------------------------------
        clear  tempU*
        % ----------------------------------------------------------------
        tempU = squeeze(U_start(:,:,s1,s2)) ./ prop_dist .*  ...
            exp(-j * prop_dist .* tempK(:,:,s1,s2));
        % ----------------------------------------------------------------
        tempU = reshape(tempU, (prm.pts * prm.pts), 1);
        tempU = sum(tempU);
        % ----------------------------------------------------------------
        U_end((sY + tempYsamples_centre), s1, s2) = tempU;
        % ----------------------------------------------------------------
      end
      % --------------------------------------------------------------
    end
    % ----------------------------------------------------------------
    sprintf('prism angular position (s2) = %d of %d',  ...
        s2, prm.prism.number_angles)
    % ----------------------------------------------------------------
end
% ----------------------------------------------------------------

% ----------------------------------------------------------------
prm.detector.PSF_Xsamples_centre = tempX_end;
prm.detector.PSF_Ysamples_centre = tempY_end;
% ----------------------------------------------------------------

% ----------------------------------------------------------------
% find the peak intensity of the PSF samples, and the corresponding
%    index in the array, along the PSF centres radial for all spectral
%    wavelengths, for each angular position of prism rotation
% ----------------------------------------------------------------
tempU_end = reshape(U_end, length(tempYsamples_total),  ...
    prm.lambda_bands * prm.prism.number_angles);
[tempU_end_peak  tempU_end_peak_index] =  ...
    max((tempU_end .* conj(tempU_end)),[],1);
tempU_end_peak = reshape(tempU_end_peak,  ...
    prm.lambda_bands, prm.prism.number_angles);
tempU_end_peak_index = reshape(tempU_end_peak_index,  ...
    prm.lambda_bands, prm.prism.number_angles);
% ----------------------------------------------------------------
prm.detector.U_6_peak = tempU_end_peak;
prm.detector.U_6_peak_index = tempU_end_peak_index;
% ----------------------------------------------------------------

% ----------------------------------------------------------------
% use the corresponding index in the array to compute the offsets,
%    Xcentre_offset and Ycentre_offset, and thus aid with designating
```

```
%     the centres of the respective PSFs for all spectral wavelengths,
%     for each angular position of prism rotation
%  ----------------------------------------------------------------
%  s2 ==> angle of rotation for the direct vision prism
%  ----------------------------------------------------------------
for s2 = 1 : prm.prism.number_angles;
    %  ----------------------------------------------------------------
    %  s1 ==> spectral bands of radiation
    %  ----------------------------------------------------------------
    for s1 = 1 : prm.lambda_bands
        %  ----------------------------------------------------------------
        prm.detector.PSF_Xcentre_offset(s1,s2) = squeeze(prm.detector.  ...
            PSF_Xsamples_centre(tempU_end_peak_index(s1,s2),s1,s2)) -  ...
            Xcentre(s1,s2);
        prm.detector.PSF_Ycentre_offset(s1,s2) = squeeze(prm.detector.  ...
            PSF_Ysamples_centre(tempU_end_peak_index(s1,s2),s1,s2)) -  ...
            Ycentre(s1,s2);
        %  ----------------------------------------------------------------
    end
    %  ----------------------------------------------------------------
end
%  ----------------------------------------------------------------


%  ----------------------------------------------------------------
%  assign the ordinates, Xcentre and Ycentre, as centres of the respective
%     PSFs for all spectral wavelengths, for each angular position of
%     prism rotation
%  ----------------------------------------------------------------
prm.detector.PSF_Xcentre = Xcentre + prm.detector.PSF_Xcentre_offset;
prm.detector.PSF_Ycentre = Ycentre + prm.detector.PSF_Ycentre_offset;
%  ----------------------------------------------------------------
prm.detector.PSF_FPA_Xcentre = round(prm.detector.PSF_Xcentre / prm.system.dx6) *  ...
    prm.system.dx6;
prm.detector.PSF_FPA_Ycentre = round(prm.detector.PSF_Ycentre / prm.system.dy6) *  ...
    prm.system.dy6;
%  ----------------------------------------------------------------


%  ----------------------------------------------------------------
clear  temp*  prop_dist;
%  ----------------------------------------------------------------
sprintf('Computation has completed for all wavelengths and prism rotations')
sprintf('----------------------------------------------------------------')
%  ----------------------------------------------------------------


%  ----------------------------------------------------------------
return
%  ----------------------------------------------------------------
%  END
%  ----------------------------------------------------------------
```

```
function[U_end, prm] = propagate_05_IR_array_03_image(prm, U_start);
%  ----------------------------------------------------------------
%  propagate_05_IR_array_03_image.m
%  ----------------------------------------------------------------
%  -  computes the propagation of the electric field from the
%         IR DETECTOR LENS PLANE to the IR DETECTOR InSb ARRAY PLANE.
%  -  computes the propagation of the electric field (denoted U),
%         starting at the transverse plane where the electric field
%         is denoted U_start, and ending at the transverse plane where
%         the electric field is denoted U_end.
%  ----------------------------------------------------------------
%  EENG799 (Independent Study)   Hyperspectral Chromotomography
%  Date:  06 January 2004
%  FLTLT Anthony J. Dearinger
%  Royal Australian Air Force
%  GE-04M
%  ----------------------------------------------------------------


%  ----------------------------------------------------------------
%  START
%  ----------------------------------------------------------------


%  ----------------------------------------------------------------
sprintf('----------------------------------------------------------------')
sprintf('Propagation from the IR DETECTOR FOCUSSING LENS PLANE to')
sprintf('IR DETECTOR InSb ARRAY PLANE')
sprintf('----------------------------------------------------------------')
sprintf('Computation has commenced for all wavelengths and prism rotations')
%  ----------------------------------------------------------------


%  ----------------------------------------------------------------
%  establish some variables of interest
%  ----------------------------------------------------------------
clear  temp*
%  ----------------------------------------------------------------
tempX_start = reshape(prm.system.x5_index,  ...
    prm.pts, (prm.pts * prm.lambda_bands * prm.prism.number_angles));
tempY_start = reshape(prm.system.y5_index,  ...
    prm.pts, (prm.pts * prm.lambda_bands * prm.prism.number_angles));
%  ----------------------------------------------------------------
dx = prm.system.dx6;
dy = prm.system.dy6;
%  ----------------------------------------------------------------
Xsamples = 20;
Ysamples = 20;
Xsamples_centre = Xsamples + 1;
Ysamples_centre = Ysamples + 1;
%  ----------------------------------------------------------------


%  ----------------------------------------------------------------
%  compute the lens thickness function
%  -  thickness of the lens across the transverse plane to the
%         optic axis of the system
%  ----------------------------------------------------------------
lens_thick_detector = [];
%  ----------------------------------------------------------------
lens_thick_detector = prm.delta_0_detector  -  ...
    (tempX_start.^2 + tempY_start.^2) *  ...
    ( (prm.R1_detector) / (2*(prm.R1_detector)^2) -  ...
    (prm.R2_detector) / (2*(prm.R2_detector)^2) );
%  ----------------------------------------------------------------
prm.lens_thick_detector = lens_thick_detector;
```

```
% ----------------------------------------------------------------

% ----------------------------------------------------------------
%  re-establish some variables of interest
% ----------------------------------------------------------------
clear  temp*
% ----------------------------------------------------------------
tempX_start = prm.system.x5_index;
tempY_start = prm.system.y5_index;
tempZ = prm.focal_detector;
% ----------------------------------------------------------------

% ----------------------------------------------------------------
%  establish the IR radiation field, U_start, and the wavenumber parameter,
%     tempK, representing the wavenumber for each wavelength band at the
%     centre wavelength for each wavelength band
% ----------------------------------------------------------------
U_start = reshape(U_start, prm.pts,  ...
    (prm.pts * prm.lambda_bands * prm.prism.number_angles));
% ----------------------------------------------------------------
tempK = ones((prm.pts * prm.pts * prm.prism.number_angles), 1) * prm.k;
tempK = reshape(tempK, prm.pts, prm.pts, prm.prism.number_angles, prm.lambda_bands);
tempK = permute(tempK, [1 2 4 3]);
% ----------------------------------------------------------------

% ----------------------------------------------------------------
%  apply the PHASE effects introduced by the lens thickness function
%     to the optical IR radiation field propagating through the lens,
%     for each wavelength band of the optical IR electromagnetic radiation
% ----------------------------------------------------------------
U_start = U_start .* exp( -j * (prm.n_detector - 1) * lens_thick_detector .*  ...
    reshape(tempK, prm.pts, (prm.pts * prm.lambda_bands * prm.prism.number_angles)) );
% ----------------------------------------------------------------
U_start = reshape(U_start, prm.pts, prm.pts, prm.lambda_bands,  ...
    prm.prism.number_angles);
% ----------------------------------------------------------------

% ----------------------------------------------------------------
clear  lens_thick_detector  Xcentre  Ycentre
% ----------------------------------------------------------------

% % ----------------------------------------------------------------
% %  compute the centre for each location where point spread function (PSF)
% %     is expected to be imaged on the IR detector focal plane array
% % ----------------------------------------------------------------
% %  -  the centre for each PSF is based on:
% % ----------------------------------------------------------------
% %  --   each rotation angle of the direct vision prism
% %  --   each wavelength band represented by each centre wavelength
% % ----------------------------------------------------------------
% Xcentre = - tempZ * sin(prm.prism.epsilon_4bX_CW);
% Ycentre = - tempZ * sin(prm.prism.epsilon_4bY);
% % ----------------------------------------------------------------

% ----------------------------------------------------------------
%  establish some variables of interest
% ----------------------------------------------------------------
prm.detector.Xsamples = [];
prm.detector.Xsamples = [-Xsamples : Xsamples];
prm.detector.Ysamples = [];
prm.detector.Ysamples = [-Ysamples : Ysamples];
prm.detector.Xsample_distances = [];
prm.detector.Xsample_distances = [-Xsamples : Xsamples] * dx;
prm.detector.Ysample_distances = [];
prm.detector.Ysample_distances = [-Ysamples : Ysamples] * dy;
```

```matlab
% ---------------------------------------------------------------

% ---------------------------------------------------------------
for s2 = 1 : prm.prism.number_angles
    % ---------------------------------------------------------------
    for s1 = 1 : prm.lambda_bands
        % ---------------------------------------------------------------
        for sX = prm.detector.Xsamples
            % ---------------------------------------------------------------
            for sY = prm.detector.Ysamples
                % ---------------------------------------------------------------
                tempX_end = [];
                tempX_end = (sX * dx) + prm.detector.PSF_FPA_Xcentre(s1,s2);
                % ---------------------------------------------------------------
                tempY_end = [];
                tempY_end = (sY * dy) + prm.detector.PSF_FPA_Ycentre(s1,s2);
                % ---------------------------------------------------------------
                tempX = [];
                tempX = tempX_end - tempX_start(:,:,s1,s2);
                % ---------------------------------------------------------------
                tempY = [];
                tempY = tempY_end - tempY_start(:,:,s1,s2);
                % ---------------------------------------------------------------
                prop_dist = [];
                prop_dist = sqrt( tempX.^2  +  tempY.^2  +  tempZ.^2 );
                % ---------------------------------------------------------------


                % ---------------------------------------------------------------
                clear  temp_U*
                % ---------------------------------------------------------------


                % ---------------------------------------------------------------
                % expression A - approximated Rayleigh-Sommerfield diffraction propagation
                % expression A - was originally used
                % ---------------------------------------------------------------
                % temp_U = squeeze(U_start(:,:,s1,s2)) ./ prop_dist .*  ...
                %     exp(-j * prop_dist .* tempK(:,:,s1,s2));
                % ---------------------------------------------------------------


                % ---------------------------------------------------------------
                % expression B - approximated Rayleigh-Sommerfield diffraction propagation
                % expression B - more accurate numerical approximation compared to
                %     propagation using expression A
                % ---------------------------------------------------------------
                temp_U_amplitude =  ...
                    sinc( (sX * dx) * pi * prm.system.dx5(s1,s2) ./ tempZ ./  ...
                    prm.lambda(s1) ) .* ...
                    sinc( (sY * dy) * pi * prm.system.dy5(s1,s2) ./ tempZ ./  ...
                    prm.lambda(s1) ) .* ...
                    prm.system.dx5(s1,s2) .* prm.system.dy5(s1,s2) .* tempZ ./  ...
                    j ./ prm.lambda(s1);
                % ---------------------------------------------------------------
                temp_U  =  U_start(:,:,s1,s2) .* temp_U_amplitude ./ prop_dist.^2 .*  ...
                    exp(-j * prm.k(s1) .* prop_dist);
                % ---------------------------------------------------------------


                % ---------------------------------------------------------------
                temp_U = reshape(temp_U, (prm.pts * prm.pts), 1);
                temp_U = sum(temp_U);
                % ---------------------------------------------------------------
                U_end((sY + Ysamples_centre),(sX + Xsamples_centre),s1,s2) = temp_U;
                % ---------------------------------------------------------------
            end
            % ---------------------------------------------------------------
        end
```

```
        %  ----------------------------------------------------------------
    end
    %  ------------------------------------------------------------------
    sprintf('prism angular position (s2) = %d of %d',  ...
        s2, prm.prism.number_angles)
    %  ------------------------------------------------------------------
end
%  ----------------------------------------------------------------


%  ----------------------------------------------------------------
clear  temp*  prop_dist;
%  ----------------------------------------------------------------
sprintf('Computation has completed for all wavelengths and prism rotations')
sprintf('-----------------------------------------------------------------')
%  ----------------------------------------------------------------


%  ----------------------------------------------------------------
return
%  ----------------------------------------------------------------
%  END
%  ----------------------------------------------------------------
```

Bibliography

1. "The AVIRIS (Airborne Visible / Infrared Imaging Spectrometer) Homepage." http://aviris.jpl.nasa.gov, December 2003.

2. Hecht, Eugene. *Optics* (4th Edition). San Francisco: Addison Wesley (Pearson Education Inc.), 2002.

3. Lillesand, Thomas M. and Ralph W. Keifer. *Remote Sensing and Image Interpretation* (4th Edition). New York: John Wiley and Sons, 2000.

4. Mooney, Jonathon M. "Angularly Multiplexed Spectral Imager," *The International Society of Optical Engineers (SPIE)*, *2480*:65 to 77 (1995).

5. Mooney, Jonathon M. and Virgil E. Vickers and Myoung An and Andrzej K. Brodzik. "High-throughput Hyperspectral Infrared Camera," *Optical Society of America*, *14*(11):2951 to 2960 (November 1997).

6. Mooney, Jonathon M. and William S. Ewing. "Characterization of a Hyperspectral Imager," *Infrared Interferometer Spectrometer (IRIS) Proceedings on CD-ROM* (1998).

7. Murguia, James E. and Toby D. Reeves and Jonathon M. Mooney and William S. Ewing and Freeman D. Shepherd and Andrzej Brodzik. "A Compact Visible / Near Visible Infrared Hyperspectral Imager." Reeves Mooney and Ewing from Air Force Research Laboratory (AFRL/SNHI), Murguia Shepherd and Brodzik from Solid State Scientific Corporation, worldwide web site http://www.solidstatescientific.com, post 1999.

8. Bulygin, F.V. and G.N. Vishnyakov and G.G. Levin and D.V. Karpukin. "Spectrotomography - a new method of obtaining spectrograms of 2-D objects," *Opt. Spektrosk. (USSR), copyright 1992 - The Optical Society of America pp 561 to 563*, *71*(6):974 to 978 (December 1991).

9. Okamoto, T. and I. Yamaguchi. "Simultaneous acquisition of spectral image information," *Optics Letters*, *16*:1277 to 1279 (1991).

10. Brodzik, Andrzej K. and Jonathon M. Mooney. "Convex projections algorithm for restoration of limited-angle chromotomographic images," *The Optical Society of America*, *16*(2):246 to 257 (February 1999).

11. Descour, Michael and Eustace Dereniak. "Computed-tomography imaging spectrometer: experimental calibration and reconstruction results," *The Optical Society of America*, *34*(22):4817 to 4826 (August 1995).

12. Descour, M. R. and C. E. Volin and E. L. Dereniak and K. J. Thome and A. B. Schumacher and D. W. Wilson and P. D. Maker. "Demonstration of a high-speed nonscanning imaging spectrometer," *Optics Letters*, *22*(16):1271 to 1273 (August 1997).

13. Volin, Curtis E. and Bridget K. Ford and Michael R. Descour and John P. Garcia and Daniel W. Wilson and Paul D. Maker and Gregory H. Bearman. "High-speed spectral imager for imaging transient fluorescence phenomena," *Applied Optics*, *37*(34):8112 to 8119 (December 1998).

14. Scholl, James F. and Eustace L. Dereniak and Michael R. Descour and Christopher P. Tebow and Curtis E. Volin. "Phase grating design for a dual-band snapshot imaging spectrometer," *Applied Optics*, *42*(1):18 to 29 (January 2003).

15. Ford, Bridget K. and Michael R. Descour and Ronald M. Lynch. "Large-image-format computed tomography imaging spectrometer for fluorescence microscopy," *Optics Express*, *9*(9):444 to 453 (October 2001).

16. Goodman, Joseph W. *Introduction to Fourier Optics* (2nd Edition). Boston: McGraw-Hill, 1996.

REPORT DOCUMENTATION PAGE

Form Approved
OMB No. 074-0188

1. REPORT DATE (DD-MM-YYYY) 23-03-2004	2. REPORT TYPE **Master's Thesis**	3. DATES COVERED (From – To) Jun 2003 – Mar 2004

4. TITLE AND SUBTITLE

SIMULATING A CHROMOTOMOGRAPHIC SENSOR FOR HYPERSPECTRAL IMAGING IN THE INFRARED

5a. CONTRACT NUMBER

5b. GRANT NUMBER

5c. PROGRAM ELEMENT NUMBER

6. AUTHOR(S)

Dearinger, Anthony, J., Flight Lieutenant, RAAF

5d. PROJECT NUMBER

5e. TASK NUMBER

5f. WORK UNIT NUMBER

7. PERFORMING ORGANIZATION NAMES(S) AND ADDRESS(S)
Air Force Institute of Technology
Graduate School of Engineering and Management (AFIT/EN)
2950 Hobson Way, Building 641
Wright-Patterson AFB OH 45433-7765

8. PERFORMING ORGANIZATION REPORT NUMBER

AFIT/GE/ENG/04-05

9. SPONSORING/MONITORING AGENCY NAME(S) AND ADDRESS(ES)
NASIC / DEMS
Attn: Ms. Susan Boyd
4180 Watson Way,   DSN: 257-3615
Wright-Patterson AFB OH 45433-5648   e-mail: Susan.Boyd@wpafb.af.mil

10. SPONSOR/MONITOR'S ACRONYM(S)

11. SPONSOR/MONITOR'S REPORT NUMBER(S)

12. DISTRIBUTION/AVAILABILITY STATEMENT

APPROVED FOR PUBLIC RELEASE; DISTRIBUTION UNLIMITED.

13. SUPPLEMENTARY NOTES

14. ABSTRACT

Hyperspectral imaging systems passively sense radiant electromagnetic energy from a remote scene to form a three dimension profile of the remote scene. The data contained in this profile describes real images of the remote scene for a certain number of spectral wavelength bands across a finite spectral range of electromagnetic radiation. Typical grating type hyperspectral imaging systems collect spectral electromagnetic radiation in the visible and near infrared spectral range, by incrementally scanning across the spatial extent of the remote scene. The legacy of low optical throughput because of the optical scanning techniques employed in these systems means adapting these systems for spectral ranges extending into the mid wave and long wave infrared is difficult. A chromotomographic imaging system utilizing a sensor optics system with significantly greater optical throughput of electromagnetic radiation has been reported to demonstrate reasonable quality hyperspectral images for finite spectral ranges in the visible, mid wave, and long wave infrared. The spectral electromagnetic radiation collected through the sensor optics system angularly multiplexes the electromagnetic radiation collected from the remote scene using a rotating prism to disperse and spatially separate the electromagnetic radiation spectral components onto a focal plane array detector. Using optics principles and wave optics propagation theory, a software model was designed to emulate the attributes of the sensor optics system loosely detailed in reports on the chromotomographic imaging system.

15. SUBJECT TERMS

hyperspectral imagery, spectrotomography, chromotomography, computed tomography, spectroscopy, spectrometers, infrared, spectra, spectrometry, radiometry, diffraction, continuous spectra, spectral energy distribution, electromagnetic spectra, electromagnetic radiation, refraction, wavefronts, optical analysis, dispersion, dispersing, spatial distribution, separation, infrared images, software tools, simulation, modeling, wave optics, propagation

16. SECURITY CLASSIFICATION OF:			17. LIMITATION OF ABSTRACT	18. NUMBER OF PAGES	19a. NAME OF RESPONSIBLE PERSON Matthew E. Goda, Maj, USAF, Ph. D. (ENG)
a. REPORT	b. ABSTRACT	c. THIS PAGE			19b. TELEPHONE NUMBER (Include area code)
U	U	U	UU	154	(937) 785 - 2024, e-mail: Matthew.Goda@afit.edu

Standard Form 298 (Rev. 8-98)
Prescribed by ANSI Std. Z39-18